UNIVERSITY OF SOUTHAMPTON

Optical Frequency Comb Locked Signal Synthesis

by

David Sze-too Wu

A thesis submitted in partial fulfillment for the
degree of Doctor of Philosophy

in the
Faculty of Physical Sciences and Engineering
Optoelectronics Research Centre

December 2014

UNIVERSITY OF SOUTHAMPTON

ABSTRACT

FACULTY OF PHYSICAL SCIENCES AND ENGINEERING
Optoelectronics Research Centre

Doctor of Philosophy

Optical Frequency Comb Locked Signal Synthesis

by David Sze-too Wu

Highly stable optical frequency combs (OFCs), particularly those generated by mode-locked lasers, have become important tools for frequency and time metrology, and spectroscopy. This is due to their ability to span wide bandwidths, to act as highly accurate frequency references, and to provide a direct link between the optical and radio frequencies. However, the narrow comb spacing of most mode-locked OFCs makes it difficult to access their individual modes for a wide range of other potential applications.

This thesis investigates comb mode extraction from a 250 MHz spaced OFC by phase locking semiconductor lasers (slave lasers) to individual comb modes. This was achieved using optical injection locking in combination with a low bandwidth electronic feedback loop. The locking process forced a slave laser to emit at the same frequency as the comb mode it was locked to, but at its natural output power. Hence a locked slave laser effectively behaved as a ultra-narrowband filter with active gain.

The locking process was characterised in terms of its long-term frequency stability over a period of 8 hours (minimum Allan deviation of less than 10^{-18}) and its short term phase noise across a bandwidth from 100 Hz to 500 MHz (minimum integrated phase noise of 0.02 rad^2). Amplification of the residual comb modes was measured and found to have a dependence on the master-slave frequency detuning. The results from numerical modelling found that this was due to phase modulation induced in the slave laser by the injected OFC and could always be suppressed by controlling the frequency detuning.

Fourier synthesis of high repetition rate waveforms was explored as one of the potential applications of this phase locking technique. Multiple lasers were made coherent with one another by locking them to different modes of a common OFC. This enabled them to behave as different frequency components of a Fourier series to generate various waveforms. This was achieved by independently controlling the relative amplitude and phase of each slave laser, and combining them together. The generation of stable waveforms with flat-top, triangular, parabolic, and sawtooth intensity profiles was demonstrated at a repetition rate of 100 GHz.

Contents

Declaration Of Authorship

I, David Sze-too Wu, declare that the thesis entitled *Optical Frequency Comb Locked Signal Synthesis* and the work presented in the thesis are both my own, and have been generated by me as the result of my own original research. I confirm that:

- this work was done wholly or mainly while in candidature for a research degree at this University;
- where any part of this thesis has previously been submitted for a degree or any other qualification at this University or any other institution, this has been clearly stated;
- where I have consulted the published work of others, this is always clearly attributed;
- where I have quoted from the work of others, the source is always given. With the exception of such quotations, this thesis is entirely my own work;
- I have acknowledged all main sources of help;
- where the thesis is based on work done by myself jointly with others, I have made clear exactly what was done by others and what I have contributed myself;
- parts of this work have been published as: [see *List of Publications*];

Signed: .....

Date

List of Figures

List of Acronyms and Symbols

α	Linewidth Enhancement Factor
$\Delta\omega$	Master-Slave Frequency Detuning
$\Delta\omega_L$	Locking Range / Locking Bandwidth
$\Delta\phi_L$	Optical Injection Locking Phase Shift
f_{ceo}	Carrier-Envelope Offset Frequency
f_r	Repetition Rate / Comb Spacing
AOM	Acousto-Optic Modulator
ASE	Amplified Spontaneous Emission
AWG	Arrayed Waveguide Grating
BPF	Band-Pass Filter
CEO	Carrier-Envelope Offset
Co-OFDM	Coherent Optical Orthogonal Frequency Division Multiplexing
CPA	Chirped Pulse Amplification
cw	Continuous Wave
DC	Direct Current
EDFA	Erbium Doped Fibre Amplifier
EOM	Electro-Optic Modulator
FFT	Fast Fourier Transform
FPF	Fabry-Pérot Filter
FWHM	Full Width at Half Maximum
FWM	Four-Wave Mixing
GPS	Global Positioning System
HLNF	Highly Non-Linear Fibre
LC-SLM	Liquid Crystal Spatial Light Modulator
LCoS-SLM	Liquid Crystal on Silicon Spatial Light Modulator
LO	Local Oscillator
LPF	Low-Pass Filter

OFC	Optical Frequency Comb
OFCG	Optical Frequency Comb Generator
OFDM	Orthogonal Frequency Division Multiplexing
OIL	Optical injection Locking
OIPLL	Optical Injection Phase Lock Loop
OPLL	Optical Phase Lock Loop
OSA	Optical Spectrum Analyser
OSNR	Optical Signal-to-Noise Ratio
OSO	Optical Sampling Oscilloscope
PC	Polarisation Controller
PD	Photodetector
PCB	Printed Circuit Board
PI	Proportional-Integral (controller)
PIC	Photonic Integrated Circuit
PLL	Phase Lock Loop
PM	Polarisation Maintaining
PM-F	Polarisation Maintaining Fibre
PSA	Phase Sensitive Amplifier
PSD	Power Spectral Density
PZT	Lead Zirconate Titantate (piezoelectric material)
RF	Radio Frequency
RIN	Relative Intensity Noise
rms	Root Mean Squared
SMF	Single Mode Fibre
SSFBG	Superstructured Fibre Bragg Grating
TEC	Thermo-Electric Cooler
VCO	Voltage Controlled Oscillator
VOA	Variable Optical Attenuator

List of Publications

Journal Papers

1. **D.S. Wu**, R. Slavík, G. Marra, and D.J. Richardson, "Direct selection and amplification of individual narrowly spaced optical comb modes via injection locking: design and characterization," *Journal of Lightwave Technology*, vol. 31, no. 14, pp. 2287–2295, 2013

2. Z. Liu, J. Kim, **D.S. Wu**, D.J. Richardson, and R. Slavík, "Homodyne OFDM with Optical Injection Locking for Carrier Recovery," *Journal of Lightwave Technology* (accepted), 2014

3. **D.S. Wu**, D.J. Richardson, and R. Slavík, "Optical Fourier synthesis of high repetition rate pulses", *Optica*, (accepted), 2014

Conference Proceedings

1. J. Kim, **D.S. Wu**, G. Marra, D.J. Richardson, and R. Slavík. "Wavelength Conversion by Injection Locking to an Optical Comb for Optical Frequency Transfer Applications," in *6th EPS-QEOD Europhoton Conference*, Neuchatel, ThB-T1-O-02, 2014.

2. J. Kim, **D.S. Wu**, G. Marra, D.J. Richardson, and R. Slavík. "Stability Characterization of an Optical Injection Phase Locked Loop for Optical Frequency Transfer Applications," in *2014 Conference on Lasers and Electro-optics (CLEO)*, San Jose, SW3O.7, 2014.

3. Z. Liu, **D.S. Wu**, D.J. Richardson, and R. Slavík. "Homodyne OFDM using Simple Optical Carrier Recovery," in *2014 Optical Fiber Communication Conference*, San Francisco, W4K.3, 2014.

4. **D.S. Wu**, D.J. Richardson, and R. Slavík, "Stable 100 GHz Pulses Generated by Injection Locking of Multiple Lasers to an Optical Frequency Comb", in *2013 Conference on Lasers and Electro-optics Europe and International Quantum Electronics Conference (CLEO/Europe-IQEC)*, Munich, CI.5.3, 2013.

5. **D.S. Wu**, D.J. Richardson, and R. Slavík, "Selective amplification of frequency comb modes via optical injection locking of a semiconductor laser: influence of adjacent unlocked comb modes," in *SPIE Optics & Optoelectronics 2013*, Prague, 87810J, 2013.

6. **D.S. Wu**, R. Slavík, G. Marra, and D.J. Richardson, "Phase noise and jitter characterization of pulses generated by optical injection locking to an optical frequency comb," in *Frontiers in Optics (FiO/LS XXVIII)*, Rochester, FW2A.3, 2012.

7. **D.S. Wu**, R. Slavík, G. Marra, and D.J. Richardson, "Phase noise characterization of injection locked semiconductor lasers to a 250 MHz optical frequency comb," in *2012 Conference on Lasers and Electro-optics and Quantum Electronics and Laser Science Conference (CLEO/QELS)*, San Jose, JW2A.89, 2012.

8. **D.S. Wu**, R. Slavík, G. Marra, and D.J. Richardson, "Robust optical injection locking to a 250 MHz frequency comb without narrow-band optical pre-filtering," in *2011 International Quantum Electronics Conference and Conference on Lasers and Electro-optics Pacific Rim (IQEC/CLEO-PR)*, Sydney, C258, 2011.

Acknowledgements

- Dave Richardson – for taking me on as his PhD student and providing me with his guidance, encouragement and advice.
- The Optoelectronics Research Centre – for funding my studentship and providing me with the opportunity to pursue a PhD degree.
- Guiseppe Marra (National Physical Laboratory) – for sharing his knowledge and advising me on the various noise measurements made in this thesis and his help with designing the feedback controllers.
- Various members of the telecommunications group, in particular Francesca Parmigiani – for generously sharing their equipment and helping me out in the lab.
- Radan Slavík – for mentoring me; for teaching and training me; for his regular support; for his insightful advice; for his encouragement and motivation; and for his friendship. In other words, for being an amazing supervisor.
- All the friends I've made in Southampton – for keeping me (relatively) sane.
- My family – for getting me to where I am today.

Chapter 1

Introduction

Independent oscillators will rarely be synchronised in their free running (natural) state without some form of interaction between them. Even with careful engineering, it is unlikely[1] two oscillators will have exactly the same frequency and phase, and be able to maintain it indefinitely. This is why time keeping has been, and continues to be, an active area of research. Oscillators can of course be actively synchronised by comparing the two oscillators and adjusting their frequencies and phases accordingly; this is analogous to synchronising a watch with a more accurate clock. This compare and adjust technique can be repeated continuously to keep the oscillators synchronised indefinitely. This technique is commonly used in modern electronics and is known as a phase lock loop (PLL) [1] since it is specifically the relative phase of the oscillators which is measured and compared.

Given the right conditions, oscillators can also naturally synchronise with one another via coupling. A popular experiment demonstrating this involves two or more metronomes, with very small differences in frequencies, placed close to one another on a common frame which is free to move. The unsynchronised metronomes will, over time, synchronise on their own[2] as the momenta from the swinging pendula can couple to each other through the freely moving frame [2].

This coupling induced synchronisation, as well as active synchronisation, can be applied to optical systems. In particular, a laser (optical oscillator) can be phase locked to another such that it adopts the same frequency and becomes coherent with it. Since the frequency is a key parameter describing a laser, these locking techniques are sometimes referred to as *'coherent cloning'* [3] since the phase locked laser effectively becomes a copy of the laser it is locked to. This thesis is a study of the use of optical phase locking to replicate individual modes of a specific optical device known as an optical frequency comb.

[1] Although not impossible: atomic clocks kept in exactly the same environment is an example of where this might be feasible

[2] The reader is encouraged to search for videos of this on the internet

1.1 Optical Frequency Combs – a revolutionary tool for metrology and spectroscopy

While the basis of this thesis is about phase locking, it is also important to understand the original laser which is being 'cloned'. This laser is referred to as the *master laser*. In this thesis, the master laser will primarily be an optical frequency comb generator (OFCG). An optical frequency comb (OFC) has an optical spectrum which consists of many modes with a fixed frequency spacing between them, as shown in Figure 1.1. OFCs can be generated either by modulating a single frequency, continuous wave (cw) laser or they can be generated directly by a mode-locked laser. OFCs can span very wide bandwidths, with some covering over an octave. The frequency of each of the OFC modes has been reported to have a fractional uncertainty as low as 1.4×10^{-19} when measured with an atomic reference [4]. This very high stability allows the comb to be used as a 'frequency ruler', where arbitrary frequencies can be measured with high accuracy, provided they lie within the bandwidth of the comb spectrum [5].

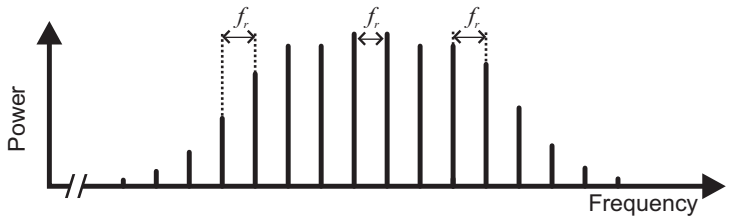

FIGURE 1.1: An example of an optical frequency comb. The comb modes are all separated by a frequency, f_r, equal to the repetition rate.

Another key feature which made the OFC a revolutionary tool for frequency metrology was their ability to perform optical to microwave frequency conversion. Current instruments are much too slow to be able to directly measure the frequency of the oscillating electric field of an optical signal. Frequency measurements are instead made by comparing the unknown frequency with a known one, for example, from an atomic transition. The beat signal generated by the two signals is a down-conversion of the difference frequency between them, and can then be measured by a photodetector with sufficient bandwidth. However, these optical frequency references, still needed to first be accurately measured. To do so, metrology laboratories around the world built long and cumbersome frequency chains to bridge the gap from directly measurable microwave atomic references, to their unknown optical atomic references [6]. This involved generating harmonics of the microwave reference using a nonlinear element and phase locking a higher frequency oscillator to one of the harmonics. This process was repeated by locking a subsequent oscillator to one of the harmonics of the second oscillator. The chain was continued using a range of oscillators (e.g. electronic oscillators, masers, lasers) to reach the desired optical frequency. OFCs can provide a direct link between the optical and microwave domains since the comb spacing (and offset[3]) can be locked to a microwave

[3]The will be discussed further in next chapter

reference. The frequency of each of the comb modes is therefore known with the same relative accuracy as the microwave reference. This has made frequency measurements significantly easier and also more accessible to non-metrology laboratories.

OFCs are also important tools for spectroscopy since they can be used as a reference to accurately calibrate a higher power single frequency cw laser for use in traditional single laser spectroscopy [7]. There are also spectroscopic methods which take advantage of the entire OFC spectrum where several comb modes perform parallel measurements of multiple transitions [8, 9, 10]. Since OFCs can also generate very wide spectra (through non-linear broadening), it is possible to generate wavelengths which are of interest for spectroscopy but are not easily accessible via cw lasers such as the ultraviolet and long-wavelength infrared regimes. The broad spectral coverage, uniform spacing and high precision of OFCs have also allowed them to be used as a replacement for various gas discharge lamps used to calibrate high resolution astronomical spectrographs [11]. A less obvious benefit of OFCs for astronomical spectrometry is the relative ease in which they can be amplified compared to gas lamps. Low intensity references require spectrograms to be measured with long integration times which is not possible for bright sources such as the Sun [12].

The high stability of OFCs also makes them ideal for use as part of an optical atomic clock. Similar to traditional microwave atomic clocks, an optical counterpart uses an atomic (or molecular or ionic) transition as a reference, only at optical frequencies instead of microwave frequencies. The frequency stability of a transition scales up with frequency and therefore optical atomic clocks can provide superior performance as compared to microwave ones [13]. One of the OFC modes can be locked to an atomic reference, which will in turn stabilise the entire OFC with respect to that reference [14]. This is the reverse of what was previously discussed, where now an optical atomic reference is used to provide a highly accurate comb spacing which is measurable at microwave frequencies. In other words, as depicted in Figure 1.2, the OFC acts as the clockwork (analogous to the many gears inside a mechanical clock) which converts the 'ticking' of an oscillator (e.g. a pendulum) into something which can be read (e.g. a clock face).

The success of OFCs in the fields of time and frequency metrology, and spectroscopy led to two of the early pioneers of high precision frequency combs, John L. Hall and Theodor W. Hänsch, being awarded half of the Nobel Prize in Physics[4] in 2005 [15].

1.2 Other OFC applications

The large number of stable and narrow linewidth modes found in OFCs gives rise to a number of applications in fields other than metrology. One such application is for

[4]The prize was shared in 2005. Half was awarded to Hall and Hänsch, with the other half awarded to Roy J. Glauber for his (unrelated) contribution to the quantum theory of optical coherence

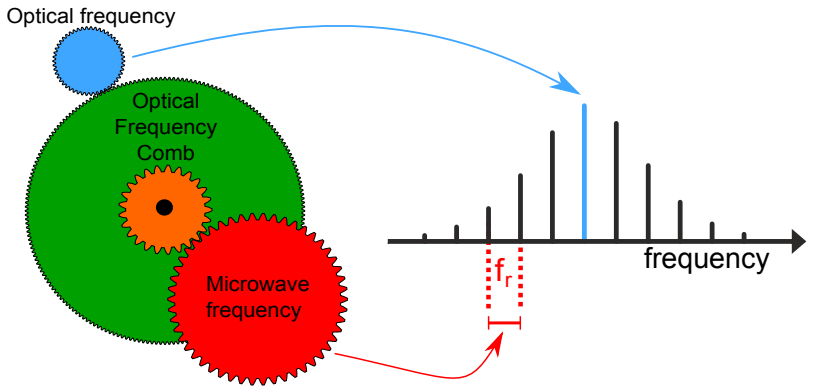

FIGURE 1.2: An analogy of an OFC behaving as clockwork to translate the optical frequency into microwave frequency

optical frequency synthesis, where a highly stabilised OFC acts as a bank of frequency references for a cw laser to accurately tune its operating frequency. This is achieved by phase locking the cw laser to one of the comb modes such that it will also emit at that frequency (or at an offset frequency). Discrete frequency [16] and continuous tuning systems [17] have been demonstrated, with algorithms developed to automatically tune the laser to the desired frequency.

Another OFC application is in the field of optical arbitrary waveform generation[5]. This is achieved through a process known as line-by-line pulse shaping [18], where the amplitude and phase of all the individual comb modes of an OFC are manipulated to give the desired output. This has been demonstrated with 108 comb modes [19] using a programmable liquid crystal modulator array to control phase and amplitude. Arbitrary optical waveforms could open a wide range of applications in fields [20] ranging from high speed optical communications, coherent control of molecules, and improved spectroscopic techniques.

It has been envisioned that OFCs can also have applications in telecommunications. One possible application is to use an OFC generated from a single high power laser, with comb modes covering one or more telecommunications bands. This could be used to replace the bank of individual lasers used for each communication channel [21]. OFCs have also been proposed for use in coherent optical orthogonal frequency division multiplexing (Co-OFDM). This is similar to radio frequency OFDM where high data rates are achieved by splitting a channel into multiple slower sub-channels. In the optical equivalent, the individual modes of the OFC can be used as the sub-channels [22]. The fixed phase relationship of the OFC is used to cancel cross-talk between the sub-channels since they beat together in a deterministic manner [23].

[5]This will be discussed in more detail in Chapter 6

OFCs also have applications in microwave (0.3—300 GHz) and terahertz (0.3—3 THz) generation[6]. These signals can be generated optically by combining two optical signals with a frequency difference equal to the desired microwave (or THz) frequency. The down-convertion of the optical heterodyne signal into a microwave signal can be achieved by direct photodetection using ultra-fast photodetectors [24, 25], or by interactions with non-linear materials [26]. An OFC is not a necessary requirement to generate these signals. However, by using two modes from an OFC, it allows microwave signals to be generated with high stability at a defined frequency. This could be particularly useful for THz spectroscopy, where many molecules have distinct spectra [27].

1.3 Processing OFCs

In many of the applications discussed in the previous sections, the raw output of the OFC is not directly used in the application. OFCs often require pre-processing before use, commonly in the form of filtering and amplification.

For many applications the entire OFC bandwidth is not required and in some cases is actually prohibitive to the application. For example, photonic microwave generation only requires two of the comb modes. There are also cases where the comb spacing is too small for a given application. This is particularly true for applications that require the OFC to be decomposed into its constituent modes, for example, for use in optical arbitrary waveform generation and astronomical spectrographs. This is generally not possible for narrow spaced combs due to the limited ability of spectral dispersers such as gratings. These issues can generally be resolved by using a spectral filtering system. For a narrow spaced OFC (< 1 GHz), a high finesse (narrowband) Fabry-Perot filter could be used to select every, for example, one out of 20 comb modes to widen the comb spacing [12, 28]. This requires the free spectral range of the filter to be carefully matched to a multiple of the comb spacing. Also, due to the high finesse, any spectral misalignment of the filter, for example due to temperature variations, is transferred into amplitude variations in the output, hence creating a source of noise [29].

It is also desirable for many applications to have high power per comb mode with high optical signal-to-noise ratios (OSNR). Wide bandwidth OFCs generally have low power per mode and require amplification, for example, using an erbium doped fibre amplifier (EDFA). However, optical amplifiers operate over a limited bandwidth which restricts the spectral region of the OFC which can be amplified. Also, conventional (phase insensitive) amplifiers will always add a noise penalty of at least 3 dB due to spontaneous emission [30]. This limitation can be overcome by using phase sensitive amplifiers (PSA) with a demonstrated noise figure of 1.1 dB [31].

[6]There are no strict frequencies which separate the different regions of the electromagnetic spectrum. These ranges are provided as a guide.

This thesis is based primarily on using phase locking to simultaneously perform the filtering, to select a single mode, and strongly amplify it with only a small noise penalty. This is achieved by phase locking a cw laser to a single comb mode; the laser then becomes a *'clone'* of the comb mode by adopting the same frequency properties. However, the laser will continue to emit at its free running power which can be many orders of magnitude larger than the comb mode it is locked to. Thus, the laser is effectively an amplified copy of an individual comb mode.

This is commonly achieved using optical phase lock loops (OPLL), where the frequency and phase of the laser is actively adjusted to match one of the comb modes via a feedback loop. In fact, Menlo Systems GmbH, a leading manufacturer of metrology grade OFCs, offer a standard package with their OFCs which includes the equipment to do this. However, the performance of OPLLs are limited since these feedback loops are electronic in nature. The locking bandwidth, the proportion of the comb mode being 'copied', has a limited bandwidth governed by the delay in the feedback loop from all the various components. For example, The Menlo Systems SYNCRO system is specified to have a maximum bandwidth of approximately 1.3 MHz.

My work presented in this thesis is based on a different phase locking technique known as optical injection locking. This is achieved by coupling the laser to one of the comb modes by injecting the comb into the optical cavity of a cw laser. This is similar to the metronomes described at the beginning of the chapter, which can couple by vibrations transmitted between them. Optical injection locking allows for significantly larger locking bandwidths as compared to OPLLs. To get the laser to lock to a single comb mode from a narrowly spaced OFC in a stable, low noise manner is non-trivial and is addressed in this thesis. The application of this technique is then demonstrated by using it in one of the previously discussed applications: Fourier synthesis of arbitrarily shaped optical waveforms.

1.4 Thesis Outline

Chapter 2 — Background This chapter will provide a review of the common types of OFCGs and their operating principles. It will also review the current techniques for optical phase locking.

Chapter 3 — Locking to an Optical Frequency Comb This chapter will begin with a review of the current state of the art for locking individual lasers to OFCs. This will be followed by the discussion, design and demonstration of my phase locking technique to extract individual comb modes.

Chapter 4 — Noise Characterisation The quality of my locking technique is evaluated in this chapter by measuring the long-term frequency stability, and short-term phase noise of the phase locked laser.

Chapter 5 — Residual Comb Mode Amplification This chapter will investigate how the presence of multiple injected frequencies (the OFC) influences the injection locking process. In particular, numerical modelling was used to look at how comb modes which are adjacent to the locked one can experience amplification.

Chapter 6 — Waveform Synthesis One of the applications for my phase locking technique, optical Fourier synthesis, is explored in this chapter. The current state of the art and the applications of arbitrary waveform generation are reviewed. The use of my phase locking technique for waveform synthesis will be discussed and followed by the design and demonstration of a system capable of generating arbitrarily shaped optical waveforms.

Chapter 7 — Conclusions The key findings in this thesis will be summarised and some insight into potential future work utilising my phase locking technique will be discussed.

1.5 References

[1] F. M. Gardner, *Phaselock Techniques*. John Wiley & Sons, 2nd ed., 1979.

[2] M. Bennett, M. F. Schatz, H. Rockwood, and K. Wiesenfeld, "Huygens's clocks," *Proceedings of the Royal Society of London A: Mathematical, Physical and Engineering Sciences*, vol. 458, no. 2019, pp. 563–579, 2002.

[3] N. Satyan, W. Liang, and A. Yariv, "Coherence cloning using semiconductor laser optical phase-lock loops," *IEEE Journal of Quantum Electronics*, vol. 45, no. 7, pp. 755–761, 2009.

[4] L. S. Ma, Z. Y. Bi, A. Bartels, L. Robertsson, M. Zucco, R. S. Windeler, G. Wilpers, C. Oates, L. Hollberg, and S. A. Diddams, "Optical frequency synthesis and comparison with uncertainty at the 10(-19) level," *Science*, vol. 303, no. 5665, pp. 1843–1845, 2004.

[5] T. Udem, R. Holzwarth, and T. W. Hänsch, "Optical frequency metrology," *Nature*, vol. 416, no. 6877, pp. 233–237, 2002.

[6] J. Ye, H. Schnatz, and L. W. Hollberg, "Optical frequency combs: From frequency metrology to optical phase control," *IEEE Journal of Selected Topics in Quantum Electronics*, vol. 9, no. 4, pp. 1041–1058, 2003.

[7] S. A. Diddams, "The evolving optical frequency comb," *Journal of the Optical Society of America B-Optical Physics*, vol. 27, no. 11, pp. B51–B62, 2010.

[8] V. Gerginov, C. E. Tanner, S. A. Diddams, A. Bartels, and L. Hollberg, "High-resolution spectroscopy with a femtosecond laser frequency comb," *Optics Letters*, vol. 30, no. 13, pp. 1734–1736, 2005.

[9] S. A. Diddams, L. Hollberg, and V. Mbele, "Molecular fingerprinting with the resolved modes of a femtosecond laser frequency comb," *Nature*, vol. 445, no. 7128, pp. 627–630, 2007.

[10] I. Coddington, W. Swann, and N. Newbury, "Coherent Multiheterodyne Spectroscopy Using Stabilized Optical Frequency Combs," *Physical Review Letters*, vol. 100, no. 1, p. 013902, 2008.

[11] M. T. Murphy, T. Udem, R. Holzwarth, A. Sizmann, L. Pasquini, C. Araujo-Hauck, H. Dekker, S. D'Odorico, M. Fischer, T. W. Hänsch, and A. Manescau, "High-precision wavelength calibration of astronomical spectrographs with laser frequency combs," *Monthly Notices of the Royal Astronomical Society*, vol. 380, no. 2, pp. 839–847, 2007.

[12] H.-P. Doerr, T. Steinmetz, R. Holzwarth, T. Kentischer, and W. Schmidt, "A laser frequency comb system for absolute calibration of the VTT echelle spectrograph," *Solar Physics*, vol. 280, pp. 663–670, Mar. 2012.

[13] J. Ye and S. T. Cundiff, *Femtosecond optical frequency comb: principle, operation, and applications*. Kluwer Academic Publishers/Springer, 2005.

[14] J. Ye, T. H. Yoon, J. L. Hall, A. A. Madej, J. E. Bernard, K. J. Siemsen, L. Marmet, J.-M. Chartier, and A. Chartier, "Accuracy Comparison of Absolute Optical Frequency Measurement between Harmonic-Generation Synthesis and a Frequency-Division Femtosecond Comb," *Physical Review Letters*, vol. 85, no. 18, pp. 3797–3800, 2000.

[15] T. N. Foundation, *Press Release: The 2005 Nobel Prize in Physics*. Nobelprize.org. Nobel Media: Accessed 28 December 2013, http://www.nobelprize.org/nobel_prizes/physics/laureates/2005/press.htm.

[16] S. H. Lee, H. Y. Ryu, W. K. Lee, Y. P. Kim, and H. S. Suh, "Discretely tunable optical frequency synthesizer utilizing a femtosecond fiber laser injection-locking technique," *IEEE Photonics Technology Letters*, vol. 21, no. 19, pp. 1435–1437, 2009.

[17] J. D. Jost, J. L. Hall, and J. Ye, "Continuously tunable, precise, single frequency optical signal generator," *Optics Express*, vol. 10, no. 12, pp. 515–520, 2002.

[18] A. M. Weiner, D. E. Leaird, J. S. Patel, and J. R. Wullert, "Programmable femtosecond pulse shaping by use of a multielement liquid-crystal phase modulator," *Optics Letters*, vol. 15, no. 6, pp. 326–328, 1990.

[19] Z. Jiang, C. B. Huang, D. E. Leaird, and A. M. Weiner, "Optical arbitrary waveform processing of more than 100 spectral comb lines," *Nature Photonics*, vol. 1, no. 8, pp. 463–467, 2007.

[20] S. T. Cundiff and A. M. Weiner, "Optical arbitrary waveform generation," *Nature Photonics*, vol. 4, no. 11, pp. 760–766, 2010.

[21] T. J. Kippenberg, R. Holzwarth, and S. A. Diddams, "Microresonator-Based Optical Frequency Combs," *Science*, vol. 332, no. 6029, pp. 555–559, 2011.

[22] S. Chandrasekhar and L. Xiang, "Terabit superchannels for high spectral efficiency transmission," in *36th European Conference and Exhibition on Optical Communication (ECOC)*, p. Tu.3.C.5, 2010.

[23] A. D. Ellis and F. C. G. Gunning, "Spectral density enhancement using coherent WDM," *IEEE Photonics Technology Letters*, vol. 17, no. 2, pp. 504–506, 2005.

[24] H. Ito, T. Furuta, and S. Kodama, "InP/lnGaAs uni-travelling-carrier photodiode with 310GHz bandwidth," *Electronics Letters*, vol. 36, no. 21, pp. 1809–1810, 2000.

[25] S. Preu, G. H. Dohler, S. Malzer, L. J. Wang, and A. C. Gossard, "Tunable, continuous-wave Terahertz photomixer sources and applications," *Journal of Applied Physics*, vol. 109, no. 6, p. 061301, 2011.

[26] Y. Ding, "High-power tunable terahertz sources based on parametric processes and applications," *IEEE Journal of Selected Topics in Quantum Electronics*, vol. 13, no. 3, pp. 705–720, 2007.

[27] M. Tonouchi, "Cutting-edge terahertz technology," *Nature Photonics*, vol. 1, no. 2, pp. 97–105, 2007.

[28] S. A. Diddams, M. Kirchner, T. Fortier, D. Braje, A. M. Weiner, and L. Hollberg, "Improved signal-to-noise ratio of 10 GHz microwave signals generated with a mode-filtered femtosecond laser frequency comb," *Optics Express*, vol. 17, no. 5, pp. 3331–3340, 2009.

[29] S. Ayotte, F. Costin, M. Aube, Y. Painchaud, M. Morin, M. Poulin, and C. Latrasse, "Semiconductor laser white noise suppression by optical filtering with ultra-narrowband FBG," in *Optical Fiber Communication Conference and Exposition and the National Fiber Optic Engineers Conference (OFC/NFOEC)*, p. OThP5, 2011.

[30] R. Olshansky, "Noise figure for erbium-doped optical fibre amplifiers," *Electronics Letters*, vol. 24, no. 22, pp. 1363–1365, 1988.

[31] Z. Tong, C. Lundström, P. A. Andrekson, C. J. McKinstrie, M. Karlsson, D. J. Blessing, E. Tipsuwannakul, B. J. Puttnam, H. Toda, and L. Grüner-Nielsen, "Towards ultrasensitive optical links enabled by low-noise phase-sensitive amplifiers," *Nature Photonics*, vol. 5, no. 7, pp. 430–436, 2011.

Chapter 2

Background

The previous chapter briefly introduced the concept of phase locking and also discussed OFCs and some of their applications. The first part of this chapter will provide a background into the fundamentals of OFCs: the different types of OFCs, how they are generated, and their properties. The second part of this chapter will discuss the three most common techniques for optical phase locking.

2.1 Types of Optical Frequency Combs

The term optical frequency comb refers to any optical signal which has a spectrum consisting of multiple modes[1] which have an equal frequency spacing between them. The three most common mechanisms to generate coherent OFCs will be discussed in this section: mode-locking, active modulation, and non-linear modulation.

2.1.1 Mode-locked laser frequency combs

Mode-locking

Mode-locked lasers are devices which are best known for generating ultra-short pulse trains in the time domain. The term mode-locking refers to the frequency domain, where the pulse train can be described as being composed of a very large number of different frequencies (modes) with a fixed (locked) phase relationship. Historically, the development of mode-locked lasers was motivated by the desire to generate pulses with shorter and shorter durations. Mode-locking can be achieved by utilising a mechanism which provides the laser with higher gain for short pulses than for cw operation. This

[1]There are various different names for the comb modes, these include: comb lines, comb teeth or frequency tones. The term *comb mode* will be used exclusively in this thesis.

mechanism is usually achieved by reducing the loss inside the laser cavity for a short period of time. This can be done either actively or passively.

An example of active mode-locking utilises an amplitude modulator inside the laser cavity, which behaves as a transmission gate. The modulator is driven at a frequency equal to, or a multiple of, the cavity round trip frequency. The modulator is set up in such a way that there is net gain for only a fraction of the round trip time. In the frequency domain, this corresponds to a lasing cavity mode acquiring modulation sidebands as a result of the active modulator.

Passive mode-locking occurs when the pulse inside the laser modulates itself (self-modulation) to reduce its duration. Pulses are shortened by passing through a saturable absorber element, which may be either real or artificial [1]. A saturable absorber is a lossy element (due to absorption) which increases in transparency as the intensity of light increases, due to saturation effects. As a result, only the portion of a pulse with sufficient intensity can propagate in the laser cavity. Real saturable absorbers refer to materials which actually exhibit saturable absorption. Dyes and semiconductors are common examples of real saturable absorbers.

Artificial saturable absorbers are elements which also exhibit a similar intensity dependent loss, without relying on saturable absorption. They generally rely on very fast optical nonlinear effects, which can be considered instantaneous relative to the pulse envelope, and as a result can be used to generate ultra-short pulses. One example is Kerr-lens mode-locking, where intensity dependent self-focussing is used to focus only the most intense portion of the pulse through an aperture inside the cavity. Another example, more common in mode-locked fibre lasers, is nonlinear polarisation rotation [2], where an intensity dependent polarisation shift is employed. The polarisation is aligned in such a way that only the high intensity portion of the pulse is transmitted [3]. Pulse durations of less than 5 fs [4] have been demonstrated using artificial saturable absorbers. Group velocity dispersion inside the laser cavity and net gain bandwidth ultimately limit the minimum pulse duration [1].

Mode-locked lasers as frequency combs

A mode-locked laser which generates a continuous train of identical pulses is in fact an OFC. This can be seen by looking at the frequency domain of the output, which can be obtained by taking the Fourier transform of the pulse train. The result is a frequency spectrum composed of a large number of discrete frequencies equally spaced from one another, i.e. a frequency comb, as shown in Figure 2.1. The comb spacing is equal to the repetition rate of the laser, f_r, which is the inverse of the time between successive pulses. The repetition rate is dependent on the round trip time of the pulse within the laser cavity, T_R, and hence depends on the cavity length.

Dispersion inside the laser cavity causes the group and phase velocity of the pulse to vary from one another, meaning that the pulse envelope has a different velocity compared to the carrier. This results in the relative phase between the carrier and the envelope, ϕ_{ce}, to evolve with time. As shown in Figure 2.1, the pulse-to-pulse carrier-envelope phase varies by an amount

$$\Delta\phi_{ce} = \phi_{ce}(t) - \phi_{ce}(t - T_R) \ , \tag{2.1}$$

where t is time. This regular change in the carrier-envelope phase causes the entire frequency spectrum to shift (in the positive direction) by an amount [5] given by

$$f_{ceo} = \frac{\Delta\phi_{ce}}{2\pi} f_r \ , \tag{2.2}$$

where f_{ceo} is known as the carrier-envelope offset (CEO) frequency.

The frequency of every comb mode of an OFC can be described using the repetition rate and the carrier-envelope offset frequency through the equation

$$\nu_n = f_{ceo} + n f_r \ , \tag{2.3}$$

where n is an integer and ν_n is the frequency of the n^{th} mode. Both f_{ceo} and f_r are typically radio frequencies (RF). This provides the direct link between the optical domain and the RF domain, which is what makes OFCs so valuable in metrology (as discussed in Section 1.1).

Comb mode stabilisation

It has been long known that the spectrum of a regular pulse train corresponds to a frequency comb, with a frequency spacing equal to the repetition rate of the pulses. However, it was not until 1999 when Udem et al. [6] verified this to an accuracy of 6.0×10^{-16} that the metrology community began to embrace the mode-locked laser as a frequency measurement tool. One of the requirements for frequency combs to be useful as a frequency reference is that the comb modes must be extremely stable, i.e. the frequency of every comb mode must not change over time.

Variations in the cavity length, e.g. due to temperature and acoustic fluctuations, causes the repetition rate to vary. This causes the OFC to 'breathe', where the spacing between the comb modes expands and contracts. The repetition rate can be easily measured by directly measuring the output of the mode-locked laser using a sufficiently fast photodetector. A phase lock loop can then be used to lock the value of f_r to a high quality RF reference, such as an atomic clock, to stabilise the comb spacing. Feedback is achieved by varying the cavity length, e.g. by using a mirror which is mounted on a piezoelectric transducer.

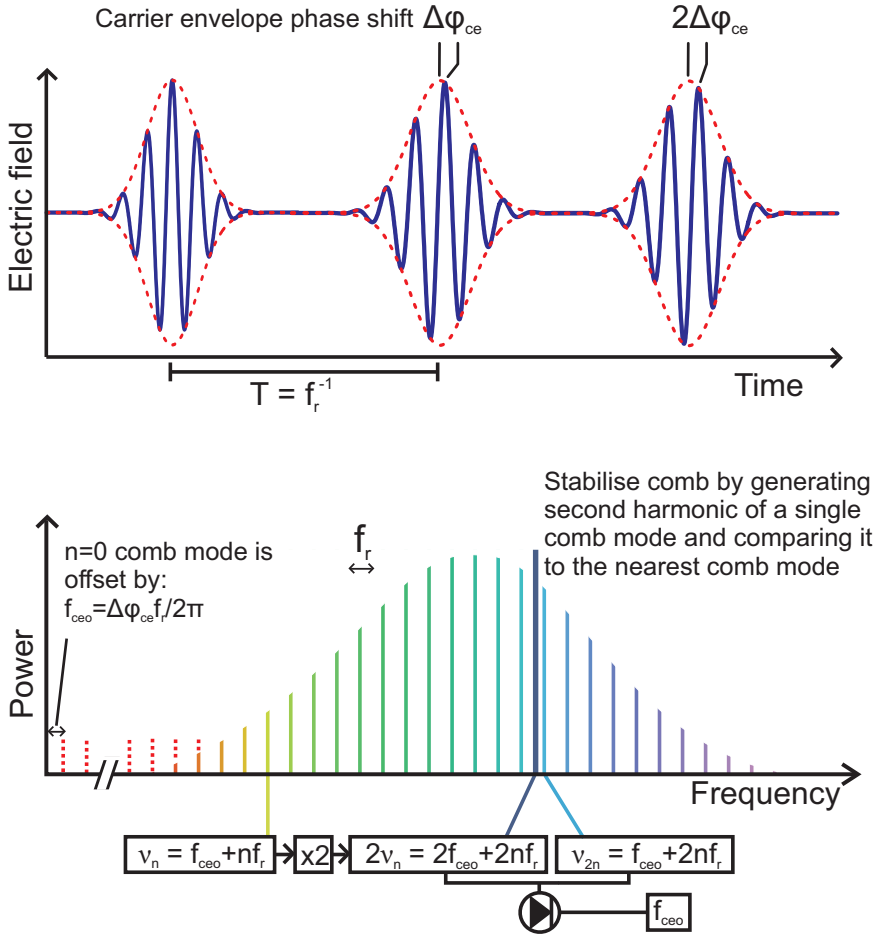

FIGURE 2.1: Output of a mode-locked laser frequency comb in the temporal (top) and frequency (bottom) domains.

With the repetition rate stabilised, the OFC still has one degree of freedom in the CEO frequency. Variations in f_{ceo} causes the entire OFC to be translated in frequency, i.e. shift the spectrum left/right. The CEO frequency is less straightforward to stabilise than f_r since it cannot be measured directly using a photodetector. This is another reason why mode-locked laser OFCs were slow to be adopted by the metrology community. It was the advent of supercontinuum generation in microstructured optical fibres [7] which enabled f_{ceo} to be measured and stabilised. One of the measurement techniques that was opened up was f-2f interferometry [8, 9]. This is a self-referencing technique where the second harmonic of the n^{th} comb mode $(2 \times \nu_n)$ is generated and combined with the $2n^{th}$ comb mode, with frequency ν_{2n} on a photodetector. The heterodyne beating between these two signals will occur at f_{ceo}, as shown in Figure 2.1. Microstructured fibres are necessary for very wide spectral broadening because it is difficult for mode-locked lasers to generate a comb which spans the required octave [10].

Similar to f_r, the measurement of f_{ceo} allows it to be phase locked to a high quality reference. f_{ceo} can be controlled by varying the dispersion inside the laser cavity. One way which the feedback can be implemented is by placing prisms inside the laser cavity

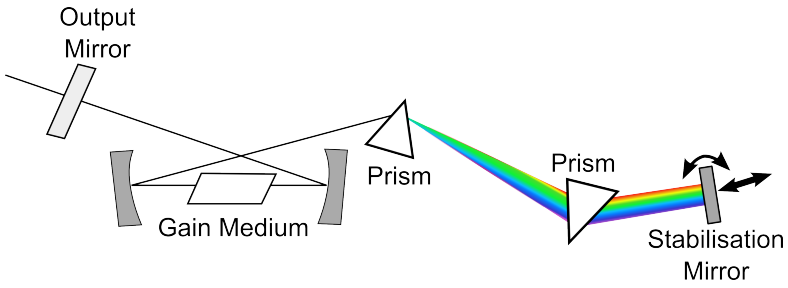

FIGURE 2.2: An example of comb mode stabilisation inside a mode-locked laser. Translating the stabilisation mirror adjusts f_r, tilting it adjusts f_{ceo}.

and controlling the tilt of one of the mirrors. This provides a linear phase shift with frequency (a group delay), which in turn changes $\Delta\phi_{ce}$ [9]. The tilt required is very small (10^{-4} rad) and the misalignment caused is considered negligible. Alternatively, the nonlinear Kerr effect can be utilised by controlling the pump power, which in turn controls the total intensity in the medium [5, 10]. The nonlinear refractive index is dependent on wavelength [11] and hence by changing the intensity it effectively changes the material dispersion, which changes $\Delta\phi_{ce}$ [12].

With f_{ceo} phase locked using f-2f interferometry, the OFC is said to be self-referenced. If both f_{ceo} and f_r are locked to an RF reference, e.g. an atomic clock, then from Equation (2.3), the frequency of every mode is known to the same accuracy as the reference. Alternatively, f_{ceo} can be stabilised by phase locking one of the comb modes to an optical reference.

Range of repetition rates

The most common form of mode-locked OFCs are fibre or titanium-sapphire (Ti:sapphire) based. Fibre based systems have proved particularly popular due to their robustness and convenient operating wavelengths (1.5 μm for erbium- and 1.0 μm for ytterbium-based systems). However, since they require moderate lengths of fibre for sufficient gain, their repetition rates are generally restricted to $\leq$ 250 MHz. The higher gain available in Ti:sapphire allows cavity lengths to be shorter and have been demonstrated to operate with f_r as high as 10 GHz [13]. However, in general, most Ti-sapphire OFCs operate with $f_r \leq 1$ GHz.

2.1.2 Electro-optic modulator based frequency combs

Externally generated OFCs refer to those which are not generated inside a laser cavity. Instead, the OFC is generated by modulating the output of a high quality, single frequency cw laser. The repetition rate is limited by the modulator bandwidth and hence can be significantly higher than passively mode-locked lasers. Wide spaced combs

(> 1 GHz) are generally a requirement for applications in optical communications, RF photonics, and optical arbitrary waveform generation. In these applications, comb modes need to be processed individually and the wider comb spacing allow for easier separation of modes, e.g. using gratings. It is primarily for this reason that these applications have traditionally favoured externally generated OFCs.

Electro-optic modulators (EOMs) are the most commonly used modulators for OFC generation because of their high bandwidth. The electro-optic effect is a change in a material's refractive index due to a change in the electric field across the material. Materials which are transparent and exhibit the linear electro-optic effect, the Pockels effect, are particularity useful for building modulators. An electric field can be applied across the material, e.g. in the form of an RF signal, which modulates the refractive index with time. An optical signal travelling through the material will experience this modulated refractive index which results in the output being phase modulated. While electro-optic effects are very fast, the speed of EOMs are limited by electrical capacitive effects of the material [14].

EOMs may be used directly as a phase modulator or set up in a Mach-Zehnder configuration for amplitude modulation to generate of the OFC. In these configurations, the number of sidebands generated (comb modes) is quite limited. One way to increase the number of comb modes is to embed the modulator inside a cavity which is resonant with the seed laser and has free spectral range that is a sub-harmonic of the modulation frequency (Figure 2.3). The resonant cavity leads to a cascade effect where the generated sidebands remain within the cavity, pass through the modulator again and generate more sidebands, increasing the spectral width of the OFC [15, 16]. An amplifier may also be placed inside the cavity to compensate for any loss within the cavity to maximise the effect of the modulator and further increase the number of modes generated [17]. In these cases, a ring cavity is usually used to prevent interactions between counter-propagating signals.

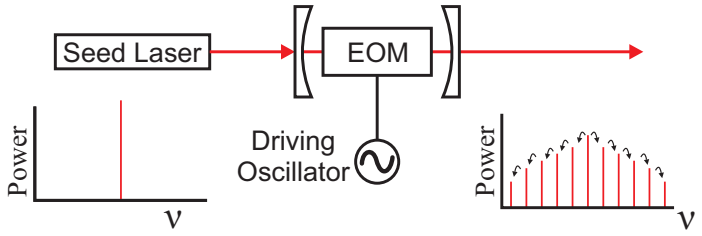

FIGURE 2.3: A double resonant EOM and cavity OFC generator. The resonant cavity allows the EOM generated sidebands to remain in the cavity and hence create more sidebands.

In the applications mentioned above, comb modes with the same optical power, i.e. a flat comb, are desired because they are easier to process. In these cases, it is advantageous to generate the OFC using multiple modulators [18]. Additional modulators allow more tuning of the shape of the OFC spectrum by changing the phase and amplitude of the

RF drive signal, and the DC bias of each modulator [19]. It has also been shown that tailored RF waveforms can be used to manipulate the shape of the OFC and has been used to generate very flat combs with < 1 dB power variation across 38 comb modes [20]. An advantage of using multiple modulators, rather than a resonant cavity, is the freedom of using any modulation frequency since there is no restriction imposed by the cavity.

Externally generated OFCs can still be described using f_r and f_{ceo} (Equation (2.3)) despite the carrier-envelope phase not being relevant. Since the entire OFC is generated with respect to the seed laser, the OFC spectrum can be shifted in frequency simply by changing the operating frequency of the seed laser. The equivalent f_{ceo} stability is dependent entirely on the frequency stability of the seed laser. In principle, it is possible to stabilise the OFC using f-2f interferometry. However, in practice this is difficult because the spectrum generated is typically much narrower than that generated by a mode-locked laser and therefore requires very wide spectral broadening. It is possible to phase lock the seed laser to a metrology grade optical reference for ultra-high stability. However, commercially available high stability lasers are generally sufficient for the above mentioned applications. The stability of f_r is dependent only the stability of the RF driver and hence active stabilisation of f_r is generally not required.

2.1.3 Microresonator based frequency combs

Nonlinear effects may also be utilised for externally generated OFCs using a cw laser. These nonlinear effects are generally very weak for cw lasers since their intensities are relatively low as compared to the peak intensity of pulsed lasers. Micrometre scale optical resonators (microresonators) can greatly enhance nonlinear interactions by trapping light inside very small volumes. The strong confinement increases the interaction length and the small volume increases the optical intensity. Whispering gallery mode microresonators, e.g. microspheres, microtoroids, and microdisks, confine light around the perimeter of the air-dielectric interface and can have Q factors $\geq 10^8$ [21, 22].

The use of microresonators for OFC generation is a recent development with the first demonstration in 2007 [23]. OFC generation can occur by coupling a cw laser with a resonant optical frequency into a microresonator. Degenerate four-wave mixing (FWM) then occurs where two pump photons (from the cw laser) are annihilated to generate a signal and an idler photon at higher and lower frequencies. Conservation of energy dictates that the frequency difference between the two generated photons and the pump photons are equal. Signal and idler photons with frequencies equal to the resonator modes are favoured and hence strong sidebands are generated at these frequencies. Non-degenerate FWM can then occur between the generated idler or signal with the original pump. These become two new pumps, but at different frequencies (i.e. non-degenerate) to generate a new idler/signal pair with the same frequency spacing as the pumps.

This continues in a cascade effect to generate more idler/signal pairs, all with the same frequency spacing hence giving rise to an OFC [22, 23], as shown in Figure 2.4.

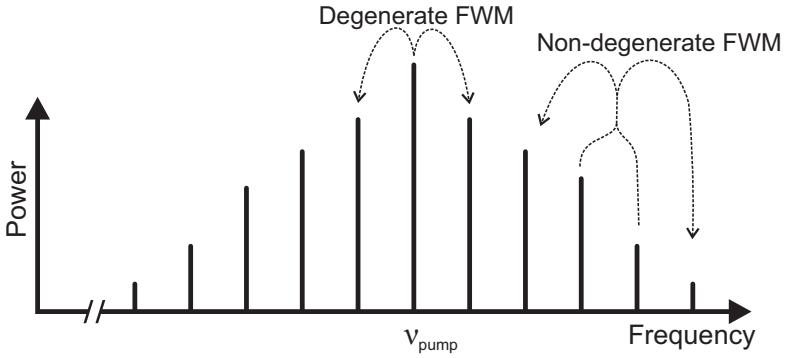

FIGURE 2.4: OFC generation using cascaded FWM in microresonators. Degenerate FWM generates the comb modes closest to the pump. Non-degenerate FWM generates further combs modes while maintaining the same frequency spacing.

It should be noted that other FWM processes can occur, namely the original pump can also generate other symmetric idler/signal pairs which match other resonator modes. Similarly, the generated signal or idler could be used as a single pump for degenerate FWM. Both of these processes are however very weak relative to the cascaded non-degenerate FWM and hence are suppressed. This is fortunate since both these processes would generate frequencies equal to the resonator modes which, due to material dispersion, would not be equidistant. The increasing mismatch between the OFC and the resonator modes as more comb modes are generated is one of the main factors limiting the bandwidth of the OFC. The transparency bandwidth of the material is another limiting factor. Equidistant mode spacing of microresonator OFCs has been confirmed to an accuracy of 7.3×10^{-18} [23].

The very short cavity lengths in microresonators allow for very wide comb spacings. Comb spacings using microresonators have ranged from as low as 13 GHz with a microresonator radius of 4 mm [24], up to 850 GHz using a microresonator with a radius of 40 μm [25]. Microresonator OFCs can also be generated with very wide bandwidths, with octave spanning bandwidths demonstrated directly at the output of the microresonator [25].

Stabilisation of microresonator OFCs is more difficult than with mode-locked lasers or EOM-based OFCs because of the very small dimensions of the microresonator which enhances thermally induced noise. For example, temperature fluctuations can cause noise in f_r via thermal-expansion of the microresonator and a thermal change in refractive index. The comb spacing dependence on temperature has been used for active stabilisation by feeding back onto the pump power which in turn adjusts the temperature of the microresonator [26]. However, the performance was relatively poor, with frequency drifts over four orders of magnitude worse than that which is possible with mode-locked

laser OFCs. Similar to EOM-based OFCs, the stability of f_{ceo} is dependent on the stability of the seed laser. If the overall noise can be sufficiently reduced, then the ability for microresonators to directly generate octave spanning OFCs brings the possibility for f-2f stabilisation of f_{ceo}.

Similar to EOM-based OFCs, the high comb spacings which are achievable with microresonators is beneficial for applications which requires comb modes to be processed individually such as for telecommunications, astronomical spectrograph calibration, and arbitrary waveform generation. Microresonator OFCs can generate a much wider bandwidth OFC compared to those using EOMs, but at the cost of additional noise. An exciting prospect of microresonator OFCs is the possibility of planar integration onto a single chip device. Many of the aforementioned applications can therefore be envisioned as very compact and portable devices.

2.2 Optical Phase Locking Techniques

The very beginning of this thesis introduced the basic concept of phase locking and Section 1.3 briefly discussed the motivation behind using optical phase locking to extract individual comb modes. To summarise: optical phase locking refers to getting a laser (the 'slave laser') to emit at a frequency which is fixed with respect to that of another laser (the 'master laser'). Phase locking is useful for improving the quality of lasers, in terms of frequency and phase noise, by locking them to higher quality master lasers. This is especially true for semiconductor lasers that have the key advantage of being low cost, but suffer from poor frequency and phase noise performance. This section will discuss three of these techniques: optical phase lock loops, optical injection locking, and a technique using a combination of the two.

2.2.1 Optical phase lock loop

A phase lock loop (PLL) is a feedback system to keep two oscillators synchronised by measuring their relative phase and actively adjusting it. It is commonly used in electronics to keep RF and microwave oscillators locked [27, 28]. An electronic PLL consists of three basic components: a phase detector, a loop filter, and a voltage controlled oscillator (VCO) as shown in Figure 2.5(a). For an analogue electronic PLL, the VCO is the slave oscillator which generates a signal with a frequency close to the master oscillator. A frequency mixer can be used as a phase detector to measure the relative phase between the master and slave signals. This phase difference is the error signal for the feedback loop and is fed into the loop filter. The loop filter processes the error signal and produces a control signal which is fed back into the VCO to compensate for the phase difference. The most basic loop filter is a low-pass filter to suppress any noise in the system, as well as the high frequency components generated by the phase detector.

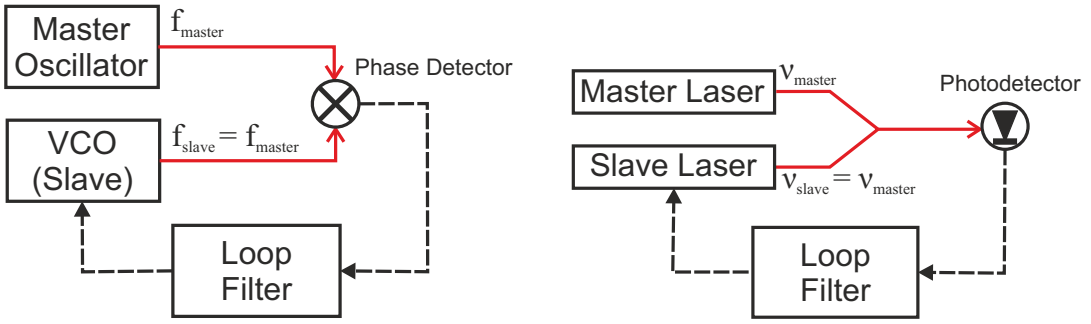

(a) PLL (b) OPLL

FIGURE 2.5: Conceptual schematics of a basic PLL and OPLL in homodyne configurations

An optical phase lock loop (OPLL) operates using the same basic principle but using optical equivalent components, as shown in Figure 2.5(b). A slave laser (optical oscillator) is used in the place of a VCO. Semiconductor lasers resemble VCOs the closest since their operating frequencies can be directly modulated by adjusting the drive current, i.e. they are current controlled oscillators [29]. Other lasers may require voltage controlled cavity length adjustment to emulate a VCO, e.g. using piezoelectric movement of a cavity mirror [30]. A photodetector may be used as a phase detector by measuring the interference between the slave and master lasers. A loop filter plays the same role of converting the measured phase signal into a control signal to be fed back into the slave laser.

OPLLs and electronic PLLs can be operated in either homodyne or heterodyne configurations. Figure 2.5 shows homodyne configurations where the slave oscillators are set to lock to the *same* frequency as the master oscillators. A heterodyne configuration is employed to lock the slave oscillator to a fixed *offset* frequency with respect to the master oscillator, as shown in Figure 2.6. This is achieved by measuring the beat signal between the two lasers, which corresponds to their frequency difference. The phase of this beat signal is then measured with respect to a reference RF oscillator to generate the error signal which is fed into the loop filter.

Heterodyne OPLL configurations add a degree of complexity to the set-up due to the additional components required as compared to homodyne configurations. They are also reliant on a high quality reference oscillator to achieve low noise performance. However, they are less susceptible to noise being generated due to power fluctuations in the master or slave oscillators. This is because in homodyne OPLL systems, the output of the photodetector is directly used as an error signal, which fluctuates with any power fluctuations of the input signals. The subsequent phase detector (RF mixer) used in heterodyne configurations only become sensitive to these power fluctuations if they are large.

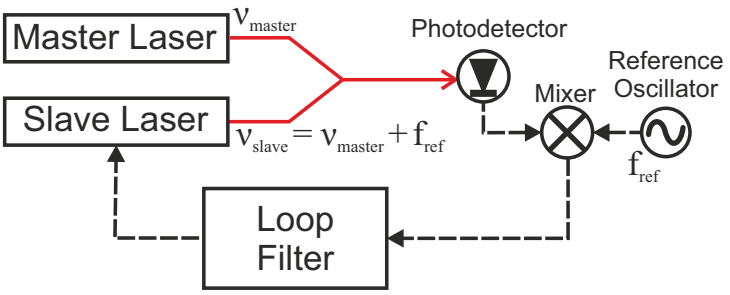

FIGURE 2.6: A conceptual schematic for heterodyne OPLL

The loop bandwidth of an OPLL is the bandwidth of the slave laser phase noise which the OPLL can compensate for. Since the phase noise of a laser is related to the laser linewidth, the bandwidth of an OPLL imposes a restriction that the slave laser must be below a certain linewidth for the OPLL to function correctly [31, 32]. This restriction makes it difficult to use semiconductor lasers as slave lasers since they traditionally have linewidths ($\geq$ 1 MHz) which exceeds typical loop bandwidths. Semiconductor lasers would otherwise be excellent candidates for OPLLs since their phase and frequency can be directly tuned by varying their drive current, they can operate over a broad range of wavelengths, and they are low cost.

The loop bandwidth is dependent on the detector bandwidth, loop delay, and frequency response of the loop filter, which is usually described by the filter cut-off frequency. The loop delay is given by the finite amount of time required for the OPLL to compensate the phase error after making the phase measurement. Loop delays can be reduced by minimising the propagation distances of signals and using miniaturised components [33]. Further reduction in loop delays can be achieved by using photonic integrated circuits, where the electronic and optical components, including the laser itself, are all integrated together onto a single chip. An OPLL photonic integrated circuit has been demonstrated [34] with an open loop bandwidth of over 1 GHz, and a loop delay of less than 1.8 ns. This was able to phase lock a 1.1 MHz linewidth laser with very low additional noise.

2.2.2 Optical injection locking

General OIL

Injection locking is the coupling of oscillators due to the transmission of oscillations from the master to the slave. This can occur in mechanical [35], electronic [36], microwave [37], and optical [38] oscillators. A conceptual diagram of optical injection locking (OIL) is shown in Figure 2.7.

Optical injection locking will only occur if the difference between the frequencies of the maser and slave lasers are within a certain bandwidth known as the locking range, $\Delta\omega_L$,

FIGURE 2.7: Optical injection locking: two lasers emitting at different frequencies (a) can be synchronised by injecting the signal from one laser into the other (b).

given by [38]

$$\Delta\omega_L = 2\gamma_e\sqrt{\frac{P_S}{P_M}}\,, \tag{2.4}$$

where γ_e is the loss rate of the slave laser due to external coupling. The detuning, $\Delta\omega = \omega_S - \omega_M$, is defined as the difference between the angular frequencies of the free running slave (ω_S) and the master (ω_M) lasers. ${}^{P_S}/_{P_M}$ is the injection ratio where P_M and P_S are the optical powers of the injected master signal and the free running slave laser respectively. The size of the locking range can therefore be controlled by varying the power of the injected signal.

If the detuning is outside the locking range ($|\Delta\omega| > \frac{1}{2}\Delta\omega_L$), then the slave laser will not lock to the master. However, the injected signal will cause a shift in the frequency of the slave laser towards the injected frequency. This frequency pulling effect becomes stronger as the injected signal approaches the locking range of the slave laser. At the edge and inside the locking range, the two frequencies will be equal which corresponds to OIL.

Although the slave laser emits at the same frequency as the injected master laser, it does experience a phase shift relative to the injected signal while in the injection locked state. This is due to the mismatch between the cavity length and operating frequency of the slave laser. This phase shift is dependent on the detuning within the locking range and is given by [38]

$$\Delta\phi_L = \sin^{-1}\left(\frac{2\Delta\omega}{\Delta\omega_L}\right). \tag{2.5}$$

Since OIL locks the frequency of the slave laser to the same frequency as the master laser, it can only be used for homodyne locking. However, heterodyne-like operation can be implemented by first frequency shifting the injected signal, e.g. by using an acousto-optic modulator.

Semiconductor OIL

OIL of semiconductor lasers was first demonstrated in 1980 by Kobayashi et al. [39] and it was found to suppress spurious modes of the laser. Similar to the general OIL, the

output will be at the same frequency as the master but with a phase shift. However, differences arise within the locking range relating to asymmetries and instability due to the strong dependence of the refractive index within the laser on the carrier density [40].

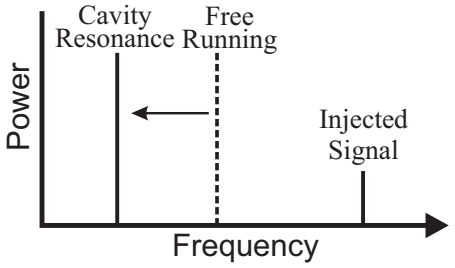

FIGURE 2.8: In a semiconductor laser, the cavity resonance frequency changes from the free running frequency due to the injection induced refractive index change.

As light is injected into the semiconductor laser, it will be regeneratively amplified by the gain medium. The amplification of this additional signal in the laser decreases the carrier density. This then increases the refractive index of the active medium, which in turn decreases the cavity resonance frequency (Figure 2.8). This can be thought of as the injected light changing the 'natural' frequency of the semiconductor laser. The optimum (zero phase shift) locking now occurs when the injected frequency matches this red-shifted resonance frequency [40], which is no longer at $\Delta\omega = 0$. The linewidth enhancement factor (α), which describes the coupling between the amplitude and phase of a semiconductor laser, is proportional to the change in refractive index with carrier density. Therefore, α can be incorporated into Equations (2.5) and (2.4) to describe the locking bandwidth and phase shift for OIL of semiconductor lasers [41]:

$$\Delta\omega_L = 2\gamma_e \sqrt{\frac{P_S}{P_M}} \sqrt{1+\alpha^2} \ , \tag{2.6}$$

$$\Delta\phi_L = \sin^{-1}\left(\frac{2\Delta\omega}{\Delta\omega_L}\right) - \tan^{-1}(\alpha) \ . \tag{2.7}$$

These equations show that the change in carrier density introduces an offset for the phase shift and increases the locking range. However, instabilities of the injection locked semiconductor laser can occur. Pulsations of the slave laser output have been observed [40, 41] where the output is unable to remain constant. This was caused by relaxation oscillations of the slave laser which can either grow or dampen depending on the carrier density i.e. the detuning [42]. The locking range can therefore be divided into stable and unstable regions, with the size of each dependent on the injection ratio [32, 43]. The locking range is unconditionally stable at low injection ratios due to the small changes in carrier density.

Many applications for OIL have been demonstrated. OIL can be used to force a semiconductor Fabry-Pérot laser to operate at different longitudinal modes by injecting light from a master laser with the corresponding wavelength [44]. This mode selection was also

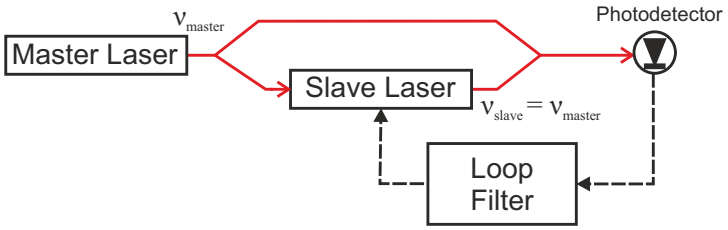

FIGURE 2.9: A conceptual schematic for an OIPLL system

found to suppress the other longitudinal modes, reducing the mode partition noise [45]. OIL can enhance the modulation properties of semiconductor lasers for use in telecommunications applications by changing the frequency and damping of the laser's relaxation oscillations [46]. This occurs because of the amplitude-phase coupling between the slave laser and the injected field (Figure 2.8), which also affects the carrier dynamics and changes the relaxation dynamics of the laser. OIL can also be used as a high-gain amplifier where a slave laser is locked to a comparatively weak signal. Since the slave laser emits at a higher power than the injected signal, it is effectively amplifying the signal [47].

2.2.3 Optical injection phase lock loop – a hybrid technique

OIL has a locking range which is dependent on the injection ratio. While the size of this locking range is limited by instability, it can still be significantly larger than the bandwidth of conventional OPLLs. However, any long-term frequency drifts of the slave and/or master laser can allow the detuning to drift outside the locking range and cause the system to unlock. In contrast to this, OPLL systems can track these slow changes but are unable to track any fast variations due to their limited bandwidth.

A combined optical injection locking and phase locked loop (OIPLL) system was proposed by Ramos et al. [48] which would have the robust locking properties of an OIL system but would also be able to track slow long-term changes using an OPLL. An OIPLL is conceptially shown in Figure 2.9. In the frequency domain, this can be thought of as the OPLL compensating for low frequency noise while the OIL reduces the noise up to the edge of the locking range. Beyond the locking range, the phase noise of the slave laser matches its free running performance [48]. Subsequent demonstrations [49] and analysis [32] of OIPLL systems found that the combined system had an improved performance in terms of phase noise over either an OIL or OPLL system on its own.

2.3 References

[1] E. Ippen, "Principles of passive mode locking," *Applied Physics B-Lasers and Optics*, vol. 170, no. 3, pp. 159–170, 1994.

[2] M. Fermann, M. Andrejco, Y. Silberberg, and M. Stock, "Passive mode locking by using nonlinear polarization evolution in a polarization-maintaining erbium-doped fiber," *Optics Letters*, vol. 18, no. 11, pp. 894–896, 1993.

[3] M. Hofer, M. E. Fermann, F. Haberl, M. H. Ober, and A. J. Schmidt, "Mode locking with cross-phase and self-phase modulation," *Optics Letters*, vol. 16, no. 7, pp. 502–504, 1991.

[4] U. Morgner, F. X. Kärtner, S. H. Cho, Y. Chen, H. A. Haus, J. G. Fujimoto, E. P. Ippen, V. Scheuer, G. Angelow, and T. Tschudi, "Sub-two-cycle pulses from a Kerr-lens mode-locked Ti:sapphire laser," *Optics Letters*, vol. 24, no. 6, pp. 411–413, 1999.

[5] J. Ye and S. T. Cundiff, *Femtosecond optical frequency comb: principle, operation, and applications*. Kluwer Academic Publishers/Springer, 2005.

[6] T. Udem, J. Reichert, R. Holzwarth, and T. W. Hänsch, "Accurate measurement of large optical frequency differences with a mode-locked laser," *Optics Letters*, vol. 24, no. 13, pp. 881–883, 1999.

[7] J. K. Ranka, R. S. Windeler, and A. J. Stentz, "Visible continuum generation in air-silica microstructure optical fibers with anomalous dispersion at 800 nm," *Optics Letters*, vol. 25, no. 1, pp. 25–27, 2000.

[8] H. R. Telle, G. Steinmeyer, A. E. Dunlop, J. Stenger, D. H. Sutter, and U. Keller, "Carrier-envelope offset phase control: A novel concept for absolute optical frequency measurement and ultrashort pulse generation," *Applied Physics B-Lasers and Optics*, vol. 69, no. 4, pp. 327–332, 1999.

[9] D. J. Jones, S. A. Diddams, J. K. Ranka, A. Stentz, R. S. Windeler, J. L. Hall, and S. T. Cundiff, "Carrier-envelope phase control of femtosecond mode-locked lasers and direct optical frequency synthesis," *Science*, vol. 288, no. 5466, pp. 635–639, 2000.

[10] F. W. Helbing, G. Steinmayer, J. Stenger, H. R. Telle, and U. Keller, "Carrier-envelope-offset dynamics and stabilization of femtosecond pulses," *Applied Physics B-Lasers and Optics*, vol. 74, no. (supplementary), pp. S35–S42, 2002.

[11] R. Adair, L. L. Chase, and S. A. Payne, "Nonlinear refractive index of optical crystals," *Physical Review B*, vol. 39, no. 5, pp. 3337–3350, 1989.

[12] J. Stenger and H. R. Telle, "Intensity-induced mode shift in a femtosecond laser by a change in the nonlinear index of refraction," *Optics Letters*, vol. 25, no. 20, pp. 1553–1555, 2000.

[13] D. C. Heinecke, A. Bartels, and S. A. Diddams, "Offset frequency dynamics and phase noise properties of a self-referenced 10 GHz Ti:sapphire frequency comb," *Optics Express*, vol. 19, no. 19, pp. 18440–18451, 2011.

[14] B. Saleh and M. Teich, *Fundamentals of Photonics*. John Wiley & Sons, 1st ed., 1991.

[15] L. R. Brothers, D. Lee, and N. C. Wong, "Terahertz optical frequency comb generation and phase locking of an optical parametric oscillator at 665 GHz," *Optics Letters*, vol. 19, no. 4, pp. 245–247, 1994.

[16] M. Kourogi, T. Enami, and M. Ohtsu, "A monolithic optical frequency comb generator," *IEEE Photonics Technology Letters*, vol. 6, no. 2, pp. 214–217, 1994.

[17] K. P. Ho and J. M. Kahn, "Optical frequency comb generator using phase modulation in amplified circulating loop," *IEEE Photonics Technology Letters*, vol. 5, no. 6, pp. 721–725, 1993.

[18] A. D. Ellis and F. C. G. Gunning, "Spectral density enhancement using coherent WDM," *IEEE Photonics Technology Letters*, vol. 17, no. 2, pp. 504–506, 2005.

[19] T. Healy, F. C. G. Gunning, and A. D. Ellis, "Multi-wavelength source using low drive-voltage amplitude modulators for optical communications," *Optics Express*, vol. 15, no. 6, pp. 2981–2986, 2007.

[20] R. Wu, V. R. Supradeepa, C. M. Long, D. E. Leaird, and A. M. Weiner, "Generation of very flat optical frequency combs from continuous-wave lasers using cascaded intensity and phase modulators driven by tailored radio frequency waveforms," *Optics Letters*, vol. 35, no. 19, pp. 3234–3236, 2010.

[21] V. Braginsky, M. Gorodetsky, and V. Ilchenko, "Quality-factor and nonlinear properties of optical whispering-gallery modes," *Physics Letters A*, vol. 137, no. 7, pp. 393–397, 1989.

[22] T. J. Kippenberg, R. Holzwarth, and S. A. Diddams, "Microresonator-Based Optical Frequency Combs," *Science*, vol. 332, no. 6029, pp. 555–559, 2011.

[23] P. Del'Haye, A. Schliesser, O. Arcizet, T. Wilken, R. Holzwarth, and T. J. Kippenberg, "Optical frequency comb generation from a monolithic microresonator," *Nature*, vol. 450, no. 7173, pp. 1214–1217, 2007.

[24] I. S. Grudinin, N. Yu, and L. Maleki, "Generation of optical frequency combs with a CaF2 resonator," *Optics Letters*, vol. 34, no. 7, pp. 878–880, 2009.

[25] P. Del'Haye, T. Herr, E. Gavartin, M. L. Gorodetsky, R. Holzwarth, and T. J. Kippenberg, "Octave spanning tunable frequency comb from a microresonator," *Physical Review Letters*, vol. 107, no. 6, p. 063901, 2011.

[26] P. Del'Haye, O. Arcizet, A. Schliesser, R. Holzwarth, and T. J. Kippenberg, "Full stabilization of a microresonator-based optical frequency comb," *Physical Review Letters*, vol. 101, no. 5, p. 53903, 2008.

[27] F. M. Gardner, *Phaselock Techniques*. John Wiley & Sons, 2nd ed., 1979.

[28] D. Abramovitch, "Phase-locked loops: A control centric tutorial," in *Proceedings of the American Control Conference*, (Anchorage, AK), pp. 1–15, 2002.

[29] R. C. Steele, "Optical Phase-Locked Loop Using Semiconductor Laser Diodes," *Electronics Letters*, vol. 19, no. 2, pp. 69–71, 1983.

[30] L. H. Enloe and J. L. Rodda, "Laser phase-locked loop," *Proceedings of the IEEE*, vol. 53, no. 2, pp. 165–166, 1965.

[31] R. T. Ramos and A. J. Seeds, "Delay, linewidth and bandwidth limitations in optical phase-locked loop design," *Electronics Letters*, vol. 26, no. 6, pp. 389–391, 1990.

[32] A. C. Bordonalli, C. Walton, and A. J. Seeds, "High-performance phase locking of wide linewidth semiconductor lasers by combined use of optical injection locking and optical phase-lock loop," *Journal of Lightwave Technology*, vol. 17, no. 2, pp. 328–342, 1999.

[33] L. N. Langley, M. D. Elkin, C. Edge, M. J. Wale, U. Gliese, X. Huang, and A. J. Seeds, "Packaged semiconductor laser optical phase-locked loop (OPLL) for photonic generation, processing and transmission of microwave signals," *IEEE Transactions on Microwave Theory and Techniques*, vol. 47, no. 7, pp. 1257–1264, 1999.

[34] R. J. Steed, F. Pozzi, M. J. Fice, C. C. Renaud, D. C. Rogers, I. F. Lealman, D. G. Moodie, P. J. Cannard, C. Lynch, L. Johnston, M. J. Robertson, R. Cronin, L. Pavlovic, L. Naglic, M. Vidmar, and A. J. Seeds, "Monolithically integrated heterodyne optical phase-lock loop with RF XOR phase detector," *Optics Express*, vol. 19, no. 21, pp. 20048–20053, 2011.

[35] M. Bennett, M. F. Schatz, H. Rockwood, and K. Wiesenfeld, "Huygens's clocks," *Proceedings of the Royal Society of London A: Mathematical, Physical and Engineering Sciences*, vol. 458, no. 2019, pp. 563–579, 2002.

[36] B. van der Pol, "The nonlinear theory of electric oscillations," *Proceedings of the Institute of Radio Engineers*, vol. 22, no. 9, pp. 1051–1086, 1934.

[37] K. Kurokawa, "Injection locking of microwave solid-state oscillators," *Proceedings of the IEEE*, vol. 61, no. 10, pp. 1386–1410, 1973.

[38] A. E. Siegman, *Lasers*. Mill Valley, CA: University Science Books, 1986.

[39] S. Kobayashi and T. Kimura, "Coherence of injection phase-locked AlGaAs semiconductor laser," *Electronics Letters*, vol. 16, no. 17, pp. 668–670, 1980.

[40] R. Lang, "Injection locking properties of a semiconductor laser," *IEEE Journal of Quantum Electronics*, vol. 18, no. 6, pp. 976–983, 1982.

[41] F. Mogensen, H. Olesen, and G. Jacobsen, "Locking conditions and stability properties for a semiconductor laser with external light injection," *IEEE Journal of Quantum Electronics*, vol. 21, no. 7, pp. 784–793, 1985.

[42] C. H. Henry, N. A. Olsson, and N. K. Dutta, "Locking range and stability of injection locked 1.54 μm InGaAsP semiconductor lasers," *IEEE Journal of Quantum Electronics*, vol. 21, no. 8, pp. 1152–1156, 1985.

[43] R. Q. Hui, A. Dottavi, A. Mecozzi, and P. Spano, "Injection locking in distributed feedback semiconductor lasers," *IEEE Journal of Quantum Electronics*, vol. 27, no. 6, pp. 1688–1695, 1991.

[44] L. Goldberg, H. F. Taylor, and J. F. Weller, "Intermodal injection locking and gain profile measurement of GaAlAs lasers," *IEEE Journal of Quantum Electronics*, vol. 20, no. 11, pp. 1226–1229, 1984.

[45] K. Iwashita and K. Nakagawa, "Suppression of mode partition noise by laser diode light injection," *IEEE Journal of Quantum Electronics*, vol. 18, no. 10, pp. 1669–1674, 1982.

[46] E. K. Lau, L. J. Wong, and M. C. Wu, "Enhanced modulation characteristics of optical injection-locked lasers: a tutorial," *IEEE Journal of Selected Topics in Quantum Electronics*, vol. 15, no. 3, pp. 618–633, 2009.

[47] R. Slavík, F. Parmigiani, J. Kakande, C. Lundstrom, M. Sjodin, P. A. Andrekson, R. Weerasuriya, S. Sygletos, A. D. Ellis, L. Gruner-Nielsen, D. Jakobsen, S. Herstrom, R. Phelan, J. O'Gorman, A. Bogris, D. Syvridis, S. Dasgupta, P. Petropoulos, and D. J. Richardson, "All-optical phase and amplitude regenerator for next-generation telecommunications systems," *Nature Photonics*, vol. 4, no. 10, pp. 690–695, 2010.

[48] R. T. Ramos, P. Gallion, D. Erasme, A. J. Seeds, and A. Bordonalli, "Optical-injection locking and phase-lock loop combined systems," *Optics Letters*, vol. 19, no. 1, pp. 4–6, 1994.

[49] C. Walton, A. C. Bordonalli, and A. J. Seeds, "High-performance heterodyne optical injection phase-lock loop using wide linewidth semiconductor lasers," *IEEE Photonics Technology Letters*, vol. 10, no. 3, pp. 427–429, 1998.

Chapter 3

Locking to an Optical Frequency Comb

The previous chapters provided a detailed background on OFCs and the different phase locking techniques. This chapter will combine these two fields to demonstrate how optical phase locking, in particular an OIPLL, can be used to extract and amplify individual comb modes. Firstly, a brief history of phase locking to OFCs will be discussed. This will be followed by a demonstration of how I implemented an OIPLL to selectively amplify comb modes from a 250 MHz spaced mode-locked laser OFC.

3.1 Locking to an OFC – literature review

Although OFCs were not common during the 1980s, techniques to selectively phase lock lasers to multi-frequency lasers were pursued for various signal processing applications such as microwave photonics and frequency multiplexing. The earliest demonstration was in 1982 by Goldberg et al. [1] where a slave laser was injection locked to one of the sidebands of a directly modulated laser. This was followed up by locking two slave lasers to different sidebands of a common multi-frequency laser to generate a strong microwave signal at 10.5 GHz [2], showing an early demonstration of coherent combination using OIL. This technique was eventually used in 1998 for radio-over-fibre experiments where a microwave signal at 64 GHz with data encoded at 155 Mb/s, was optically transmitted over optical fibre [3].

It was around this time that OIPLL was beginning to be demonstrated as a locking technique with very low residual phase noise [4]. Similar to the case with OIL, two slave lasers were locked using OIPLL to the sidebands of a modulated master laser for photonic microwave generation at 36 GHz with low phase noise [5].

An early example of locking to an actual OFC for microwave generation was demonstrated in 2003 by Fukushima et al. [6]. In this case, the OFC was generated using an EOM-embedded resonant cavity, with a comb spacing of 17.5 GHz, and spanning a bandwidth of 1.8 THz. OIL was employed to lock two lasers to generate a microwave signal of 110 GHz, which was limited by the bandwidth of the photodiodes available to measure these signals. Locking to OFCs using OIPLLs was also demonstrated for optical frequency synthesis with high switching speeds [7] for telecommunication applications. By changing the driving current of the slave laser, it was made to lock to different modes of an 18 GHz spaced OFC with a 40 nm tuning range. The switching speed of < 10 ns was limited by the speed of the laser current controller.

Phase locking of cw lasers to frequency stabilised (f_r & f_{ceo}) mode-locked laser OFC was first pursued for spectroscopy applications to make use of the OFC as an accurate frequency ruler. An early demonstration of this was by Jost et al. [8] using an OPLL to lock a laser to a 100 MHz spaced self-referenced OFC. This employed a heterodyne configuration to allow the frequency of the locked laser to be continuously tunable.

OIL to a frequency stabilised mode-locked OFC with a repetition rate of 1.05 GHz was demonstrated by [9] using an injection ratio of approximately –50 dB. Their attempts to lock to a lower repetition rate (100 MHz) OFC were unsuccessful due to multiple modes being within the locking range. I believe that the relatively wide linewidth slave laser was limiting the minimum injection ratio possible for injection locking. OIL was also used to create a continuously tunable frequency synthesiser by locking to a 1 GHz OFC [10]. Since the slave laser locks to the same frequency as the comb mode it is locked to, f_r was changed to allow for continuous tuning.

Continued work was undertaken to achieve OIL to sub-GHz repetition rate OFCs. Ryu et al. [11] demonstrated direct OIL of a semiconductor laser to a 250 MHz repetition rate OFC. It was found that environmental fluctuations caused path length and polarisation fluctuations of the injected signal in the optical fibre. This would have resulted in a fluctuating locking range which caused unlocking. Passive fibre stabilisation using polystyrene casing was employed to maintain the locking for approximately one hour.

OIL for repetition rates of 100 MHz or less continued to be challenging with the only demonstrations reported requiring pre-filtering of the OFC [12]. This used a diffraction grating to first extract a 100 GHz bandwidth of the OFC (approximately 1000 adjacent comb modes) followed by an ultra-narrowband Fabry-Pérot filter (67 MHz passband) to suppress all but one comb mode. A slave laser could then easily injection lock to the unsuppressed comb mode using relatively high injection ratios. A similar set-up was later adapted into an OIPLL system [13]. The OPLL error signal was obtained by measuring the relative phase of the slave laser and the adjacent comb modes which were reflected by the laser. However, these modes were also within the locking range and

hence they also experienced injection locking, although at much smaller power levels due to their attenuated injected power. The phases of these adjacent modes were therefore also dependent on the OIL detuning (Equation 2.5) which prevented an RF mixer from being directly used as a phase detector. The phase of the slave laser was recovered using a dithering technique which enabled the OPLL part of the OIPLL to operate correctly and allowed the locking to be maintained for over 24 hours.

A recent study by Criado et al. [14] directly compared the performance of using the combination of a Fabry-Pérot filter and EDFAs with OIL to selectively amply an individual comb mode from a 10 GHz spaced OFC. It was found that, in terms of long-term frequency and power stability, OIL had superior performance. This was due to the precise electronic feedback required to keep the Fabry-Pérot filter aligned with the desired comb mode. The OSNR was also found to be higher for OIL due to the additional noise contribution from amplified spontaneous emission from the EDFAs.

3.2 My approach – principle and realisation

One of the major challenges of injection locking a laser to an OFC is to avoid locking to multiple comb modes. This occurs when the locking range of the slave laser is wide enough to encompass multiple comb modes injected into the laser. This can be overcome by using an OFC with a high repetition rate (e.g. in [5]), or by using narrowband prefiltering of the injected comb (e.g. in [12]). My approach uses low injection ratios such that the slave laser only locks to a single comb mode (Figure 3.1). The corresponding small locking range makes it difficult to keep the laser locked due to frequency drifts. This drifting occurs due to the limited stability of the laser temperature and current controllers. The implementation of an OIPLL allows the slow frequency drifts to be compensated and hence the injection locking can be maintained for long periods of time.

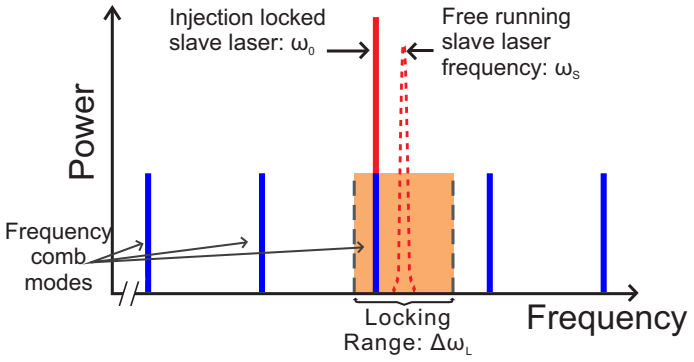

FIGURE 3.1: A slave laser can be injection locked to a single comb mode if it has a locking range which is smaller than the comb spacing.

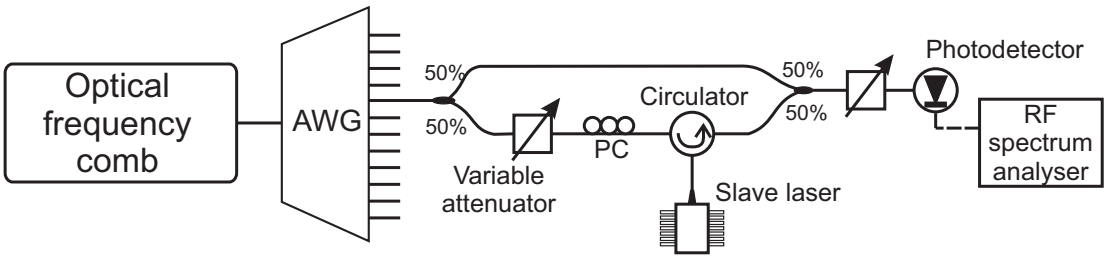

FIGURE 3.2: The set-up for measuring the beating between the slave laser and the injected master laser. PC: polarisation controller, AWG: arrayed waveguide grating

3.2.1 Demonstration of OIL to an OFC

All of the experiments presented in this thesis were conducted using a fibre mode-locked laser OFC (FC1500-250-WG, Menlo Systems GmbH) with a repetition rate of 250 MHz and a central wavelength of 1560 nm. The mode-locking mechanism was non-linear polarisation rotation. The repetition rate and carrier envelope offset frequency were stabilised to a quartz oscillator (TimeTech GmbH) which in turn was phase locked to a Global Position System (GPS) clock.

The slave lasers used were narrow linewidth (specified at < 200 kHz) discrete mode semiconductor lasers [15] from Eblana Photonics. These lasers were fibre pigtailed in a butterfly package, which was hermetically sealed with a thermo-electric cooler (TEC) for temperature tuning. The packaging did not include an optical isolator which allowed for optical injection from the front facet of the laser. The output power of these lasers in the pigtailed fibre varied from +3 to +12 dBm.

The OIL set-up is shown in Figure 3.2. Standard non-polarisation maintaining fiberised (SMF-28) telecommunications components were used in this set-up. The frequency comb was loosely filtered prior to injection using an arrayed waveguide grating (AWG) with a passband of 50 GHz and channel spacing of 100 GHz. The output channel of the AWG injected into the slave laser is shown in Figure 3.3(a) and contained over 200 adjacent comb modes. The AWG acted as a broadband filter and was used as a precaution to prevent any damage to the isolator-free laser and to avoid saturating the photodetector. A variable optical attenuator was used to control the injected power and hence the injection ratio, while a polarisation controller was used to align the injected signal with the slave laser. It should be noted that throughout this thesis, the injection ratio is defined as the power *per comb mode* (not the total power) injected into the slave laser divided by the output of the slave laser (+12 dBm in this case). For this experiment, the slave laser was operated using a combined current and temperature controller (ILX Lightwave LDC-3724B). A circulator was used to inject the signal into the slave laser via the front facet and to keep the slave laser output separate from the input. A list of component parameter is given in Table 3.1. The losses provided in Table 3.1 includes the connector losses, which was estimated to be 0.2 dB per connector.

TABLE 3.1: Component parameters for Figure 3.2

Component	Parameter	Value
AWG	Insertion loss (per channel)	3–5 dB
	Channel bandwidth (3 dB)	50 GHz
	Passband shape	Gaussian
	Connector type	FC/APC
	Fibre type	SMF-28
50/50 Coupler	Excess Loss	0.5 dB
	Connector type	FC/APC
	Fibre type	SMF-28
Variable attenuator	Excess Loss	1.5 dB
	Connector type	FC/APC
	Fibre type	SMF-28
Polarisation controller	Insertion loss	<0.5 dB
	Connector type	FC/APC
	Fibre type	SMF-28
Circulator	Insertion loss	1.1 dB
	Connector type	FC/APC
	Fibre type	SMF-28
Slave laser	Type	Discrete mode
	Output Power	+12 dBm
	Operating Current	129.83 mA
	Operating Temperature	26.73°C
	Connector type	FC/APC
	Fibre type	SMF-28
Photodetector	Bandwidth	800 MHz
	Responsivity	1.0 A/W
	Optical input type	FC

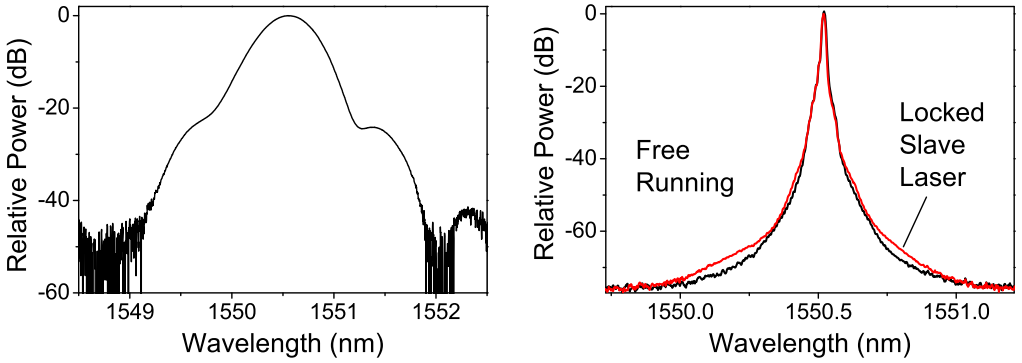

(a) Injected AWG channel

(b) Slave laser in the free running (no injected power) and injection locked (−60 dB injection ratio) states

FIGURE 3.3: The measured optical spectra of (a) an AWG output channel, and (b) the slave laser output. Resolution: 0.01 nm.

The spectrum of the slave laser output was measured with an optical spectrum analyser (OSA) and is shown in Figure 3.3(b) for the injection locked state and when there is no signal injected into the laser (free running). The injection locked state shows additional noise in the wings of the signal. This is due to the partial reflection of the residual comb modes injected into the slave laser, which is investigated further in Chapter 5. This

figure shows that the slave laser retains its free running OSNR of approximately 75 dB (resolution of 0.01 nm) when it is injection locked.

The limited resolution of the OSA prevented it from being used as a tool to confirm whether injection locking has actually taken place. The OIL process could be observed by combining the output of the slave laser with the original injected signal and generating a beat signal on a photodetector as shown in Figure 3.2. A variable optical attenuator was placed before the photodetector to ensure that the photodetector was not saturated. This beat signal was then monitored on an RF spectrum analyser. Narrow linewidth (less than the measurement resolution) RF signals were present at frequencies which were multiples of the repetition rate of the frequency comb (250, 500, 750 MHz etc.) due to the comb modes beating with one another. Figure 3.4 shows the RF spectra of when the slave laser was unlocked and when it was injection locked with an injection ratio of –60 dB. In the unlocked state (Figure 3.4(a)) there were also two relatively wide bandwidth signals between 0 and 250 MHz which correspond to the beating between the slave laser and the two nearest comb modes. These are repeated every 250 MHz corresponding to beating with comb modes located further away in the frequency domain.

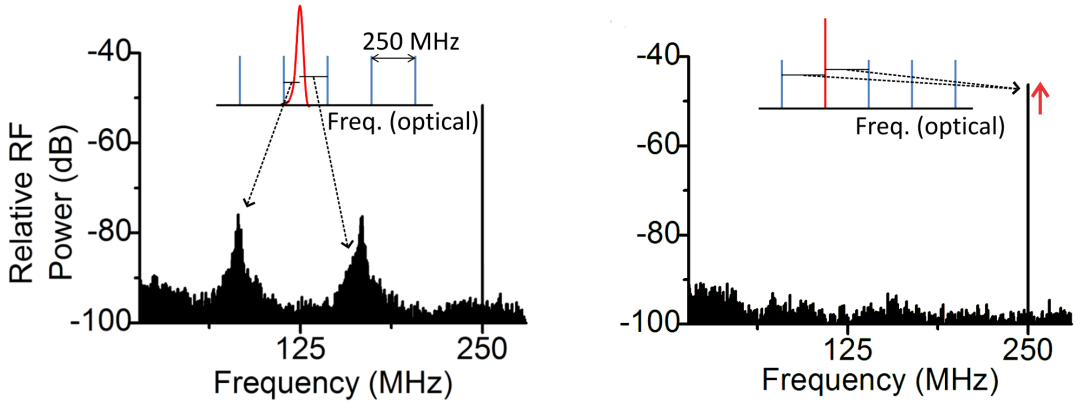

(a) Unlocked (b) Locked

FIGURE 3.4: The beating between the slave laser and the nearest comb modes in the unlocked and locked state. The insets are illustrations showing the origins of the RF beat signals in the optical frequency domain.

The beating signals between 0 – 250 MHz move in opposite directions as the slave laser frequency is tuned towards one of the adjacent comb modes. This continues until they are 'absorbed' by the 0 and 250 MHz beat signals, which corresponds to the injection locked state (Figure 3.4(b)). The 250 MHz signal also shows an increase in RF power which is due to the additional contribution from the locked slave laser. The linewidth of the 250 MHz component in the locked state was measured to be less than 1 Hz, the resolution of the spectrum analyser, which confirms that the frequency of the slave laser is matched with one of the comb modes. The ability to tune the slave laser into the locked and unlocked states shows that OIL to a single comb mode was achieved and that the locking range was smaller than the repetition rate of 250 MHz. With larger

injection ratios where the locking range was wider than the comb spacing, the unlocked state was not observed since the slave laser would always be locked to at least one of the modes.

Estimating the injection ratio

It is not straightforward to directly measure the power of each individual comb mode of the OFC used in these experiments. As a result, the injection ratio needed to be measured indirectly. The power per comb mode injected into the slave laser was estimated by measuring the optical power directly before the circulator used for injection. Since this was the output of an AWG channel, it contained approximately 200 (–23 dB) comb modes within a 3 dB bandwidth, as specified by the manufacturer. The circulator loss was considered to have 1 dB insertion loss. The coupling efficiency of the fibre pigtail of the laser was estimated to be 50% (–3 dB) [16]. From these factors, the power per comb mode injected into the slave laser was estimated to be:

$$P_M \approx \text{Total power at circulator input (dBm)} - (23 + 1 + 3)\ \text{dB}.$$

Similarly, the output power of the slave measured at the output of the circulator (with no injected power). The actual output of the slave laser also needs to account for the fibre coupling efficiency and circulator loss.

$$P_S \approx \text{Power at circulator output with no injection (dBm)} + (1 + 3)\ \text{dB}.$$

The injection ratio was therefore estimated to be the measured injection ratio, from the input and output of the circulator, minus 31 dB. This adjustment factor of –31 dB is used consistently throughout the experimental work in this thesis when quoting the injection ratio.

OIL stability

The locking process could only be maintained for tens of seconds as the slave laser was found to be jumping between a locked and unlocked state. The cause of this instability was traced down to the fibre between the slave laser and the circulator, which was sensitive to perturbations (e.g. tapping on the fibre). Since the laser had no isolator, this fibre behaved as an external cavity to the laser with the circulator behaving as an isolator. The external cavity may have been set up due to back-reflections from the FC/APC connectors or the circulator, which were specified as –60 and $<$ –50 dB respectively. This generates many closely spaced longitudinal cavity modes which the

slave laser can couple to. The longitudinal mode spacing of the fibre cavity, $\Delta\nu_{cavity}$, is given by

$$\Delta\nu_{cavity} = \frac{c}{2nL} \ , \tag{3.1}$$

where c is the vacuum speed of light, $n \approx 1.5$ is the refractive index of the fibre, and L is the fibre length. The fibre lengths of the laser and circulator pigtails were approximately 65 cm each, resulting in a cavity mode spacing of 83 MHz (for the total length of 1.3 m) as illustrated in Figure 3.5(a). The FC/APC connection between the fibre pigtails was found to affect the stability of the slave laser. When loss was introduced in the laser pigtail, by creating a small bend radius, the mode jumping occurred less often. In contrast, when the fibre loss was increased in the circulator pigtail, after the fibre connection, mode jumping did not become less frequent. This suggests that the main source of the back reflection was from the connector interface. It was later discovered from the circulator manufacturer test report that although the circulator back reflection was specified as $<$ –50 dB, the measured value was actually $<$ –60 dB, which was limited by their measurement set-up. This means that the back reflection from the circulator was either comparable or less than from the connector.

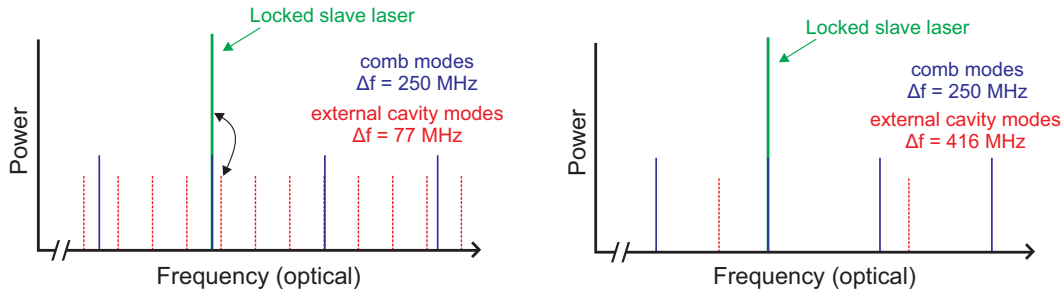

(a) Long cavity (b) Short cavity

FIGURE 3.5: Illustration of the lasing (green), external cavity (dashed, red) and injected comb (blue) modes of a slave laser for fibre lengths of (a) 130 cm, and (b) 24 cm.

This issue were addressed by fusion splicing the laser pigtail with the circulator pigtail. With a high quality splice, the back reflection from the splice are expected to be less than from the connector interface and hence the circulator was expected to produce the dominant back reflection. An exception to this may arise when dissimilar fibres are spliced together, e.g. a strong Fresnel reflection may occur for fibres with different core materials. However, as stated in Table 3.1, both fibres in this case were specified to be SMF-28.

Fusion splicing also allows the length of fibre to be significantly reduced. This would increase the spacing of the external cavity modes formed by parasitic back-reflection from the circulator, and hence reduce the likelihood of mode jumping (Figure 3.5(b)). For this demonstration, the fibre length was reduced to 24 cm (Figure 3.6), which increased the mode spacing to 416 MHz. Mode jumping was no longer observed after the fusion splicing

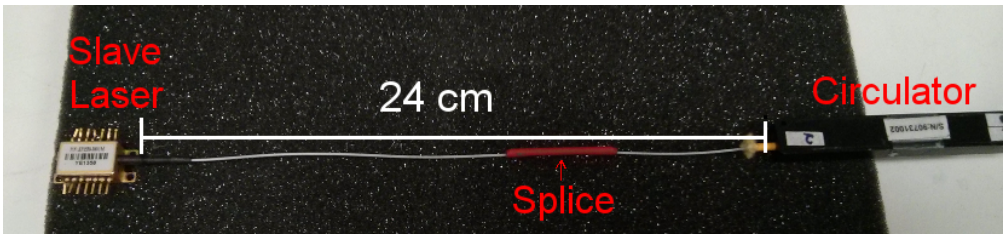

FIGURE 3.6: A photograph of a slave laser fusion spliced directly to a circulator

and the slave laser was able to maintain injection locking for up to 10 minutes. However, further investigation is required to truly understand the reason for this improvement.

3.2.2 OIPLL design

The previous section showed that it was possible to lock to an individual comb mode using OIL with low injection ratios. However, the locking could not be maintained indefinitely due to frequency variations in the slave laser, which occurred because of the limited stability of the laser controller. This caused the frequency detuning between the slave and master ($\Delta\omega$) to drift outside the locking range. To implement long-term locking, a feedback mechanism was needed to compensate for the frequency variations of the slave laser and keep the detuning between the free running slave laser and the master laser within the locking range.

The detuning could not be directly measured in the injection locked state since the slave laser does not emit at its free running frequency, but rather at the same frequency as the master. However, it is known from Equation (2.7) that the slave laser acquires a phase shift, $\Delta\phi_L$, which is dependent on $\Delta\omega$. An OIPLL is formed by measuring this phase shift and actively adjusting the free-running frequency of the slave laser to keep $\Delta\omega$ at a fixed value.

The OPLL required the phase of the slave laser to be measured relative to the original injected signal. In principle, this could be achieved by tapping off part of the master signal prior to injection and recombining it with the slave laser output, similar to that in Figure 3.2. However, this method is very sensitive to any path mismatch between the two arms which causes an additional phase shift [4]. Careful path matching would have been required to avoid this, and fluctuations in path lengths would have occurred in the optical fibre due to refractive index variations caused by acoustic pickup and thermal drift.

An alternative method which can be used with OFC master lasers is to measure the phase of the slave output with respect to the adjacent comb modes. This measurement can be made by measuring the beat signal between the slave output and the *reflected* comb modes from the slave laser cavity. An illustration of the output spectrum of the locked slave laser is shown in Figure 3.7. The residual comb modes (the ones not being

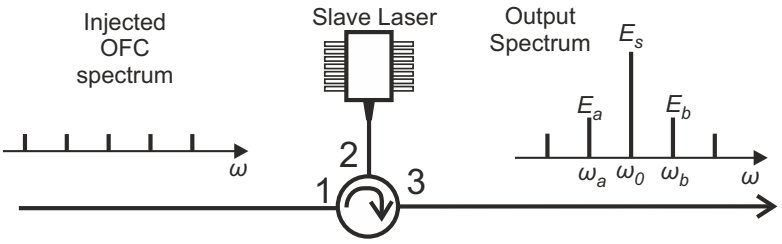

FIGURE 3.7: Illustration of OIL via the front facet using a circulator. A sufficiently narrow locking range results in injection locking to a single comb mode. Note: adjacent modes experience some gain from the laser medium.

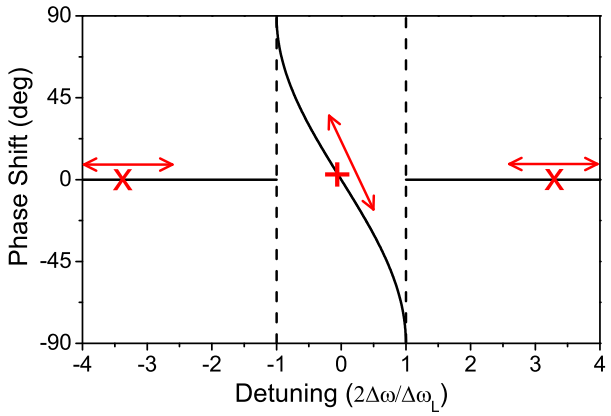

FIGURE 3.8: Illustration of OIL phase shift incurred by the locked mode (+) as a function of detuning. The adjacent comb modes (×) are outside the locking range and do not experience a phase shift. For simplicity, the α-factor was considered to be 0.

injection locked to) do not experience any phase shift with changes in $\Delta\omega$ (Figure 3.8). They do however experience some amplification due to travelling through the laser gain medium[1]. While these residual comb modes are undesirable in terms of slave laser spectral purity, they do allow a beat signal to be measured at the output of the slave laser. If only the locked output of the slave laser and the two adjacent comb modes (which experience the most residual amplification) are considered, the total electric field at a detector is given by

$$E_{tot} = E_a e^{i(\omega_a t - k_a L + \phi)} + E_S e^{i(\omega_0 t - k_0 L + \Delta\phi_L + \phi)} + E_b e^{i(\omega_b t - k_b L + \phi)} \ , \tag{3.2}$$

where E_j is the electric field amplitude, ω_j is the angular frequency, and $k_j L$ is the phase evolution due to propagation from the OFC to the detector (k_j is the wavenumber and L is the propagation length). The subscript $j = 0$ refers to the locked comb mode, E_S is the electric field amplitude of the slave laser output, and $j = a, b$ refer to the lower and higher frequency comb modes adjacent to the locked comb mode respectively. The initial phase, ϕ, of each mode is assumed to be the same for the three comb modes. This is true for OFCs which are generated by amplitude modulation of a cw laser and is also a reasonable assumption for mode-locked lasers (since the modes are closely

[1]This is investigated further in Chapter 5

spaced). Only the two nearest residual comb modes were considered in this analysis because the contribution from the other comb modes to the beat signal was assumed to be significantly smaller and negligible.

The optical power measured by the detector is given by $P_{tot} = E_{tot}E_{tot}^{*}$, where * denotes the complex conjugate. P_{tot} consists of a direct current (DC) component and time varying beat components. The RF beat signal given by the locked slave laser and the two adjacent combs modes is given by

$$P_{\Delta\Omega_r} = \cos\left(\Delta\Omega_r t + (k_0 - k_a)L - \Delta\phi_L\right) + \cos\left(\Delta\Omega_r t + (k_b - k_0)L + \Delta\phi_L\right) \ , \qquad (3.3)$$

where $\Delta\Omega_r = 2\pi f_r$ is the angular comb spacing. The amplitude of the beat signal has been normalised for simplicity, since it is phase which is of interest. Since the comb spacing of the OFC is only 250 MHz (approximately 2 pm in wavelength) and L is of the order of metres, we can consider dispersion to be negligible and that $(k_0 - k_a)L = (k_b - k_0)L = \psi$.

$P_{\Delta\Omega_r}$ can be isolated from the DC and higher frequency components of P_{tot} by using a suitable RF band-pass filter. An RF mixer[2] can be used to convert $P_{\Delta\Omega_r}$ to baseband using a local oscillator at the same frequency and with phase, θ, given by $\cos\left(\Delta\Omega_r + \theta\right)$. The baseband output, S, which can be isolated using a low-pass filter, is given by

$$S = \cos[\psi - \theta]\ \cos\left[\sin\left(2\Delta\omega/\Delta\omega_L\right) + \tan^{-1}(\alpha)\right] \ , \qquad (3.4)$$

where Equation (2.7) has been substituted for ϕ_L. S can be optimised by tuning the relative phases of the RF signals entering the mixer such that $|\cos(\psi - \theta)| = 1$. If $\tan^{-1}(\alpha) \approx \pi/2$, S is directly proportional to $\Delta\omega$ within the locking range, which would be an ideal error signal. This is not possible since α is finite; Figure 3.9 shows S as an error signal for different values of α. The slave lasers used here have an α-factor of approximately[3] 5, corresponding to $\tan^{-1}(\alpha) \approx 1.37$. S is therefore not perfectly linear (Figure 3.9), but is sufficiently close for use as a feedback error signal. It should be noted that for non-semiconductor lasers with α-factors of 0, this error signal would not be expected to be approximately linear.

Comparison of OIPLL with others

The first demonstration of an OIPLL using the common path adjacent comb modes to measure the slave laser phase was by Johansson and Seeds [5]. A significantly wider spaced OFC (12 GHz) was used in comparison to the one used in this thesis. The wider spacing relaxes the constraints on the maximum size of the locking range, but required higher speed RF components, such as mixers, amplifiers, and filters.

[2] A more detailed explanation of using a mixer as a phase detector is given in Section 4.1.3.
[3] This information was provided after discussions with the manufacturer

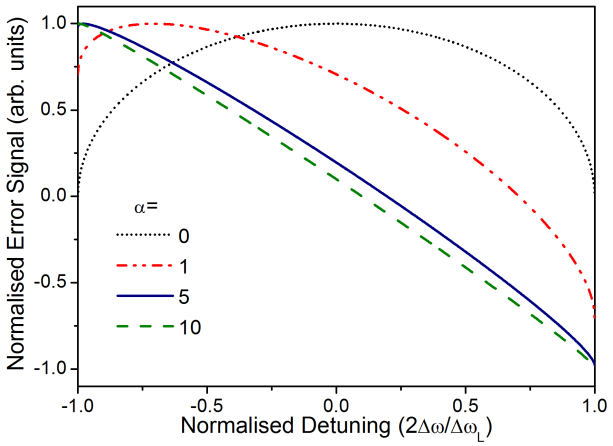

FIGURE 3.9: The error signal, S, given by Equation (3.4) for various values of α.

An OIPLL was also used by Kim et al. [13] to lock a laser to a low repetition rate OFC. Similar to my technique, their error signal was also based on the phase of the locked slave laser with respect to the residual adjacent comb modes. Their lower repetition rate (100 MHz) motivated them to pre-filter their OFC prior to injection locking using a narrowband Fabry-Pérot filter. This allowed them to use larger injection ratios with locking ranges that included the adjacent comb modes. These modes were attenuated by the filter which allowed the slave laser to lock to the strong unattenuated comb mode. However, their analysis showed that the adjacent comb modes still experienced an OIL phase shift. In order to generate a suitable error signal, they required their slave laser to be dithered.

In contrast, my technique does not require narrowband pre-filtering of the OFC. This is due to the wider comb spacing of the OFC used by a factor of 2.5. Also, by using low injection ratios, the residual comb modes in my technique do not lie within the slave laser locking range and hence do not experience the OIL phase shift (Figure 3.8). Dithering was therefore not required to generate a suitable feedback error signal. The lack of dithering and narrowband filtering significantly simplified the set-up.

3.2.3 Implementation of OIPLL

The implementation of the OIPLL described in the previous section is shown in Figure 3.10. The OIPLL significantly extended the time which the slave laser remained locked from a couple of minutes to hours (over 24 hours).

Injection locking

The injection locking portion of the set-up is the same as in Section 3.2.1. A fibre coupler was used to tap off 10% of the slave laser output for use in the feedback loop.

Slow electronic feedback

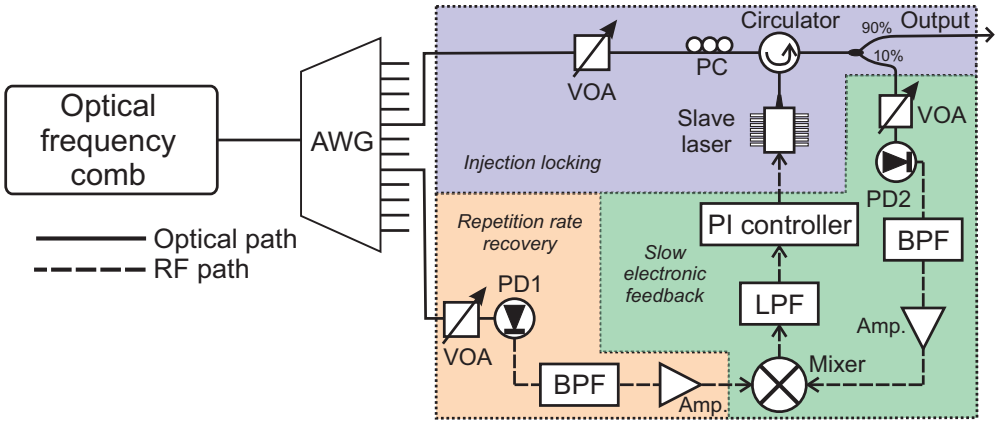

FIGURE 3.10: Schematic of the OIPLL. VOA: variable optical attenuator, PC: polarisation controller, PD: photodetector, BPF: band-pass filter, LPF: low-pass filter, PI: proportional-integral controller

The signal tapped off from the slave laser output was fed into a photodetector (PD2) to measure the beat signal between the locked mode and the adjacent residual comb modes. The beat signal at f_r was isolated from the DC signal and higher harmonics using RF band-pass filters (BPF) with a passband of 205–270 MHz. The filtered beat signal was very weak (electrical power: < -65 dBm) and was amplified using a cascade of three low-noise RF amplifiers (Mini-Circuits, ZFL-500LN+) with a total gain of approximately 72 dB such that the beat signal was larger than 0 dBm. This was then strong enough to be fed into an RF frequency mixer along with a local oscillator, which was derived directly from the OFC (repetition rate recovery). This was able to convert the beat signal to baseband, which was extracted from the higher harmonics using a low-pass filter. The low-pass filter (LPF) was a simple RC (resistor-capacitor) filter with a 3 dB cut-off frequency of 3.3 kHz.

The signal, S (Equation (3.4)), was then fed into a proportional-integral (PI) controller. This was the feedback controller which produced an output voltage which was proportional to the error signal, and also depended on the accumulated past errors (the integral). This feedback signal was then fed into the modulation port of the laser current driver, which changed the driving current and hence changed the free running frequency of the slave laser. In principle, the feedback could act on the laser temperature instead of driving current. This was not employed because frequency changes due to temperature are significantly slower than driving current.

It should be noted that the combination of the LPF and PI controller make up the *loop filter* discussed in the PLL theory in Section 2.2.

Repetition rate recovery

The RF mixer required a local oscillator signal with the same frequency as the beat signal to downconvert it to baseband. An RF synthesiser could be used for this, but would result in a noisy error signal due to the relative frequency noise between the beat

signal and synthesiser. A separate PLL would be required to lock the frequency of the synthesiser with the beat signal, which would increase the complexity of the set-up.

I implemented a simpler alternative where the local oscillator was generated by directly measuring the repetition rate of the OFC. This ensured that the local oscillator was always at the same frequency as the beat signal. One of the AWG ports, which was not used for OIL, was connected directly to a photodetector (PD1) which would measure relatively strong signals at f_r and its higher harmonics. The signal at f_r was isolated using a band-pass filter (passband: 205–270 MHz) and amplified (gain: 43 dB) to the required power for the RF mixer (+7 dBm).

3.3 Conclusions

In this chapter I have demonstrated OIL of a discrete mode semiconductor laser to a single comb mode of a low repetition rate OFC (250 MHz). This was achieved using low injection ratios such that the locking range is smaller than the comb spacing. The locking stability was passively improved by fusion splicing the laser pigtail directly to a circulator which had the effect of eliminating the back reflection from the fibre connector interface. It also allowed a shorter fibre length between the laser and the circulator, increasing the spacing between the external cavity modes to reduce the likelihood of mode jumping. This allowed OIL to be maintained for over one minute.

The locking duration was significantly extended by implementing an OIPLL set-up. The feedback error signal was based on the OIL induced phase shift which was measured with respect to the residual comb modes which are reflected by the laser cavity. In contrast to similar techniques in the literature [13], my technique does not require a single comb mode to be isolated using narrowband filters, and the feedback mechanism does not require any dithering.

3.4 References

[1] L. Goldberg, H. F. Taylor, and J. F. Weller, "FM sideband injection locking of diode-lasers," *Electronics Letters*, vol. 18, no. 23, pp. 1019–1020, 1982.

[2] L. Goldberg, H. F. Taylor, J. F. Weller, and D. M. Bloom, "Microwave signal generation with injection-locked laser diodes," *Electronics Letters*, vol. 19, no. 13, pp. 491–493, 1983.

[3] R. P. Braun, G. Grooskopf, D. Rohde, and F. Schmidt, "Low-phase-noise millimeter-wave generation at 64 GHz and data transmission using optical sideband injection locking," *IEEE Photonics Technology Letters*, vol. 10, no. 5, pp. 728–730, 1998.

[4] C. Walton, A. C. Bordonalli, and A. J. Seeds, "High-performance heterodyne optical injection phase-lock loop using wide linewidth semiconductor lasers," *IEEE Photonics Technology Letters*, vol. 10, no. 3, pp. 427–429, 1998.

[5] L. A. Johansson and A. J. Seeds, "Millimeter-wave modulated optical signal generation with high spectral purity and wide-locking bandwidth using a fiber-integrated optical injection phase-lock loop," *IEEE Photonics Technology Letters*, vol. 12, no. 6, pp. 690–692, 2000.

[6] S. Fukushima, C. F. C. Silva, Y. Muramoto, and A. J. Seeds, "Optoelectronic millimeter-wave synthesis using an optical frequency comb generator, optically injection locked lasers, and a unitraveling-carrier photodiode," *Journal of Lightwave Technology*, vol. 21, no. 12, pp. 3043–3051, 2003.

[7] C. C. Renaud, M. Düser, C. F. C. Silva, B. Puttnam, T. Lovell, P. Bayvel, and A. J. Seeds, "Nanosecond Channel-Switching Exact Optical Frequency Synthesizer Using an Optical Injection Phase-Locked Loop (OIPLL)," *IEEE Photonics Technology Letters*, vol. 16, no. 3, pp. 903–905, 2004.

[8] J. D. Jost, J. L. Hall, and J. Ye, "Continuously tunable, precise, single frequency optical signal generator," *Optics Express*, vol. 10, no. 12, pp. 515–520, 2002.

[9] H. S. Moon, E. B. Kim, S. E. Park, and C. Y. Park, "Selection and amplification of modes of an optical frequency comb using a femtosecond laser injection-locking technique," *Applied Physics Letters*, vol. 89, no. 18, p. 181110, 2006.

[10] S. E. Park, E. B. Kim, Y. H. Park, D. S. Yee, T. Y. Kwon, C. Y. Park, H. S. Moon, and T. H. Yoon, "Sweep optical frequency synthesizer with a distributed-Bragg-refiector laser injection locked by a single component of an optical frequency comb," *Optics Letters*, vol. 31, no. 24, pp. 3594–3596, 2006.

[11] H. Y. Ryu, S. H. Lee, W. K. Lee, H. S. Moon, and H. S. Suh, "Absolute frequency measurement of an acetylene stabilized laser using a selected single mode from a femtosecond fiber laser comb," *Optics Express*, vol. 16, no. 5, pp. 2867–2873, 2008.

[12] Y. J. Kim, J. H. Jin, Y. S. Kim, S. W. Hyun, and S. W. Kim, "A wide-range optical frequency generator based on the frequency comb of a femtosecond laser," *Optics Express*, vol. 16, no. 1, pp. 258–264, 2008.

[13] Y. J. Kim, Y. Kim, B. J. Chun, S. Hyun, and S. W. Kim, "All-fiber-based optical frequency generation from an Er-doped fiber femtosecond laser," *Optics Express*, vol. 17, no. 13, pp. 10939–10945, 2009.

[14] A. Criado, C. de Dios, E. Prior, G. H. Dohler, S. Preu, S. Malzer, H. Lu, A. C. Gossard, and P. Acedo, "Continuous wave sub-THz photonic generation with ultra-narrow linewidth, ultra-high resolution, full frequency range coverage and high long-term frequency stability," *IEEE Transactions on Terahertz Science and Technology*, vol. 3, no. 4, pp. 461–471, 2013.

[15] B. Kelly, R. Phelan, D. Jones, C. Herbert, J. O'Carroll, M. Rensing, J. Wendelboe, C. B. Watts, A. Kaszubowska-Anandarajah, P. Perry, C. Guignard, L. P. Barry, and J. O'Gorman, "Discrete mode laser diodes with very narrow linewidth emission," *Electronics Letters*, vol. 43, no. 23, pp. 1282–1284, 2007.

[16] T. Wipiejewski, *The Photonics Handbook: Photonic Packaging*. http://www.photonics.com/EDU/Handbook.aspx?AID=25514: Accessed 16/05/2014, 2014.

Chapter 4

Noise Characterisation

The ability for the OIPLL presented in the previous chapter to selectively amplify individual comb modes from an OFC could potentially allow it to be used for many of the applications discussed in Section 1.2. The performance of these applications is largely determined by the noise characteristics of the locked slave laser. Typical examples include: high OSNR for telecommunications; narrow linewidth for spectroscopy; and good long-term stability for metrological frequency dissemination [1]. In this chapter, I present and discuss the long- and short-term noise characterisation of the locking process described in the previous chapter (Section 3.2.3).

4.1 Background

The noise of an oscillator refers to the random variations of amplitude and/or phase, which degrades the signal of interest. A noisy signal (optical or electrical) can be described by:

$$E(t) = [E_0 + \epsilon(t)] \cos(\omega_0 t + \phi_0 + \varphi(t)) \ , \tag{4.1}$$

where t is time, $E(t)$ is the electric field, E_0 is the amplitude, ω_0 is the angular frequency, and ϕ_0 is the initial phase. Noise is introduced into the amplitude through the term $\epsilon(t)$ and the phase through $\varphi(t)$, both of which vary with time. These variations are shown in Figure 4.1. Frequency variations are sometimes considered as another form of noise, however, it is closely related to phase noise since instantaneous frequency is proportional to the time derivative of phase [2].

The remainder of this section will discuss how to measure these two forms of noise in optical systems.

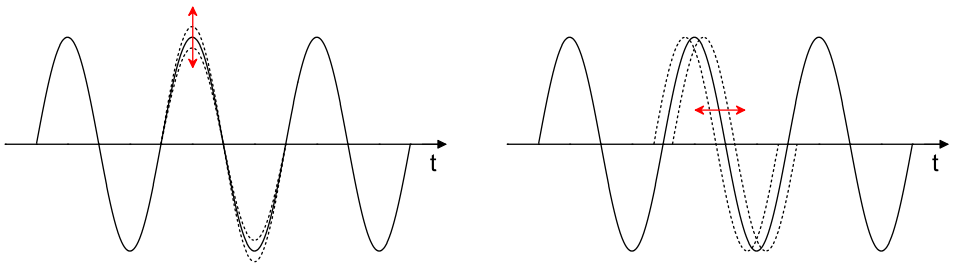

(a) Amplitude noise (b) Phase noise

FIGURE 4.1: Diagrams showing examples of (a) amplitude, and (b) phase variations.

4.1.1 Relative intensity noise

The amplitude noise of an optical signal is usually quoted as relative intensity noise (RIN). The RIN is defined as

$$\text{RIN} = \frac{\langle \delta P(t)^2 \rangle}{P_0^2} \ , \tag{4.2}$$

where $\delta P(t)$ is the fluctuation in optical power, P_0 is the average optical power, and $\langle \delta P(t)^2 \rangle$ is the mean-square of the optical power fluctuations [3]. A simple technique to measure RIN is to directly detect the optical power using a photodetector to convert the optical signal into an electrical signal. RIN measurements are usually presented as a power spectral density (PSD) plot to show the different frequency components of the noise. This can be done by measuring the photodetector signal using an RF spectrum analyser. Modern fast Fourier transform (FFT) spectrum analysers are able to simultaneously measure the DC (average) and the alternating current (AC) photodetector power. Alternatively, a bias tee can be used to split the DC and AC components of the photodetector signal.

This simple method to measure RIN is unable to distinguish between the noise of the optical system and any instrument noise. A more accurate method which minimises the contribution to the measurement from instrument noise can be found in [4].

4.1.2 Frequency stability – the Allan deviation

As discussed in Section 1.1, the frequency of optical signals (100s of THz) is too high for the individual optical cycles to be directly measured. The optical frequency therefore needs to be downconverted to the RF domain. This can be done by combining it with another optical signal and measuring the beat signal using a photodetector. The accuracy of this measurement is dependent on both the stability and accuracy of the reference signal, which is one of the reasons why highly stabilised OFCs have been an invaluable tool in frequency metrology.

The frequency of the beat signal can be accurately measured using an RF frequency counter, which counts the number times a signal crosses zero over a certain time period (the gate time). If a highly stable optical signal is used as the reference, the frequency stability of a test signal can be measured by taking repeated frequency counter measurements to track changes in the frequency. The frequency stability can then be described by calculating some form of statistical variance.

Although the standard deviation is commonly used as a general tool to quantify the spread of a data set, it is not suitable to describe frequency stability. This is because the standard deviation for many frequency sources, which is calculated based on the mean of the entire data set, is not stationary and will vary depending on the number of samples in the data set [5]. This is caused by the presence of noise which is correlated with time (non-white noise), e.g. $1/f$ flicker of phase noise. The metrology community has adopted the Allan deviation, σ_y, as a standard tool to quantify frequency stability[1]. The Allan variance, σ_y^2, is calculated as

$$\sigma_y^2(\tau) = \frac{1}{2(M-1)} \sum_{i=1}^{M-1} (y_{i+1} - y_i)^2 \ , \tag{4.3}$$

where y_i is the fractional frequency measured over a sampling time of τ, with the subscript i referring to the i^{th} measurement out of M number of measurements. The fractional frequency is defined as

$$y_i = \frac{\nu_i - \nu_0}{\nu_0} \ , \tag{4.4}$$

where ν_i is the average frequency of the signal measured over the sampling time τ, and ν_0 is the nominal frequency [5, 6]. ν_0 can be the average frequency across all M measurements, or it can be a pre-specified frequency, e.g. the frequency specified by the manufacturer of an oscillator.

The main advantage of the Allan deviation as compared to the standard deviation is that for a wide range of non-white types of noise, the Allan deviation will converge to a value that is independent of the number of samples. Also, by plotting the Allan deviation for different values of τ, these different types of noises can be distinguished by their slopes (in a log-log plot), allowing for greater characterisation. This is shown in Figure 4.2. It should be noted that other types of Allan deviations exist. The *overlapping* Allan deviation has a higher confidence interval than the standard Allan deviation. The *modified* Allan deviation changes the slope of white phase noise so that it can be distinguished from flicker phase noise. For this thesis, I have chosen to use the standard Allan deviation to allow for direct comparison of my results with others.

[1] The Allan variance is also known as the 2-sample variance. It is also commonly abbreviated to AVAR.

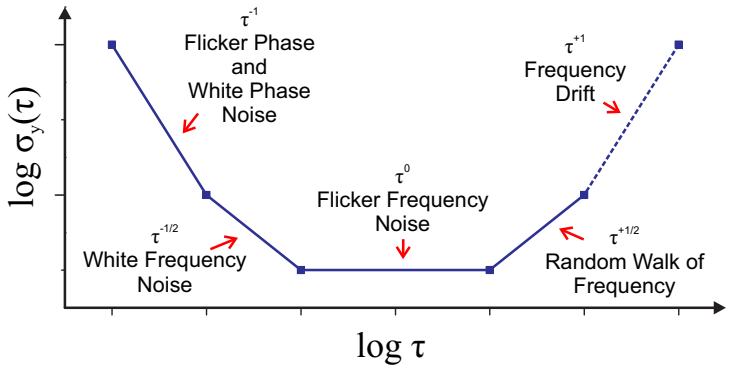

FIGURE 4.2: An example Allan deviation plot showing the different types of noise.

The stability requirements, in terms of Allan deviation, are dependent on the application targeted with highly sensitive applications requiring higher stability. A source with an Allan deviation of 5×10^{-15} at 1 s averaging time phase locked to a laser cooled Ca atom was considered sufficient for the development of optical clocks [7]. For gravitational wave detection, which requires higher sensitivity, an Allan deviation of 10^{-21} at 100 ms was targeted by the VIRGO interferometer in Italy [8].

4.1.3 Phase noise measurements

Although the frequency stability and the corresponding Allan deviation measurements are caused by phase noise, the actual term 'phase noise', by convention, generally refers to the noise which occurs over very short time scales. As a rough guide, most Allan deviation measurements are made up to long sampling times $\gg 1$ s (which corresponds to frequencies $\ll 1$ Hz), where as phase noise measurements are plotted in the frequency domain up to high frequencies $\gg 1$ Hz. Phase noise is detrimental to many applications. For example, it was calculated [9] that for a 16-quadrature amplitude modulated (16-QAM) Co-OFDM signal with 128 sub-carriers, an increase in laser linewidth (a measure of integrated phase noise) from 10 kHz to 100 kHz would increase the bit error ratio (BER) from approximately $10^{-8.5}$ to $10^{-2.5}$.

Similar to frequency stability measurements, phase noise can only be measured with respect to a reference signal which, in general, should be significantly quieter than the signal under test [10]. This allows for the assumption that the noise of the reference signal has a negligible contribution to the measurement. The frequency of the reference signal should be such that the beating with the test signal can be measured using a sufficiently fast photodetector and RF spectrum analyser. In cases where a higher quality reference is not available, the phase noise can be measured using a self-referenced heterodyne technique [11]. In this case, the signal is split into two arms, one of which is delayed and frequency shifted with respect to the other. The delay needs to be longer than the coherence length of the signal such that when the two signals are recombined they are

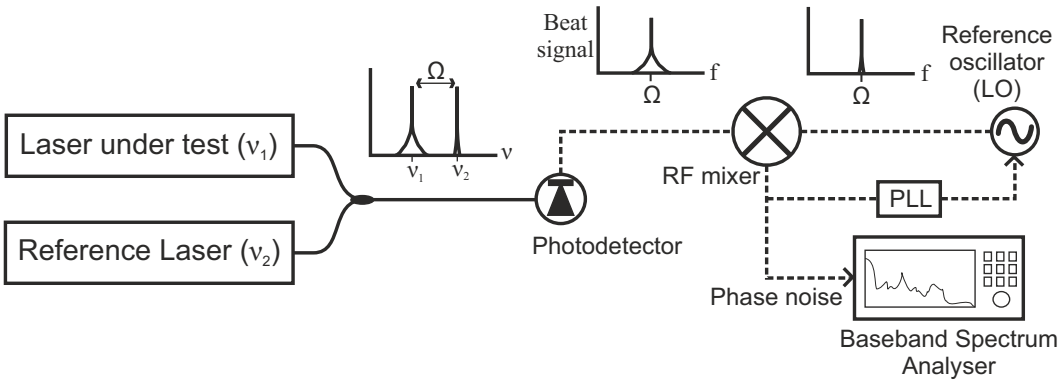

FIGURE 4.3: Schematic for measuring the phase noise of a laser using a low noise reference laser and RF source.

de-correlated. Assuming that the noise is stationary, the measured phase noise will have equal contributions from each arm.

The measurement of the phase noise spectrum can be made by simply measuring the PSD of the beat signal. The data is usually presented with the PSD normalised to the power of the RF carrier (the central frequency of the beat signal). The resulting spectrum shows the sideband power due to noise, referenced to the carrier, and is given in units of dBc/Hz (decibels with respect to the carrier per Hz). The main limitation of this measurement is that the PSD of the beat signal is unable to distinguish between amplitude noise and phase noise, since both forms of noise generates sidebands. Also, this measurement requires the frequency of the beat signal to not drift (be highly stable) compared to the sweep time of the spectrum analyser.

Alternatively, an RF phase detector can be used to measure the phase, and any corresponding phase noise, of the beat signal. An RF frequency mixer (also known as a frequency multiplier) can be operated as a phase detector if the local oscillator (LO) and RF inputs into the mixer are at the same frequency[2]. A schematic of this type of measurement is shown in Figure 4.3. The output of the mixer will contain a signal with frequency components at the sum and difference of the LO and RF frequencies. Since the LO and RF frequencies are the same in this case, the difference frequency will be zero (baseband). For an ideal mixer,

$$\text{Mixer output} = K_m \left[A_{RF}\cos(\Omega t + \phi_{RF} + \varphi(t)) \times A_{LO}\cos(\Omega t + \phi_{LO})\right] \ ,$$

$$\text{Mixer output} = \frac{1}{2}K_m A_{RF} A_{LO}\left[\cos(\phi_{RF} - \phi_{LO} + \varphi(t)) + \cos(2\Omega t + \phi_{RF} + \phi_{LO}))\right] \ , \tag{4.5}$$

where $A_{RF,LO}$ and $\phi_{RF,LO}$ are the amplitudes and phases of the input signals, both with a frequency of Ω. The phase noise of the RF signal is given by $\varphi(t)$, while the LO was assumed to be noise free. K_m is a conversion factor of the mixer, which is dependent on the RF and LO input powers for analogue mixers. The baseband signal can be isolated

[2]This technique was utilised in Section 3.2.2 to measure the injection locking phase shift.

from the frequency doubled component using a low-pass filter.

$$\text{Mixer output (filtered)} = K_\phi \cos\left(\phi_{RF} - \phi_{LO} + \varphi(t)\right) \ , \tag{4.6}$$

where $K_\phi = \frac{1}{2} K_m A_{RF} A_{LO}$ is known as the phase detector sensitivity. If the RF and LO signals are in quadrature, i.e. $\phi_{RF} - \phi_{LO} = \frac{\pi}{2}$, then the small angle approximation ($\cos(x) \approx x$) can be used such that

$$\text{Mixer output (filtered, in quadrature)} \approx K_\phi \, \varphi(t) \tag{4.7}$$

The mixer will only operate as a linear phase detector if the LO and RF signals are kept in quadrature and the phase noise is sufficiently low for the small angle approximation to hold true. Although amplitude noise can cause the value of K_ϕ to fluctuate, these variations are usually significantly smaller than the $\varphi(t)$ contribution. To keep the input signals in quadrature, a PLL can be used to lock the frequency and phase of the LO to the RF signal. This also has the advantage of being able to compensate for any frequency drift of the RF beat signal. The phase noise can then be characterised by measuring the PSD of the mixer output using a baseband spectrum analyser to find the various frequency components of the noise.

4.2 Long-term frequency stability of the OFC locked slave laser

Long-term locking stability is important for applications such as frequency dissemination and time metrology. It is important in these cases for an oscillator to maintain the same frequency for long periods of time (ideally, it would be indefinite). For example, in precise frequency transfer, averaging frequency measurements over 1000 s is needed to achieve required level of precision [12] and hence an oscillator would need to be locked for at least that length of time. This section reports on my investigation of the long-term stability of the OIPLL.

4.2.1 Experimental set-up

The long-term stability of the locking process was characterised by measuring the long-term frequency variations using a set-up similar to the one described in Section 4.1.2. To measure how well the slave laser was locked to its target comb mode, the original comb mode was used as the optical reference by splitting the AWG output prior to optical injection. The total optical power in the reference arm was approximately –11 dBm. The set-up is shown in Figure 3.10 and parameters summarised in Table 4.1. A non-zero frequency beat signal was generated by frequency shifting the output of the slave

TABLE 4.1: Component parameters for Figure 4.4. Components within the OIPLL Slave laser are the same as in Table 3.1.

Component	Parameter	Value
AWG	Insertion loss (per channel)	3–5 dB
	Channel bandwidth (3 dB)	50 GHz
	Passband shape	Gaussian
	Connector type	FC/APC
	Fibre type	SMF-28
50/50 Coupler	Excess Loss	0.5 dB
	Connector type	FC/APC
	Fibre type	SMF-28
Slave laser	Type	Discrete mode
	Output power	+12 dBm
	Operating current	127.48 mA
	Operating temperature	26.63°C
	Connector type	FC/APC
	Fibre type	SMF-28
AOM	Insertion loss	4.8 dB
	Operating frequency	35 MHz
	Connector type	FC/APC
	Fibre type	SMF-28
Variable attenuator	Excess Loss	1.5 dB
	Connector type	FC/APC
	Fibre type	SMF-28
Photodetector	Bandwidth	125 MHz
	Responsivity	1.0 A/W
	Transimpedance gain	40 V/mA
	Optical input type	FC
Low pass filter	Cut-off frequency	48 MHz
35 MHz Source	RF output power	1 W
10 MHz GPS Reference	Phase noise	–100 dBc/Hz at 1 Hz –150 dBc/Hz at 10 kHz

laser by 35 MHz using an acousto-optic modulator (AOM) and combining it with the original signal which was injected into the slave laser. The AOM was driven using an RF synthesiser which was synchronised to the same GPS clock used to stabilise the OFC. The optical power after the AOM was approximately +6 dBm.

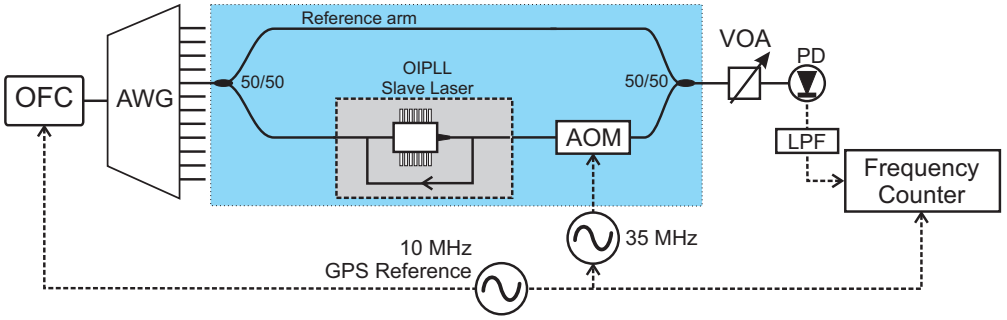

FIGURE 4.4: Schematic of the long-term frequency stability set-up. The grey shaded box represents the locked slave laser and includes all the shaded components in Figure 3.10.

The beat signal was measured using a photodetector (bandwidth: DC-125 MHz, responsivity: 1.0 A/W, transimpedance gain: 40 V/mA), with a VOA used to ensure the photodetector was not saturated. The frequency of the filtered signal was measured using a digital frequency counter (FXM50 Counter, Menlo Systems GmbH) with a gate time of 1 s. The frequency counter was referenced to the same 10 MHz GPS clock used to synchronise the AOM driver.

The AOM shifted slave laser output was not only combined with the original comb mode which it was locked to, but also all the other comb modes present in the reference arm. The beat signal between the slave laser and comb mode it was locked to (at 35 MHz) was isolated from the higher frequency beating with the other comb modes by using an RF low-pass filter (48 MHz). The filtered signal contained a component at 35 MHz which was due to the beating between the residual comb modes in the slave laser output and their corresponding (non-frequency shifted) comb modes in the reference arm. The majority of the residual comb modes did not influence the measurement since they were very weak compared to the locked mode. Also, the comb modes in the reference arm and slave laser output were not overlapped in the temporal domain when they were combined (since the comb modes form short pulses of approximately 10 ps). However, it is expected that the residual comb modes close to the locked mode, which can be amplified by the injection locking process, may contribute to the 35 MHz beat signal and affect the measurement.

The comparison of the slave laser output with the original comb mode it was locked to makes this an interferometric measurement, similar to a Mach-Zehnder interferometer. Fluctuations of optical phase in either the reference or slave laser arm would cause fluctuations of phase in the beat signal which was measured by the frequency counter. These changes in phase may not have been due to the locking process and hence they represent an error in the measurement. For example, if the OFC starts to fluctuate in phase, then these fluctuations would be followed by the locked slave laser. However, if the slave laser was then combined with the OFC from an earlier time (prior to the fluctuations), then this would appear as noise in the beat signal generated. These master laser induced fluctuations can be suppressed in the measurement by balancing the path lengths in the reference arm and the injection locking arm after the AWG output port is split. This ensures that any fluctuations in the slave laser due to the OFC will occur at the same time in the reference signal at the detector and hence no relative fluctuation will be measured.

Another source of measurement noise is due to thermal and acoustic fluctuations in the optical fibre due to variations in the environment, e.g. air temperature and vibrations. These affect the measurement by causing slow changes ($\lesssim$ 10 kHz) to the refractive index of the fibre and the polarisation of the optical signal. Path matching can also help suppress this, since these fluctuations would then be expected to occur equally in both arms. However, they can be further suppressed by shielding the set-up from these

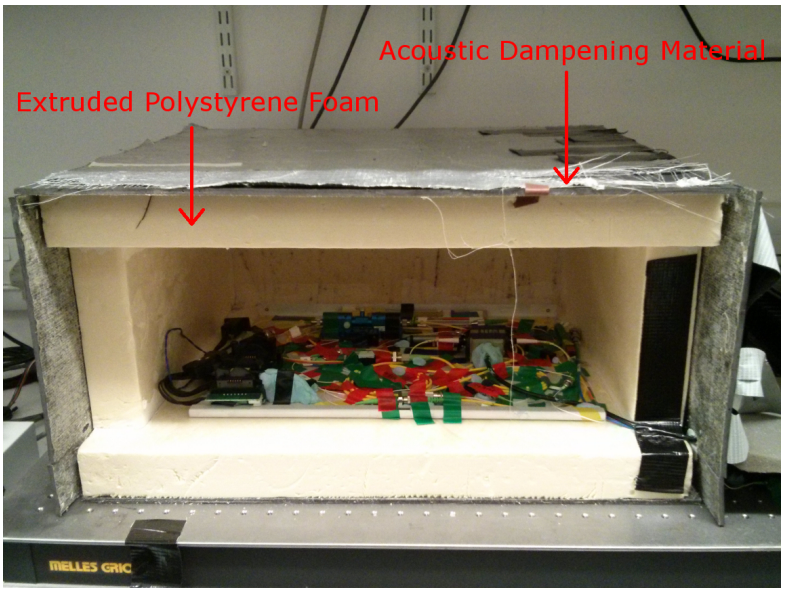

FIGURE 4.5: Photograph of the thermal and acoustic dampening box. A front panel (not shown) seals the box.

environmental changes. This was achieved in my set-up by placing the blue-shaded part of the set-up in Figure 4.4 inside a thermal and acoustic damping box. The box (shown in Figure 4.5) was constructed in-house[3] using extruded polystyrene foam for high thermal insulation and was covered with a layer of acoustic dampening material. Additional insulation was provided by filling the box with sheets of low density polystyrene foam.

4.2.2 Results

The frequency variation of the 35 MHz beat signal over a period of 8 hours is shown in Figure 4.6. These measurements were taken overnight in April 2011 using an injection ratio of –65 dB. The feedback controller used was a Newport LB1005 set with a proportional gain factor of –20 dB and a PI corner of 10 Hz.

Although the experimental set-up was strongly insulated, the measurement was still susceptible to environmental fluctuations. The laboratory air-conditioner was kept on in Figure 4.6(a). Regular spikes in frequency variation occurred approximately every half an hour, which corresponded to the air-conditioner cycle. These spikes were no longer present when the air-conditioner was turned off in Figure 4.6(b). The maximum frequency variation in this case was ±0.07 Hz with a standard deviation of 0.014 Hz. However, as discussed in Section 4.1.2, the Allan deviation is more suitable to describe frequency variations. This was calculated and plotted in Figure 4.7.

The Allan deviation improves from an initial value of 9.1×10^{-17} at 1 s as the averaging time increases. For averaging times of 1–10 s, the Allan deviation follows a τ^{-1}

[3]This was constructed by Radan Slavík

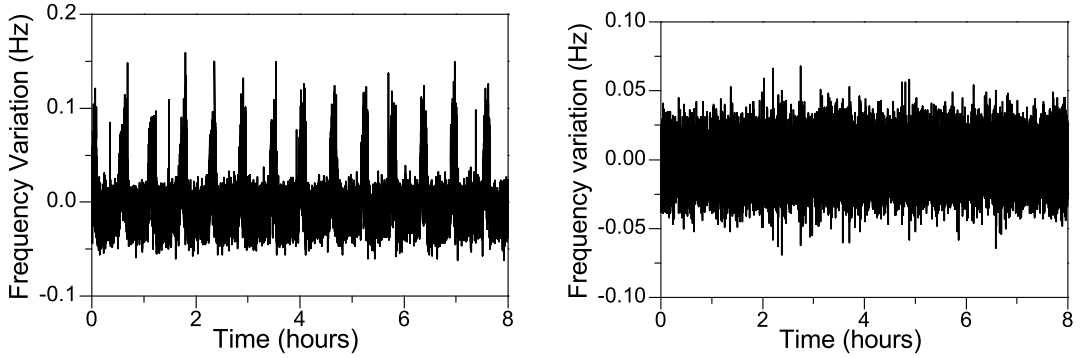

(a) Air-conditioner On (b) Air-conditioner Off

FIGURE 4.6: Frequency variations measured over 8 hours. Injection ratio: –65 dB.

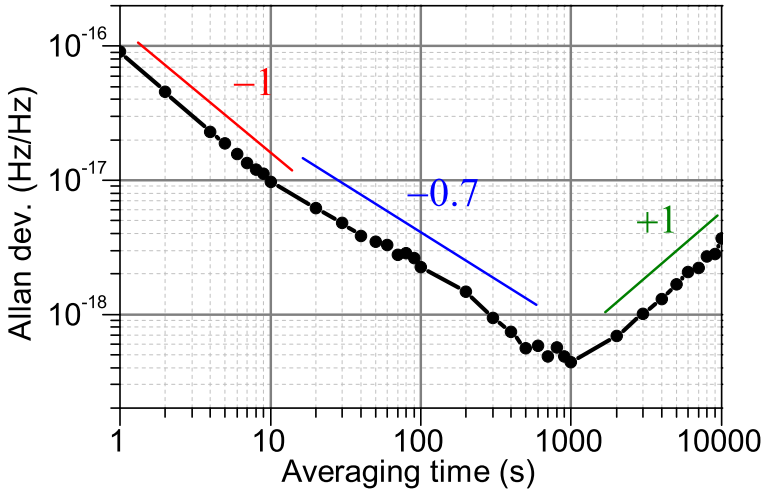

FIGURE 4.7: Allan deviation calculated from the data shown in Figure 4.6(b). The coloured numbers show the approximate slopes.

dependence indicating the dominance of phase noise. Between 10–500 s, the slope of curve shows something between a τ^{-1} and $\tau^{-\frac{1}{2}}$ dependence which suggests that there is a mix of phase noise and white frequency noise, with neither type being dominant. The Allan deviation reaches a minimum of 4.4×10^{-19} at an averaging time of 1000 s. At longer averaging times, the Allan deviation increases with a τ^{+1} dependence, which corresponds to frequency drift. The cause of this frequency drift was not clear but it may have been caused by very slow thermal fluctuations which would have induced a phase difference between the slave laser signal and the reference arm due to any optical path length mismatch. Another source for this frequency drift could be due to some form of drift in the locking point of the OIPLL feedback loop. From Equation (2.7), this would cause a drift in the phase of the slave laser relative to the reference signal. Further investigation would be required to understand the true nature of this frequency drift.

4.2.3 Discussion

Comparison of results with others

A similar measurement of the Allan deviation of an injection locked slave laser to a 250 MHz spaced OFC was performed by Ryu et al. [13]. A significant difference between my measurement and theirs was that they used a pure OIL system, not an OIPLL. As a result, they did not achieve long-term locking and hence could only measure their Allan deviation for averaging times up to 30 s. My Allan deviation measurement of 9.7×10^{-18} at an averaging time of 10 s is comparable to their value of approximately 2×10^{-17}. This small discrepancy could be due to differences in how well the experimental set-up was shielded from environmental fluctuations. It might also be attributed to their use of a higher injection ratio, which I estimate to be approximately –50 dB using the same assumptions from Section 3.2.

A comparison can also be made with Kim et al.'s results [14]. They also achieved long-term locking using an OIPLL system, but used a 100 MHz spaced OFC and required pre-injection filtering using a narrowband Fabry-Pérot filter. They measured an Allan deviation of 2.3×10^{-15} at 10 s averaging time which was more than two order of magnitude higher than my measurement. This significant improvement is likely caused by the wider spaced OFC I used, which would have resulted in less interference from neighbouring comb modes. Their use of an ultra-narrowband Fabry-Pérot filter might have been susceptible to misalignment which could have caused amplitude variations of the injected comb mode. This could have led to phase variations of the slave laser output[4] which would have degraded the frequency stability.

4.3 Short-term stability of the OFC locked slave laser

In this section, the short-term phase noise associated with the locking process is presented. These phase noise measurements complement the long-term frequency stability analysis in the previous section. Knowledge of the short-term fluctuations due to the locking mechanism is important for applications operating at high speeds, e.g. for telecommunications applications.

4.3.1 Two injection locked lasers

Two OIPLL locked lasers were used to take the phase noise measurements, with the additional slave laser placed in the reference arm from the previous section. This was done to suppress the relative power of the amplitude modulation noise introduced by the AOM

[4]This will be discussed further in Section 4.3.3

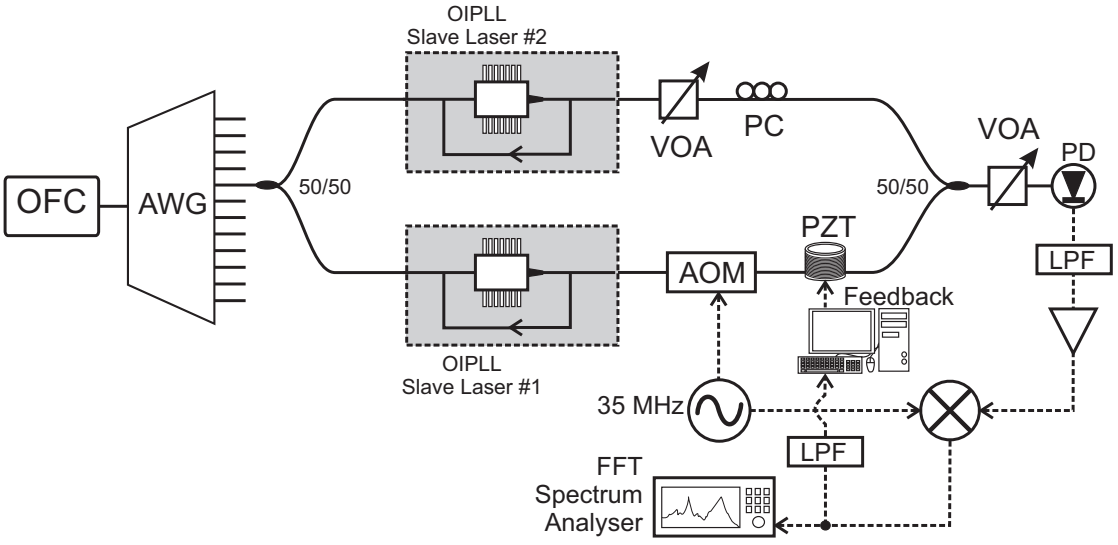

FIGURE 4.8: Schematic of the set-up used to measure phase noise. AWG: arrayed waveguide grating, AOM: acousto-optic modulator, PZT: Lead Zirconate Titantate (piezoelectric phase shifter), LPF: low-pass filter, VOA: variable optical attenuator, PC: polarisation controller.

(Appendix A). The beating signal between two injection locked lasers was significantly stronger than between one laser and an individual comb mode. Since the amplitude modulation noise remained the same, its relative power was strongly suppressed.

In this case, the measurement was no longer based on the phase of a locked slave laser as compared to the original comb mode it was locked to. Rather, the two slave lasers were compared against each other as shown in Figure 4.8. The phase noise of one of the slave lasers could be calculated under some assumptions. Firstly, it was assumed that the two slave lasers were identical. This assumption was justified because the two free running slave lasers were very similar. Both of the lasers were discrete mode lasers with similar properties, and were part of the same manufacturing batch. The slave lasers also needed to be independent, which was clearly not the case since they were both locked to the same comb mode. However, it was the phase noise due to the locking process which was of interest. Therefore, if the path lengths were matched, noise from the master would be present in both slave lasers and be cancelled out in the measurement. Therefore, the only phase noise which should be measured was primarily due to the locking process, which was assumed to be independent for each laser. Under these assumptions, it can be shown that the phase noise PSD of a single laser is simply equal to half of the measured value (Appendix B).

4.3.2 Phase noise measurement set-up

The initial set-up for measuring the phase noise is shown in Figure 4.8 with the component parameters summarised in Table 4.2. The two slave lasers were both Eblana

TABLE 4.2: Component parameters for Figure 4.8. Components within the OIPLL Slave lasers are the same as in Table 3.1.

Component	Parameter	Value
AWG	Insertion loss (per channel)	3–5 dB
	Channel bandwidth (3 dB)	50 GHz
	Passband shape	Gaussian
	Connector type	FC/APC
	Fibre type	SMF-28
50/50 Coupler	Excess Loss	0.5 dB
	Connector type	FC/APC
	Fibre type	SMF-28
Slave laser #1	Type	Discrete mode
	Output power	+12 dBm
	Operating current	107.41 mA
	Operating temperature	26.63°C
	Connector type	FC/APC
	Fibre type	SMF-28
Slave laser #2	Type	Discrete mode
	Output power	+12 dBm
	Operating current	110.50 mA
	Operating temperature	27.11°C
	Connector type	FC/APC
	Fibre type	SMF-28
Variable attenuator	Excess Loss	1.5 dB
	Connector type	FC/APC
	Fibre type	SMF-28
Polarisation controller	Insertion loss	<0.5 dB
	Connector type	FC/APC
	Fibre type	SMF-28
AOM	Insertion loss	4.8 dB
	Operating frequency	35 MHz
	Connector type	FC/APC
	Fibre type	SMF-28
PZT phase shifter	Insertion loss	0.5 dB
	Connector type	FC/APC
	Fibre type	PM-F
	Input voltage	0–10 V
Photodetector	Bandwidth	125 MHz
	Responsivity	1.0 A/W
	Transimpedance gain	40 V/mA
	Optical input type	FC
Low pass filter (after photodetector)	Cut-off frequency	48 MHz
35 MHz Source	RF output power	1 W
RF Mixer	Input frequencies	1–100 MHz
	Isolation	40 dB
	Conversion loss	4.7 dB
Low pass filter (before feedback)	Cut-off frequencies	1.9 MHz
RF amplifier	Bandwidth	0.1 – 500 MHz
	Gain	23 dB
	Noise figure	2.9 dB

discrete mode lasers with no isolators operating at +12 dBm. Both lasers were locked to the same comb mode and used Newport LB1005 PI controllers with the same settings as in Section 4.2.1 (Proportional gain: –20 dB, PI corner: 10 Hz). The output from one of the lasers was then frequency shifted by 35 MHz using an AOM and combined with the other laser output using a fibre coupler. The beating between the two lasers was measured using a photodetector.

The phase noise of the beat signal was measured using an analogue phase detector (the RF mixer in Figure 4.8). The reference signal (local oscillator) for the mixer was the same 35 MHz signal used to drive the AOM. A fibre optic piezoelectric phase shifter (fibre stretcher) was inserted after the AOM to keep the beat signal in quadrature with the reference signal at the mixer, ensuring that it behaves as a phase detector. The feedback for the phase shifter was controlled through a personal computer using LabVIEW and had a very low bandwidth ($<$ 10 Hz). The LabVIEW program was a proportional feedback controller with no integral component. This low bandwidth feedback would only compensate for very slow changes in phase due to the temperature drift in the optical fibre.

The phase detector sensitivity (K_d) was measured to be 0.32 ± 0.02 V/rad (volts per radian) when the input power was +3.6 dBm for the RF beat signal and +4.9 dBm for the local oscillator. This was measured by replacing the beat signal with a 'dummy' signal with the same RF power but with a slightly offset frequency (+600 Hz). The baseband signal from the mixer was measured on an oscilloscope and K_d was calculated from the linear region of the signal (near 0 V).

4.3.3 Phase noise results (frequencies $<$ 17.5 MHz)

The phase noise was measured for injection ratios ranging from –72.5 to –51 dB, with both lasers locked using the same injection ratio. Locking outside this range was difficult since the locking range was either too small to maintain the lock, or too large with interference from neighbouring comb modes preventing the locking from being maintained. The AOM frequency shift of 35 MHz only allowed the phase noise up to the Nyquist frequency of 17.5 MHz to be measured. However, due to the 48 MHz low-pass filter used to isolate the 35 MHz beat signal, this upper limit was reduced to 13 MHz.

The single sideband (SSB) phase noise of an individual locked slave laser is shown in Figure 4.9 for three different injection ratios. The measurement noise floor was measured by removing the OIPLL slave lasers from Figure 4.8 and measuring the phase noise of the beat signal between the AOM frequency shifted and OFC signals. From the phase noise spectrum, clear spikes in noise can be seen at frequencies of approximately 1 kHz and 8 kHz which was present regardless of the injection ratio. These features were also present in the noise floor measurement which shows that they are not inherent to the

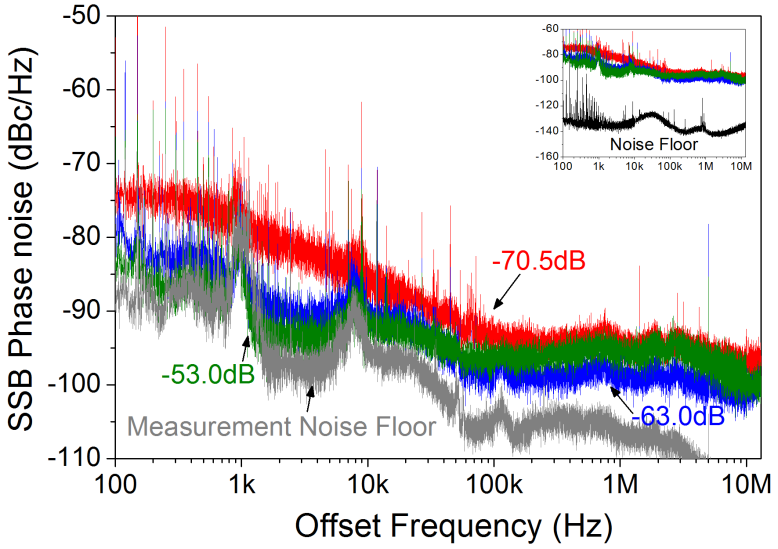

FIGURE 4.9: Single sideband (SSB) phase noise of a locked slave laser up to 13 MHz using various injection ratios. The inset shows the spectrum analyser noise floor.

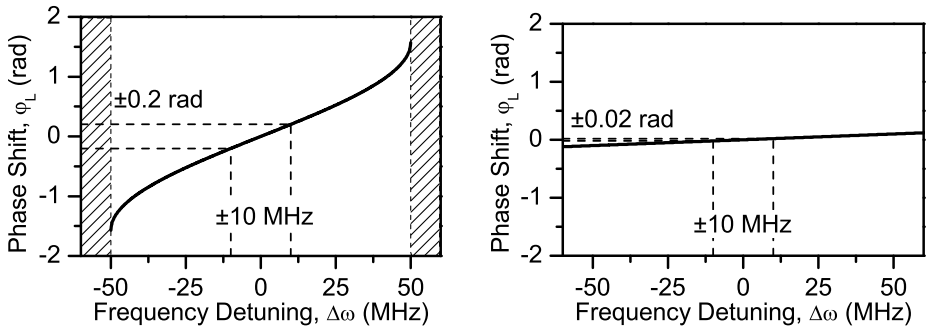

(a) $\Delta\omega_L = 100$ MHz, the shaded area is outside the locking range.

(b) $\Delta\omega_L = 1$ GHz, only a fraction of the locking range is shown

FIGURE 4.10: The injection locking induced phase shift of a slave laser ($\alpha = 0$). For a variation in detuning by 10 MHz, the resulting variation in phase is smaller for a larger locking range.

slave lasers themselves. In general, it can be seen that at low frequencies (< 50 kHz), the phase noise decreases as the injection ratio increases. The reason for this was due to the limited bandwidth (< 100 Hz) of the OPLL part of the OIPLL not compensating for frequency detuning fluctuations at higher frequencies. Recall that the injection locking phase shift (Equation (2.7)) is dependent on the detuning as a fraction of the locking range; the size of which increases with injection ratio. Therefore, for the same amount of frequency fluctuation in the slave (or master) laser, a larger locking range will result in smaller phase fluctuations in the slave laser output, as illustrated in Figure 4.10.

At higher offset frequencies (> 50 kHz), the phase noise increases with larger injection ratios. It is believed that this was caused by the neighbouring comb modes having an effect on the injection locking process. This would occur because they have a closer

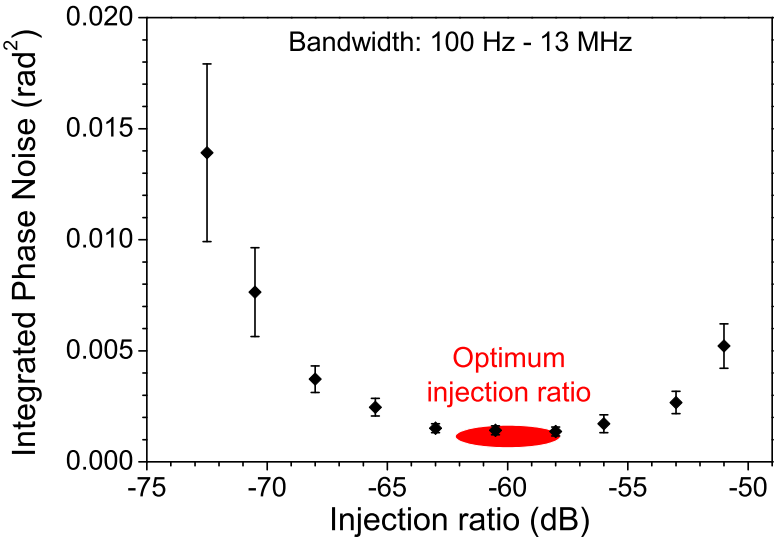

FIGURE 4.11: The integrated phase noise (100 Hz–13 MHz) for various injection ratios.

proximity to the edges of the locking range when larger injection ratios are used. Although the slave laser may not lock to the adjacent comb modes, the closer proximity may induce effects such as frequency pulling [15] and hence increase the noise.

Although the results in Figure 4.9 show the dependence of phase noise on the injection ratio, it is not clear how much noise is being generated from the various components in the set-up. Phase noise measurements should have been taken of all the various components in the set-up, including the AOM and its 35 MHz RF driver, as well as the RF amplifiers. Adding together the various sources of noise should equate to the total noise measured in Figure 4.9, and could also be used to confirm the measurements.

The total phase noise was quantified by calculating the integrated phase noise[5] across the measurement bandwidth (100 Hz—13 MHz), which is shown in Figure 4.11. This shows that an optimum injection ratio exists between –63 and –58 dB where the integrated phase noise was at a minimum of less than 0.002 rad^2. As discussed above, the increased integrated phase noise at low injection ratios was due to low frequency noise; while at high injection ratios it was due to high frequency noise.

4.3.4 Phase noise results (frequencies < 500 MHz)

The frequency range of the phase noise measurements from the previous section were limited because of the small frequency shift of the AOM. It was found that as the upper limit of those measurements was approached, the phase noise began to increase for higher injection ratios. It was speculated from this that this was due to the increased influence of the adjacent comb modes with wider locking ranges. In order to test this, the measurement bandwidth needed to be increased to be wider than the comb spacing.

[5]The integrated phase noise is also known as the *phase error variance*.

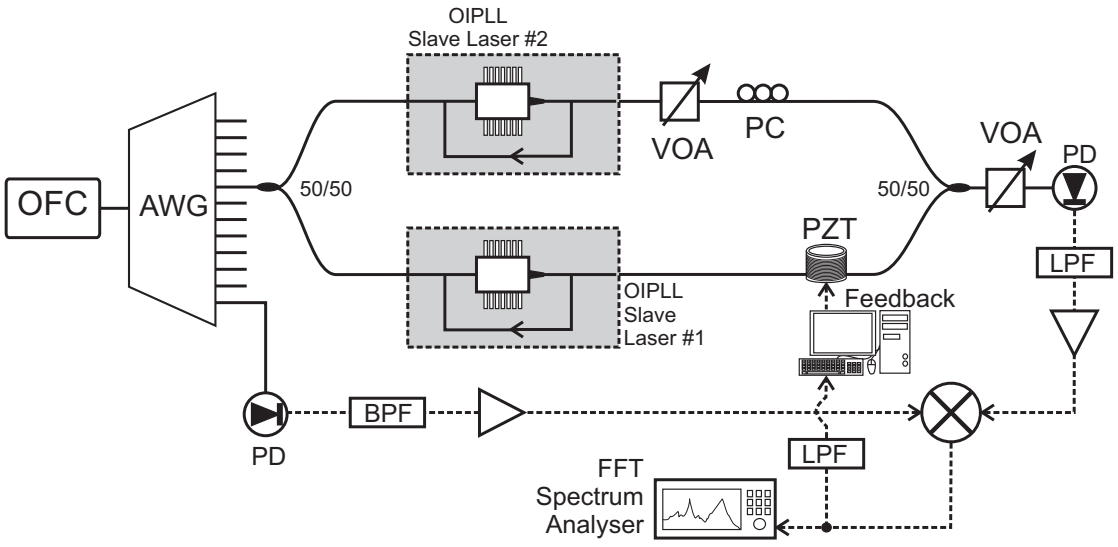

FIGURE 4.12: Schematic of the set-up used to measure phase noise without using an AOM.

AOM frequency shifters up to 1 GHz are available on the market, but are uncommon and expensive. Therefore, an alternative approach needed to be taken to increase the phase noise measurement bandwidth. To generate a higher frequency beat signal between the two slave lasers, they were locked to different comb modes, rather than the same one. It was assumed that the two comb modes used for locking had statistically identical noise properties. Therefore, it could still be assumed that the two locked slave lasers were independent, but also had identical noise properties. The slave lasers were chosen to be locked to comb modes separated by 1 GHz (4 comb modes apart), which allowed the phase noise up to 500 MHz (Nyquist frequency) to be measured. Since the measurement bandwidth was larger than the comb spacing, the effect of the residual comb modes could be further studied.

The set-up is shown in Figure 4.12 and was similar to the previous measurement set-up, but with the AOM removed. The beat signal between the slave lasers was detected with a reverse-biased photodiode (no transimpedance amplifier, responsivity: 0.95 A/W). The RF signal was low-pass filtered (cutoff freqeuency: 2 GHz), amplified (bandwidth: 10–2500 MHz, gain: 20 dB, noise figure: 5.5 dB) and sent to a frequency mixer (conversion loss: 6.05 dB, isolation: 35 dB).

The reference RF signal (local oscillator for the mixer) was extracted directly from the OFC. This was similar to the repetition rate recovery from Section 3.2.3 but was instead used to generate an RF signal at the fourth harmonic of the repetition rate. The reference signal was filtered using a band-pass filter (passband: 850–1100 MHz) and amplified (bandwidth: 10–1000 MHz, gain: 23 dB, noise figure: 4.0 dB). The power of the reference signal entering the mixer was approximately +7 dBm.

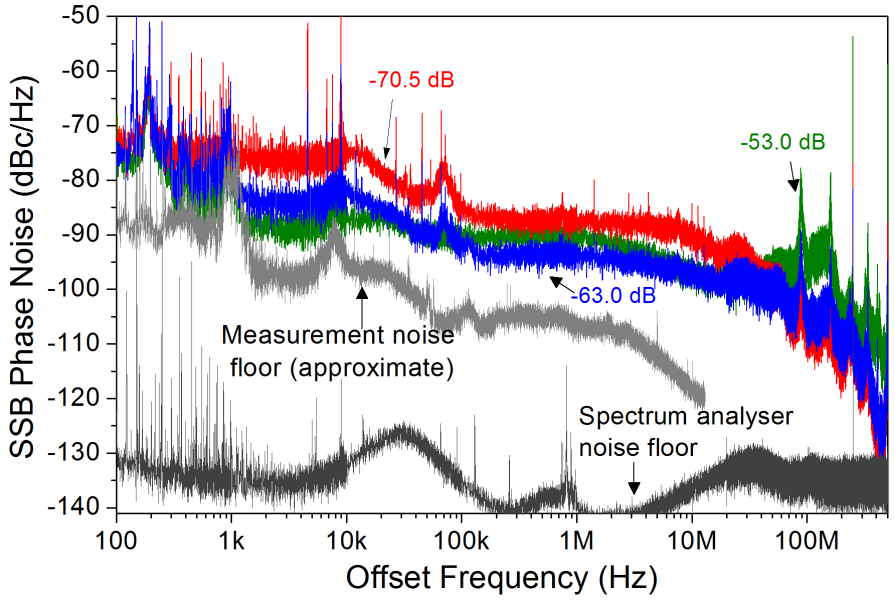

FIGURE 4.13: SSB phase noise of a locking slave laser calculated by measuring the phase noise of a 1 GHz beat signal generated by two locked slave lasers. The measurement noise floor is the same as in Figure 4.9 and is not truly representative for the current measurement.

Residual comb mode amplification

It was found while taking these measurements that the phase noise at multiples of the repetition rate (250 MHz and 500 MHz) varied with the detuning of each laser. This may have been due to the amplification of residual comb modes having a detuning dependence. Alternatively, it could have been due to the change of injection locking phase and hence the variation may have been caused by destructive and constructive interference of the RF signals.

This was briefly investigated by measuring the beat signal between one locked slave laser and one free running slave laser (with no optical injection). This removed the possibility of interfering RF signals, since the residual comb modes are only present in one laser. In this case, the power of the beat signals due to the residual comb modes were still found to have a dependence on the detuning of the locked slave laser. This implied that the amplification of the residual comb modes does have a detuning dependence and was investigated further in Chapter 5. These further investigations found that phase modulation of the slave laser was induced by residual comb modes, with the modulation depth dependent on the detuning between the slave laser and locked comb mode. For the following phase noise measurements, the slave lasers were locked to a detuning such that the residual comb modes were at a minimum.

Results and Discussion

The phase noise was measured for a similar range of injection ratios as the previous measurement; some of these are shown in Figure 4.13. The measurement noise floor was not measured for this experiment. The approximate measurement noise floor displayed in Figure 4.13 is the same as the one measured in Figure 4.9, which is the reason it is only considered to be an approximate representation of the true noise floor. The similarities in the measured phase noise spectra for the slave laser suggests that the measurement noise floor will also be similar, however, the true noise floor for this set-up should have been measured.

For offset frequencies up to 13 MHz, there is good consistency with Figure 4.9 despite not locking the slave lasers to the same comb mode, justifying the assumptions discussed above. The small differences may be attributed to the different mixer used for the phase detector, and small changes in the experimental set-up due to the entire set-up being dismantled and reassembled again between experiments.

Above 13 MHz, it can now be clearly seen that the overall phase noise decreases with increasing injection ratio. The peaks at approximately 90 and 160 MHz corresponded to amplitude noise peaks which were present in the injected OFC signal, but were converted into phase noise. It can be observed that the noise at 250 MHz associated with the residual comb modes and the amplitude-to-phase noise at 90 and 160 MHz became stronger with increasing injection ratios. This provides more evidence that as the locking range increases, the adjacent unlocked comb modes interfere more with the locking process leading to increased noise.

The integrated phase noise across the wider measurement bandwidth was again calculated and is shown in Figure 4.14. The larger values were due to the increased measurement bandwidth, however, there still existed an optimum locking region where the integrated phase noise was at a minimum (≈ 0.02 rad^2). The optimum locking region shifted to slightly lower injection ratios (between –63 and –58 dB). This was likely due to the larger measurement bandwidth which included the effects of the adjacent residual comb modes and the amplitude-to-phase converted noise.

To confirm these measurements, the integrated phase noise was also estimated by measuring the root mean squared (rms) jitter of the 1 GHz temporal waveform of the beat signal. This was done using an RF digital sampling oscilloscope (Tektronix DSA8200, bandwidth: 50 Hz — 10 GHz) and the jitter was estimated by comparing the measured waveforms with a fitted 1 GHz sine wave. The results are plotted alongside the integrated phase noise measurements in Figure 4.14. There is good agreement between the two types of measurements despite the significantly larger measurement bandwidth of the oscilloscope. This shows that there was only a small noise contribution from the additional bandwidth between 500 MHz to 10 GHz. This contribution may be due to

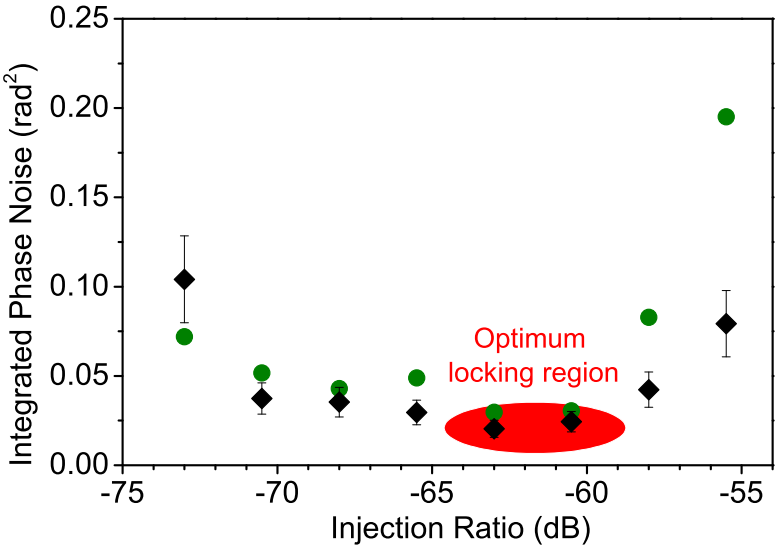

FIGURE 4.14: The integrated for various injection ratios. Black diamonds are calculated from the integrated phase noise (100 Hz to 500 MHz) and green circles are estimated from temporal waveforms measured using a sampling oscilloscope (50 Hz to 10 GHz).

both the higher harmonics of the residual comb modes and the free running white noise of the slave laser. These results also suggest that locking the two slave lasers to more spectrally distant comb modes should not significantly change the phase noise properties. This could allow for very high repetition rate optical signals to be generated without any degradation of phase noise, which could also be useful for arbitrary waveform generation. This concept is explored further in Chapter 6.

Further insight into the contribution of phase noise at various frequencies towards the total phase noise can be gained by looking at the cumulative integrated phase noise. Figure 4.15 shows the integrated phase noise starting from 100 Hz up to 500 MHz using an injection ratio of –63 dB (minimum phase noise). In this case it was found that the contribution from the residual comb modes at 250 MHz was 2×10^{-5} rad^2, which is 3 orders of magnitude smaller than the total integrated phase noise of 0.02 rad^2. More generally, it was found that this contribution was less than 10^{-4} rad^2 for all injection ratios below –58 dB. However, as previously mentioned, these measurements were taken with a detuning such that the amplification of the residual comb modes were at a minimum. When this was not the case, the contribution at 250 MHz can be of the same order as the total integrated phase noise, increasing it by up to a factor of 3 at the optimum injection ratio. This is shown in red in Figure 4.15.

These phase noise measurements have shown that using the optimum injection ratio can be crucial for potential applications where noise is required to be kept at a minimum. At the same time, it is also important to have the slave laser locked to a detuning where the residual comb modes are at a minimum.

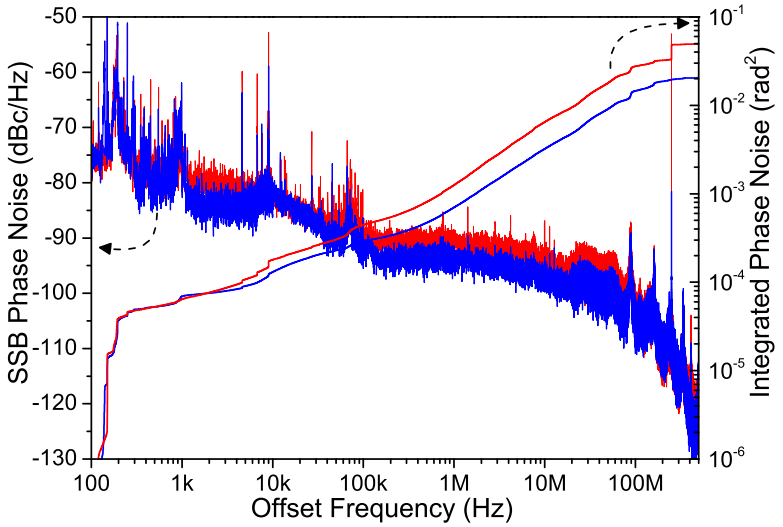

FIGURE 4.15: The SSB phase noise for an injection ratio of –63 dB and the cumulative integrated phase noise (integration from 100 Hz to 500 MHz). The blue curves were when the detuning was tuned such that the residual comb modes were at a minimum; the red curves were at a maximum.

4.4 Relative Intensity Noise

The main focus of this chapter has been on phase and frequency stability of the locking process. In this final section, amplitude noise measurements are presented to complement the previous sections. It was stated in Section 4.1.1 that in principle, RIN measurements are relatively simple. However, from a practical perspective, these measurements may be difficult for low noise lasers due to limitations imposed by instrumentation noise.

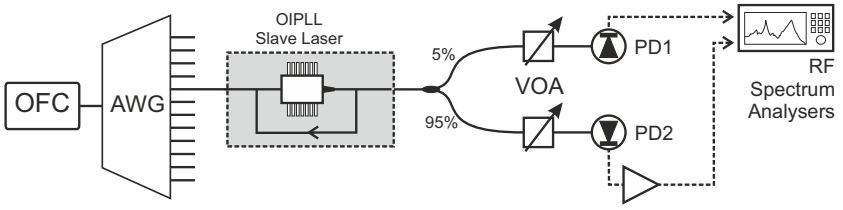

FIGURE 4.16: Schematic of the RIN measurement set-up.

The measurement set-up is shown in Figure 4.16. Two RF spectrum analysers were required for this measurement. An FFT spectrum analyser (Tektornix RSA3303A) was required since it was able to measure from very low frequencies (< 1 Hz), but had a relatively high noise floor. A swept mode RF spectrum analyser, with lower noise (Agilent E4446A with 50 kHz DC block) was used to measure the RIN from 100 kHz. Two different photodetectors were also required. Firstly a photodetector (New Focus 1811-FC) with an in-built transimpedance amplifier was able to generate a strong signal from DC–125 MHz with low additional noise. To expand the measurement bandwidth, an additional wider bandwidth photodetector was required. The only available ones at the

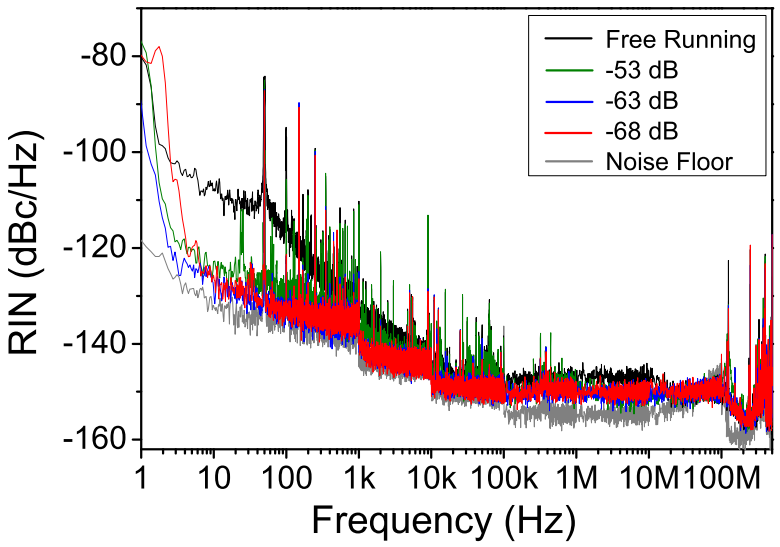

FIGURE 4.17: RIN measurement at various injection ratios

time of the measurement were unamplified (Agilent 83440C DC–20 GHz Lightwave Detector) and as such, an external RF amplifier (Mini-Circuits, ZFL-500LN+) was required to raise the signal above the spectrum analyser noise floor. A summary of the various combinations of photodetectors and spectrum analysers used for different measurements bands are given in Table 4.3.

TABLE 4.3: RIN measurement photodetectors and RF spectrum analysers

Measurement Band	Photodetector	Spectrum Analyser
1 Hz – 100 kHz	New Focus 1811-FC	FFT
100 kHz – 100 MHz	New Focus 1811-FC	Swept Mode
100 MHz – 500 MHz	Agilent 83440C	Swept Mode

The measured RIN is shown in Figure 4.17. The change in spectrum analyser at 100 kHz required the data to be stitched with a multiplicative factor so that the data is matched. Similarly, this was also required at 100 MHz to account for the change in photodetector. The stitching was done for the free running measurement first. For consistency, the phase locked measurement were subsequently stitched using the same multiplicative factors as the free running case. The instrument noise floor was measured with no optical input into the photodetectors.

It can be seen from Figure 4.17 that for frequencies less than 10 kHz, the RIN was suppressed by the locking process, particularly for frequencies less than 1 kHz. A lower RIN suppression of approximately 2–5 dB also occurred at higher frequencies (< 10 MHz). It has been reported in the literature [16, 17] that the injection locking process is expected to suppress RIN, since the amplification of the injected signal uses up more of the laser's available gain, which reduces spontaneous emission. However, Figure 4.17 shows that the RIN increased with injection ratio, which is in contrast to the what is expected from theory [16] and previous experimental results [17]. A possible reason for this is because an OFC was used in this experiment, which was not the case in [16, 17] where the master

was a single frequency cw laser. It is likely that the increase in RIN at larger injection ratios was a result of additional noise from the residual comb modes.

A contribution to the intensity noise due to the OFC injection can be seen at 250 MHz due to the residual comb modes. It should be noted that these measurements were taken with the detuning dependent residual comb mode amplification at the minimum (the same as for the phase noise measurements). The RIN at 250 MHz is expected to be larger if the residual comb amplification was not minimised.

The RIN measurements in Figure 4.17 are still limited by the instrument noise floor at frequencies below 100 kHz for injection ratios below –53 dB. This is evident in the discontinuities in the RIN where the data has been stitched together without any scaling factors (at 1 and 10 kHz), which matches the instrument noise floor. As a result of the poor stitching, the absolute values for the RIN above 1 kHz are ambiguous in Figure 4.17 and should not be taken as representative of the actual value. The measured RIN in the range 30–100 MHz was lower than the noise floor; this is believed to be due to oscillations in the transimpedance amplifier in the photodetector occurring when there is no optical input, and hence is not the true noise floor. These measurements could be improved to find the true extent of the RIN suppression by using lower noise RF spectrum analysers.

4.5 Conclusions

This chapter has investigated the noise properties of slave lasers which were phase locked using the technique from the previous chapter. The long-term frequency stability was evaluated by measuring the frequency variation of the locked laser over a period of 8 hours. The Allan deviation was calculated from this data and was found to be 9.1×10^{-17} at an averaging time of 1 s. It reached a minimum 4.4×10^{-19} at 1000 s, but was found to have a long-term frequency drift after 1000 s.

The short-term phase stability was investigated by measuring the phase noise associated with the locking process. It was found that a small locking range decreased the robustness of the locking since there was less tolerance to frequency fluctuations in the slave laser. However, a larger locking range increased the amplification of neighbouring comb modes which were simultaneously injected into the slave laser. The phase noise was minimised by locking the slave laser at a detuning which minimised the amplification of residual comb modes, and by using an injection ratio which balanced the effects of having too wide or too narrow of a locking range. At the optimum injection ratio for my measurements (–63 dB), the integrated phase noise across the measurement bandwidth (100 Hz to 500 MHz) was 0.02 rad^2. It was found that the contribution to the integrated phase noise from the amplified residual comb modes is small if the detuning was tuned to minimise this amplification. Ideally, the phase noise and Allan deviation measurements

would be done simultaneously to increase the correlation between the measurements. This can be considered for future work.

Finally, the amplitude noise of the slave laser was investigated by measuring the RIN. The RIN of the locked laser was found to be small and the measurements were limited by the instrument noise floor. Despite this, it was found that the phase locking suppressed the RIN of the slave laser, which was consistent with the literature. However, in contrast to the literature, the RIN was found to increase with injection ratio. This was believed to be because an OFC was used as the master, and by increasing the power of the residual comb modes via the injection ratio, the RIN also increased.

4.6 References

[1] S. Droste, F. Ozimek, T. Udem, K. Predehl, T. W. Hänsch, H. Schnatz, G. Grosche, and R. Holzwarth, "Optical-frequency transfer over a single-span 1840 km fiber link," *Physical Review Letters*, vol. 111, p. 110801, Sept. 2013.

[2] W. F. Walls and F. L. Walls, "Computation of time-domain frequency stability and jitter from PM noise measurements," in *Proceedings of the International Conference on Time and Frequency (ICTF)*, pp. 218–225, 2001.

[3] Eagleyard Photonics GmbH, *Application Note - Relative Intensity Noise of Distributed Feedback Lasers*. Accessed 30/01/2014, 2014.

[4] E. Rubiola, K. Volyanskiy, and L. Larger, "Measurement of the laser relative intensity noise," in *2009 IEEE International Frequency Control Symposium Joint with the 22nd European Frequency and Time forum*, pp. 50–53, 2009.

[5] W. J. Riley, *NIST Special Publication 1065: Handbook of Frequency Stability Analysis*. Boulder, CO, USA: National Institute of Standards and Technology, 2008.

[6] D. W. Allan, "Should the classical variance be used as a basic measure in standards metrology?," *IEEE Transactions on Instrumentation and Measurement*, vol. IM-36, no. 2, pp. 646–654, 1987.

[7] J. Ye and S. T. Cundiff, *Femtosecond optical frequency comb: principle, operation, and applications*. Kluwer Academic Publishers/Springer, 2005.

[8] F. Acernese, M. Alshourbagy, F. Antonucci, S. Aoudia, K. Arun, P. Astone, G. Ballardin, F. Barone, L. Barsotti, M. Barsuglia, T. Bauer, S. Bigotta, S. Birindelli, M. Bizouard, C. Boccara, F. Bondu, L. Bonelli, L. Bosi, S. Braccini, C. Bradaschia, A. Brillet, V. Brisson, H. Bulten, D. Buskulic, G. Cagnoli, E. Calloni, E. Campagna, B. Canuel, F. Carbognani, L. Carbone, F. Cavalier, R. Cavalieri, G. Cella, E. Cesarini, E. Chassande-Mottin, S. Chatterji, F. Cleva, E. Coccia, J. Colas, M. Colombini, C. Corda, A. Corsi, F. Cottone, J.-P. Coulon, E. Cuoco, S. DAntonio, A. Dari, V. Dattilo, M. Davier, R. De Rosa, M. Del Prete, L. Di Fiore, A. Di Lieto, M. Di Paolo Emilio, A. Di Virgilio, V. Fafone, I. Ferrante, F. Fidecaro, I. Fiori, R. Flaminio, J.-D. Fournier, S. Frasca, F. Frasconi, L. Gammaitoni, F. Garufi, G. Gemme, E. Genin, A. Gennai, A. Giazotto, M. Granata, V. Granata, C. Greverie, G. Guidi, H. Heitmann, P. Hello, S. Hild, D. Huet, P. La Penna, M. Laval, N. Leroy, N. Letendre, M. Lorenzini, V. Loriette, G. Losurdo, J.-M. Mackowski, E. Majorana, N. Man, M. Mantovani, F. Marchesoni, F. Marion, J. Marque, F. Martelli, A. Masserot, F. Menzinger, C. Michel, L. Milano, Y. Minenkov, S. Mitra, M. Mohan, J. Moreau, N. Morgado, A. Morgia, S. Mosca, B. Mours, I. Neri, F. Nocera, G. Pagliaroli, C. Palomba, F. Paoletti, S. Pardi, A. Pasqualetti, R. Passaquieti, D. Passuello, G. Persichetti, F. Piergiovanni, L. Pinard, R. Poggiani, M. Punturo, P. Puppo, O. Rabaste, P. Rapagnani, T. Regimbau, F. Ricci, A. Rocchi, L. Rolland, R. Romano, P. Ruggi, B. Sassolas, D. Sentenac, B. Swinkels, R. Terenzi, A. Toncelli, M. Tonelli, E. Tournefier, F. Travasso, J. Trummer, G. Vajente, J. van den Brand, S. van der Putten, D. Verkindt, F. Vetrano, A. Viceré, J.-Y. Vinet, H. Vocca, M. Was, and M. Yvert, "Laser with an in-loop relative frequency stability of 1.01021 on a 100-ms time scale for gravitational-wave detection," *Physical Review A*, vol. 79, no. 5, p. 053824, 2009.

[9] X. Yi, W. Shieh, and Y. Ma, "Phase noise effects on high spectral efficiency coherent optical OFDM transmission," *Journal of Lightwave Technology*, vol. 26, no. 10, pp. 1309–1316, 2008.

[10] R. Paschotta, "Noise in laser technology," *Optik & Photonik*, vol. 4, no. 2, pp. 48–50, 2009.

[11] T. Okoshi, K. Kikuchi, and A. Nakayama, "Novel method for high resolution measurement of laser output spectrum," *Electronics Letters*, vol. 16, no. 16, p. 630631, 1980.

[12] G. Marra, H. S. Margolis, and D. J. Richardson, "Dissemination of an optical frequency comb over fiber with 3 10(18) fractional accuracy," *Optics Express*, vol. 20, no. 2, pp. 1775–1782, 2012.

[13] H. Y. Ryu, S. H. Lee, W. K. Lee, H. S. Moon, and H. S. Suh, "Absolute frequency measurement of an acetylene stabilized laser using a selected single mode from a femtosecond fiber laser comb," *Optics Express*, vol. 16, no. 5, pp. 2867–2873, 2008.

[14] Y. J. Kim, B. J. Chun, Y. Kim, S. Hyun, and S. W. Kim, "Generation of optical frequencies out of the frequency comb of a femtosecond laser for DWDM telecommunication," *Laser Physics Letters*, vol. 7, no. 7, pp. 522–527, 2010.

[15] A. E. Siegman, *Lasers*. Mill Valley, CA: University Science Books, 1986.

[16] T. B. Simpson, J. M. Liu, and A. Gavrielides, "Bandwidth enhancement and broadband noise reduction in injection-locked semiconductor lasers," *IEEE Photonics Technology Letters*, vol. 7, no. 7, pp. 709–711, 1995.

[17] X. Jin and S. L. Chuang, "Relative intensity noise characteristics of injection-locked semiconductor lasers," *Applied Physics Letters*, vol. 77, no. 9, pp. 1250–1252, 2000.

Chapter 5

Residual Comb Mode Amplification

It was found in the previous chapter that although a slave laser can lock to an individual comb mode of an OFC, the adjacent comb modes may experience some amplification. The amount of amplification was dependent on the master-slave frequency detuning ($\Delta\omega$). Although the residual comb modes were significantly weaker than the locked mode, they still constituted unwanted signals. This phenomenon was also observed by Fukushima et al. [1] using a 10 GHz spaced OFC as the master. As they varied their detuning across the locking range, it was found that the maximum residual comb mode was –32.5 dB relative to the laser mode. This was considered to be sufficient suppression for their application (millimetre wave generation) and hence was not further investigated.

The residual comb mode amplification is studied further in this chapter to better understand its origins and how to minimise it. The experimental measurements of the residual comb mode amplification are first presented, followed by numerical modelling of the slave laser using the semiconductor laser rate equations.

5.1 Fabry-Pérot filter measurement

The narrow comb spacing of the OFC used in my experiments made it challenging to directly measure the power of the residual comb modes of the slave laser. This was due to difficulties in distinguishing between the residual comb modes from the locked laser mode. My first attempt to measure the relative power of the residual comb modes was by using a tunable narrowband Fabry-Pérot filter (FPF). This was manufactured by Micron Optics and was specified to have a free spectral range (FSR) of 69.47 GHz and a finesse of 695, which corresponded to a passband of approximately 100 MHz.

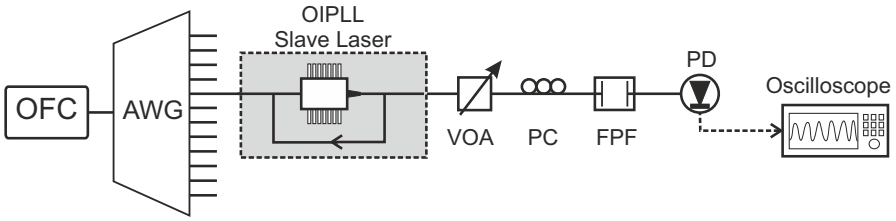

FIGURE 5.1: The set-up for measuring the relative power of the residual comb modes using a Fabry-Pérot filter (FPF).

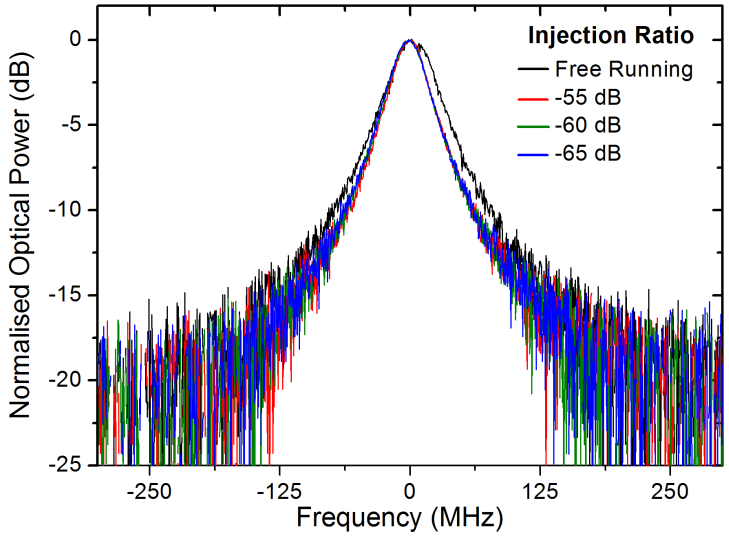

FIGURE 5.2: The measured optical power using the FPF scanned across the locked mode and the two adjacent residual comb modes for various injection ratios.

The experimental set-up is shown in Figure 5.1. The central frequency of the FPF passband was scanned by applying a linearly increasing voltage to the internal PZT. The relative residual comb mode power was to be measured by sweeping the FPF passband across the locked laser mode and the adjacent residual comb modes. The photodetector signal was recorded on an oscilloscope.

The results are shown in Figure 5.2 for a range of injection ratios. The free running spectrum was wider than the locked spectra, which was likely due to the frequency drift of the unlocked laser. The results for the locked spectra do not show the presence of any residual comb modes in the slave laser. They were likely obscured by the high level of noise at the frequencies where they were expected to be measured ($\pm$250 MHz). The noise of approximately –17.5 dB was larger than the expected residual comb mode power and hence it was not surprising that they could not be observed. There are two possible reasons for this high noise level. Firstly, the voltage scale of the oscilloscope needed to be large in order to measure the laser mode. This however, imposed a voltage resolution limit which made it difficult to accurately measure weaker signals and effectively limited the sensitivity of the measurement. The low sensitivity of the measurement could potentially be overcome by using a power meter instead of a simple photodetector. This would have significantly increased the dynamic range of the measurement. Unfortunately, a

sufficiently sensitive power meter with data logging capabilities was not readily available. The second reason behind why the residual comb modes were not measured was likely due to the FPF. The passband may not have been sufficiently narrow to be able to measure the residual comb mode with a negligible contribution from the laser mode. It was concluded from the results presented here that it was not possible to measure the relative power of the residual comb modes using the set-up in Figure 5.1.

5.2 RF-based measurement

An alternative measurement technique was required to find the relative power of the residual comb modes. RF-based measurements were attempted using the beat signal generated between the slave laser and a separate reference laser at their frequency difference, ΔF. The total electric field of a signal containing the reference laser E_{ref} and the slave laser E_S is given by

$$\tilde{E}_{tot} = \tilde{E}_{ref} + \tilde{E}_S, \tag{5.1}$$

with

$$\tilde{E}_{ref} = E_{ref}\ e^{i[(\omega_0+\Delta F)t]}\ , \tag{5.2}$$

$$\tilde{E}_S = E_{-1}\ e^{i[(\omega_0-f_r)t]} + E_0 e^{i[(\omega_0)t]} + E_{+1}\ e^{i[(\omega_0+f_r)t]}, \tag{5.3}$$

where the subscripts ± 1 refer to the two adjacent residual comb modes and 0 refers to the main mode of the locked slave laser. For simplicity, only the two adjacent comb modes are considered here and the relative phase of each component has been neglected. The photocurrent measured by a photodetector is given by $i_{\text{photo}} \propto E_{tot}E_{tot}^*$. The beat signals between the reference laser and the slave laser (and residual comb modes) are given by the cross terms of i_{photo} and are given by

$$i_{\text{beat}} \propto 2E_{ref}E_0 \cos\left[\Delta F t\right] + 2E_{ref}E_{-1} \cos\left[(f_r - \Delta F)t\right] + 2E_{ref}E_{+1} \cos\left[(f_r + \Delta F)t\right]. \tag{5.4}$$

An RF spectrum analyser, which measures electrical power, can be used to measure these different frequency signals. The electrical power is proportional to the square of the photocurrent and hence the power of each beat signal at frequency f ($P_{RF}(f)$) is given by

$$P_{RF}(f = \Delta F) \propto E_{ref}^2 E_0^2, \tag{5.5}$$

$$P_{RF}(f = f_r - \Delta F) \propto E_{ref}^2 E_{-1}^2, \tag{5.6}$$

$$P_{RF}(f = f_r + \Delta F) \propto E_{ref}^2 E_{+1}^2.$$

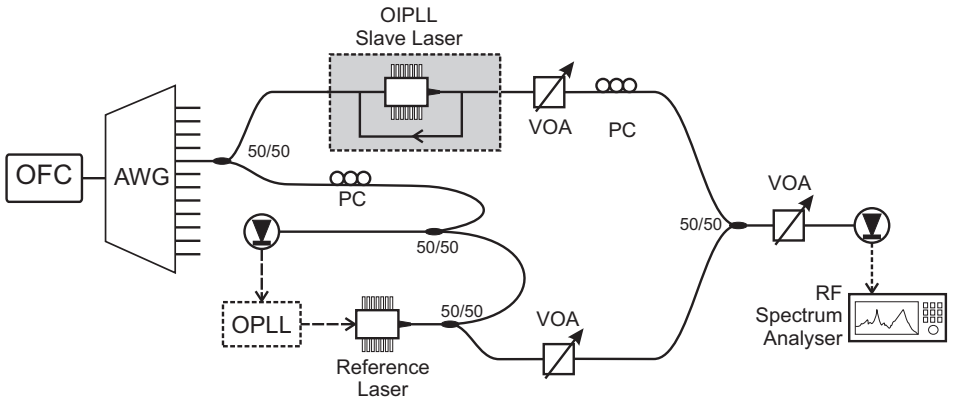

FIGURE 5.3: The experimental set-up for measuring the relative power of the residual comb modes of a slave laser based on the beating with a reference laser.

Therefore, from Equation (5.5), the relative power between the residual comb modes ($E_{\pm1}^2$) and the main mode of the slave laser (E_0^2) can be found by measuring the relative RF power of their corresponding beat signals ($^{P_{RF}(f=f_r\pm\Delta F)}/_{P_{RF}(f=\Delta F)}$). It should be noted that a beat signal at $f = f_r$ will also be present due to the main mode of the slave laser and the residual comb modes. However, these would be significantly weaker than the beat signals in Equation (5.5) if the power of reference laser is comparable to the slave laser.

The experimental set-up is shown in Figure 5.3 and the parameters of the lasers are provided in Table 5.3. The reference laser was a discrete mode semiconductor laser, similar to the slave laser, but had an in-built isolator which reduced the free-running noise. A heterodyne OPLL was employed to keep the frequency of the reference laser locked to 30 MHz away from the slave laser. This was done by locking the reference laser to the same comb mode as the slave laser using the OPLL equipment available with the Menlo Systems OFC. The locked reference laser had frequency variations of approximately ±1 MHz over 10 s. This OPLL performance was poor as compared to my phase locking technique (the OIPLL) used to lock the slave laser to the OFC. However, the OPLL was not fully optimised since this level of performance was sufficient for the residual comb mode power measurement. A VOA was placed before the photodetector to ensure it was not saturated. The photodetector was reverse biased with no transimpedance amplifier, had a bandwidth of 1.2 GHz, and a responsivity of 0.95 A/W.

An example of one of the RF spectrum measurements is shown in Figure 5.4(a). The strong signal at 30 MHz corresponds to the beating between the laser mode of the slave laser and the reference laser. The weaker signals at 220 and 280 MHz correspond to the beating between the residual comb modes and the reference laser. The relative RF powers were measured between the main beat signal (30 MHz) and the signal at 280 MHz.

TABLE 5.1: Laser parameters in Figure 5.3

Slave laser	Type	Discrete mode
	Output power	+12 dBm
	Operating current	130.98 mA
	Operating temperature	35.61°C
	Connector type	FC/APC
	Fibre type	SMF-28
	Built-in isolator	no
Reference laser	Type	Discrete mode
	Output power	+10 dBm
	Operating current	103.75 mA
	Operating temperature	31.74°C
	Connector type	FC/APC
	Fibre type	SMF-28
	Built-in isolator	yes

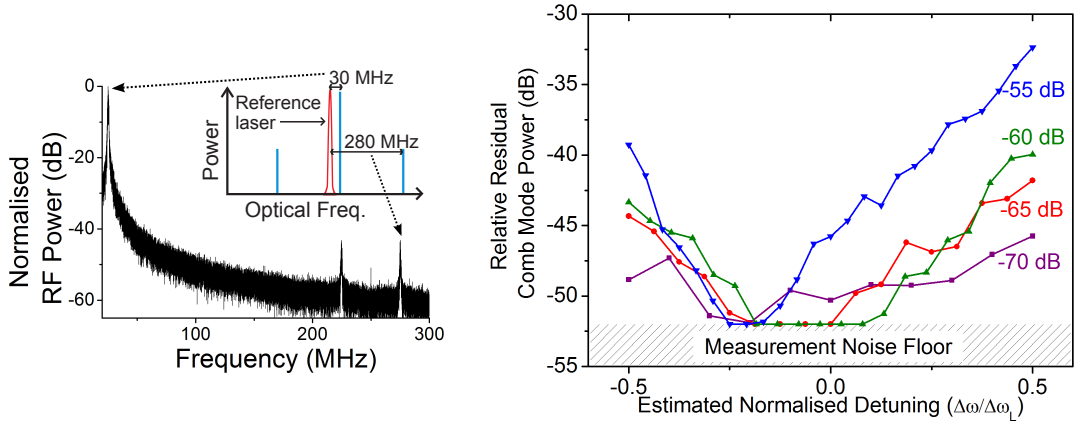

(a) RF spectrum and illustration of the corresponding optical spectrum

(b) Measurement for various injection ratios

FIGURE 5.4: RF measurement of the relative power of one of the adjacent residual comb modes of the slave laser.

The measurements of relative power were made at regular intervals of detuning across the locking range. The noise of the beat signal prevented any measurements below –52 dB. This noise floor was significantly lower than for the FPF measurements in the previous section. The detuning dependent relative power of one of the adjacent comb modes, with respect to the laser mode of the slave laser, is shown in Figure 5.4(b) for various injection ratios.

The detuning was controlled by tuning the locking position of the slave laser feedback loop by introducing an offset to the feedback error signal. The actual detuning could not be directly measured since the slave laser was emitting at the same frequency as the comb mode it was locked to. The detuning was therefore estimated based on two assumptions:

1. The entire locking range was accessible by locking the feedback loop to an offset value.
2. The error signal was linear across the locking range.

The second assumption was made based on the sufficiently large α factor of the slave laser used (Section 3.2.2, Figure 3.9). Nevertheless, it should be emphasised that the normalised detuning values in Figure 5.4(b) were estimated with a large associated uncertainty.

Despite the uncertainty in the detuning, some useful information could still be extracted from Figure 5.4(b). For locking ratios up to –55 dB, the residual comb mode power was always less than –32 dB relative to the laser mode. Compared to the injection ratios used, this represented a large amplification of the residual comb modes. The maximum amplification occurs at one edge of the locking range and as the detuning was tuned towards the other edge, the residual comb mode power decreases and drops below the measurement noise floor near the centre of the locking range. As the detuning continued to be tuned closer to the other edge of the locking range, the residual comb mode power increases again, but does not become as large as at the other edge. This trend was present for all the injection ratios measured. This was consistent with the observations made in Chapter 4, where the residual comb modes could always be minimised by tuning $\Delta\omega$. The measurement noise floor prevented an accurate measurement of the maximum suppression of the residual comb mode amplification.

It can also be seen from Figure 5.4(b) that the maximum amplification of the residual comb mode decreased as the injection ratio was decreased. The detuning dependence of the amplification appears to be more flat as the injection ratio decreases. This suggests that although the maximum residual comb mode power is reduced at low injection ratios, it cannot be suppressed as much as at high injection ratios. However, this apparent increase in flatness may be an artefact of the measurement due to the noise floor.

The results show an asymmetric behaviour of the residual comb mode power with detuning across the locking range. This was most likely due to the uncertainty in estimating the detuning. For example, it might have been incorrect to assume the entire locking range was accessible by offset locking the feedback loop. If the accessible locking range itself was asymmetric, then this asymmetry would directly map across to the estimated locking range. Furthermore, as the size of the locking range increases, the normalisation of the locking range would make the actual zero detuning diverge further away from the estimated zero detuning. This would exaggerate the artificial asymmetry effect and make the minimum in the residual comb mode power appear to drift away from zero detuning as the injection ratio increases, as observed in Figure 5.4(b).

5.3 Numerical simulations

The experimental results from the previous section showed that the residual comb mode amplification does have a dependence on both the detuning and the injection ratio. Limitations in the measurement, due to the uncertainty in the detuning and the high noise floor, prevented the true relationship between this amplification with detuning/injection ratio from being accurately measured. The remainder of this chapter will use numerical simulations in an attempt to better understand this phenomenon.

5.3.1 Laser rate equations with optical injection

For this analysis, it was assumed that the OPLL (electronic feedback) component of the OIPLL does not have an active role in the residual comb mode amplification due to its very low bandwidth with respect to the comb spacing. In other words, this will be treated as a purely optical injection locking effect.

The semiconductor laser rate equations can be readily modified to include the effects of optical injection. These have been extensively used to analytically and numerically study the process of optical injection locking in semiconductor lasers. Examples include: the derivation of the size of locking range ($\Delta\omega_L$) and phase shift ($\Delta\phi_L$) [2, 3]; the study of OIL stability [4, 5]; and to investigate the OIL modulation properties [6, 7]. Prior to my work presented here, to my knowledge, there had not been any numerical or analytical study of OIL using a multi-frequency master such as an OFC.

Optical injection by an OFC can be readily incorporated into the standard semiconductor laser rate equations. From Mogensen et al. [3], the rate equation for the electric field of a semiconductor slave laser under optical injection is given by

$$\frac{d}{dt}\tilde{E}_S(t) - \left(i\omega(N) + \frac{1}{2}\left[G(N) - \frac{1}{\tau_p}\right]\right)\tilde{E}_S(t) = \frac{K}{\tau_c}\tilde{E}_M(t)\ , \tag{5.7}$$

where $\tilde{E}_S(t)$ and $\tilde{E}_M(t)$ are the time dependent complex electric fields of the slave and master lasers; $\omega(N)$ is the angular optical frequency and $G(N)$ is the modal gain per second of the slave laser, both of which are dependent on the carrier density N; τ_p is the photon lifetime in the laser cavity; K is the external coupling efficiency of the slave laser; and τ_c is the round trip time inside the laser cavity.

The complex electric fields can be defined as:

$$\tilde{E}_S(t) = \quad E_S(t)\ e^{i[\omega_S t + \phi_S(t)]}\ , \tag{5.8}$$

$$\frac{K}{\tau_c}\tilde{E}_M(t) = \quad \sum_j \left\{E_{\text{inj}}\ e^{i[\omega_j t + \varphi]}\right\}\ , \tag{5.9}$$

where $E_S(t)$, ω_S, and $\phi_S(t)$ are the real valued amplitude, free running angular frequency and phase of the slave laser respectively. The injected OFC is described in Equation (5.9), where the subscript j is an index for each injected comb mode. For my analysis, I have assumed that each comb mode at the input of the slave laser had equal and constant amplitudes given by E_{inj}. It was also assumed that the comb modes have the same initial phase, φ, which was set to 0. The angular frequency of each comb mode is given by ω_j.

The expressions for the complex electric fields can be substituted into Equation (5.7). By separating the real and imaginary parts, and following similar steps to those taken in [3], the rate equations for the amplitude, phase, and carrier density can be written as:

$$\frac{d}{dt}E_S(t) = \frac{1}{2}G_N\left[N(t) - N_{th}\right]E_S(t) + E_{\text{inj}}\sum_j \cos\left(\delta\omega_j t - \phi_S(t)\right) \ , \tag{5.10}$$

$$\frac{d}{dt}\phi_S(t) = \frac{1}{2}\alpha G_N\left[N(t) - N_{th}\right] + \frac{E_{\text{inj}}}{E_S(t)}\sum_j \sin\left(\delta\omega_j t - \phi_S(t)\right) \ , \tag{5.11}$$

$$\frac{d}{dt}N(t) = R_p - \frac{N(t)}{\tau_s} - G_N\left[N(t) - N_{th}\right]E_S(t)^2 - \frac{1}{\tau_p}E_S(t)^2 \ . \tag{5.12}$$

Equations (5.10)–(5.11) are the modified rate equations for the electric field ampltidue and phase respectively, while Equation (5.12) is the standard (unmodified) rate equation for the carrier density $N(t)$. The definitions and values of the constants in Equations (5.10)–(5.12) are given in Table 5.2. $\delta\omega_j = \omega_j - \omega_S$ is the detuning between each comb mode and the slave laser. The gain was assumed to be independent of wavelength since only a small number of closely spaced comb modes were considered in this analysis. The injection ratio is defined as E_{inj}/E_{S0}, where E_{S0} is the steady-state electric field amplitude of the free running (no optical injection) slave laser. The values of G_N, τ_s, and τ_p were estimated based on values used by others in the literature [3, 4].

TABLE 5.2: Semiconductor laser parameters used in the rate equation modelling

$G_N = 8.1 \times 10^{-13}$ m^{3}s^{-1}	Differential gain
$N_{th} = 1.7172 \times 10^{24}$ m^{-3}	Carrier density at threshold (includes cavity losses)
$\alpha = 5$	Linewidth enhancement factor
$K = 0.2$	Injected light coupling coefficient
$\tau_c = 6 \times 10^{-12}$ s	Laser cavity round trip time
$R_p = 1.7833 \times 10^{34}$ s^{-1}	Pump rate
$\tau_s = 2 \times 10^{-9}$ s	Carrier lifetime
$\tau_p = 2 \times 10^{-12}$ s	Photon lifetime

Equations (5.10)–(5.12) are used in the next section to analyse the influence of the residual comb modes on the injection locking process. The initial values of $E_S(0)$,

$\phi_S(0)$, and $N(0)$ were chosen to correspond with the steady state solution of the free running slave laser with no optical injection.

As discussed in [8], there are some features which are overlooked in this model of the slave laser:

- The model only specifies that a semiconductor laser is the slave laser but does not specify the type of semiconductor laser. For example, any effects due to the structure of the laser (e.g. distributed feedback, Fabry-Pérot, or discrete mode) is not included in this model. The inclusion of these features would only be likely to affect the coupling efficiency between the master and slave.
- Noise of either the slave or master laser were not incorporated into this model, including the effects of spontaneous emission. Although this may improve the accuracy of the results, it will slow down the numerical calculations and the noise could obscure the effects of interest.
- This model does not include non-linear interactions such as four-wave mixing. However, these effects were likely to be weak due to the low injection ratios. Also, only a narrow bandwidth of comb modes were injected, which corresponds to long pulses in the temporal domain and hence low peak power which also weakens any non-linear effects.

Despite these shortcomings, models with the same limitations have previously been successful in providing physical insight into the injection locking process. Therefore, this model was also expected to provide some understanding of the influence of the residual comb modes and how they may be amplified.

5.3.2 Results

Residual comb mode power

An injection signal consisting of 9 comb modes with a comb spacing of 250 MHz was first considered to check for consistency with the measured results in Section 5.2. The free running frequency of the slave laser was chosen such that it would injection lock to the central comb mode. The rate equations were solved numerically in the time domain using the Matlab ODE45 ordinary differential equation solver. The output power of the injection locked slave laser was calculated ($P = E^*E$) and Fourier transformed into the frequency domain using a fast Fourier transform (FFT) algorithm.

The relative power of one of the residual comb modes with respect to the lasing mode is shown in Figure 5.5(a) as a function of detuning, which was varied in steps of 0.5 MHz. The injection ratio was also varied from –70 dB to –55 dB. Similar to the experimental

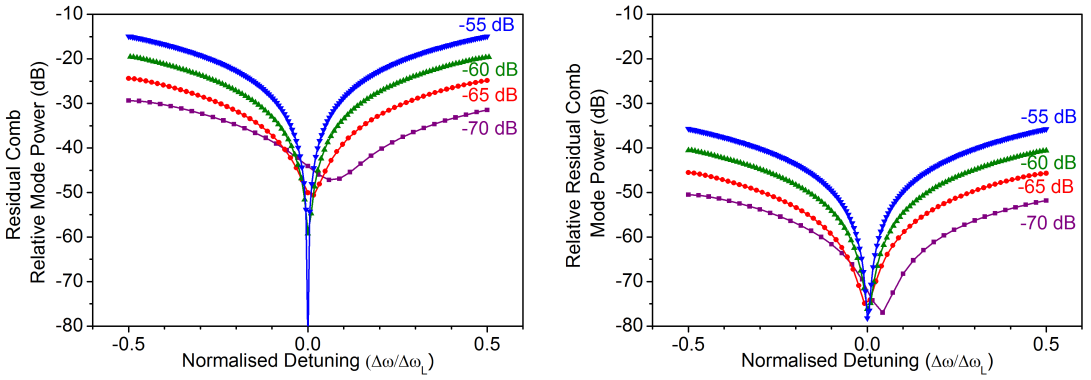

(a) 250 MHz comb spacing

(b) 2.5 GHz comb spacing

FIGURE 5.5: The calculated relative power of one the residual comb modes adjacent to the lasing mode for various injection ratios for two different spaced OFCs.

results, Figure 5.5(a) shows that regardless of the injection ratio, $\Delta\omega$ can be tuned to suppress the residual comb mode power. Surprisingly, for higher injection ratios, the residual comb mode power can be lower than its injected power. The residual comb mode power was at its maximum at the edges of the locking range and this maximum power increased with increasing injection ratios, which is consistent with the experimental measurements.

There were some discrepancies between the experimentally measured and numerically calculated results. The calculated results only showed a slight asymmetry of the residual comb mode power with detuning, and it was only noticeable at low injection ratios. The residual comb mode amplification was also larger in the numerical results as compared to the experimental results, with the relative power of the residual comb mode reaching as high as –15 dB. These discrepancies were likely due to the previously discussed inaccurate assumptions about the estimated locking range used to take the previous measurements. In particular, it was likely that the entire locking range was not accessible for the measurements which could have contributed to the strong asymmetry observed. Also, the parameters used in Table 5.2 were unlikely to accurately reflect the slave laser used in the experiment.

It was expected that the use of a wider spaced OFC would reduce the power of the residual comb modes since they would be located further away from the locking range of the slave laser. To test this hypothesis, the numerical calculations were repeated with the comb spacing increased by a factor of 10 to 2.5 GHz. The results are shown in Figure 5.5(b), where the residual comb mode powers were significantly lower than when the narrower spaced OFC was injected. The other features were still present with the wider spaced OFC such as the detuning dependent residual comb mode suppression, and the small asymmetry at low injection ratios.

Residual comb mode contribution from amplitude and phase modulation

Although there was some consistency between the experimental and numerical results, the cause of the amplification of the residual comb modes was still unclear. From Equation (5.10) and (5.11), it is evident that the injected comb modes causes amplitude and phase modulation of the slave laser. This modulation generates sidebands in the spectral domain which contribute to the power of the residual comb modes and hence causes their amplification. To more clearly study the effects of the injected adjacent comb modes, the rate equations were solved for the simpler scenario of three injected comb modes, with the slave laser locked to the central mode.

Figure 5.6 shows examples of the numerical solutions for $E_S(t)$ and $\phi_S(t)$ with three injected modes spaced 250 MHz apart and at an injection ratio of –60 dB. Figure 5.6(a)–(b) shows the amplitude (E_S) and phase (ϕ_S) with zero detuning between the slave laser and the locked mode, whereas in Figure 5.6(c)–(d) the detuning was 5 MHz. In these calculations, the slave laser was initially in its free running state with the comb modes injected at time $t = 0$. It can be seen from these figures that there was a transitional state after the comb injection where the slave laser goes from free-running to injection locked. After this transitional state (approximately 20 ns), the slave laser reached a quasi-steady state where the amplitude and phase oscillated at a frequency corresponding to the frequency spacing between the injected modes. In Figure 5.6(d), the quasi-steady phase had a linear component which was calculated to have a slope of $2\pi \times 5 \times 10^6$ rad s^{-1}. This component confirms that injection locking has occurred since this linear change in the slave laser phase with time corresponds to a 5 MHz frequency shift of the slave laser.

Figure 5.7 shows the solutions to the rate equations with the comb spacing increased to 2.5 GHz. The amplitude and phase in the quasi-steady states oscillated around the same values as in the case with a comb spacing of 250 MHz. As expected, the frequency of the oscillations increased to the same value as the comb spacing. It was found that the oscillations in the electric field amplitude were larger with the wider comb spacing, while the phase oscillations were smaller.

These oscillations in the slave laser electric field corresponded to amplitude and phase modulation respectively. From Figures 5.7 & 5.6, it can be seen that in the quasi-steady state, the amplitude and phase of the locked slave laser can be described by:

$$E_{quasi}(t) = E_{locked} + a \times sin(\Omega t), \tag{5.13}$$

$$\phi_{quasi}(t) = \phi_L + \Delta\omega \times t + b \times cos(\Omega t), \tag{5.14}$$

where a and b are the amplitude and phase modulation depths respectively, which are dependent on the injection locking detuning ($\Delta\omega$) and the angular comb spacing frequency (Ω). The term ϕ_L corresponds to the injection locking phase shift introduced in

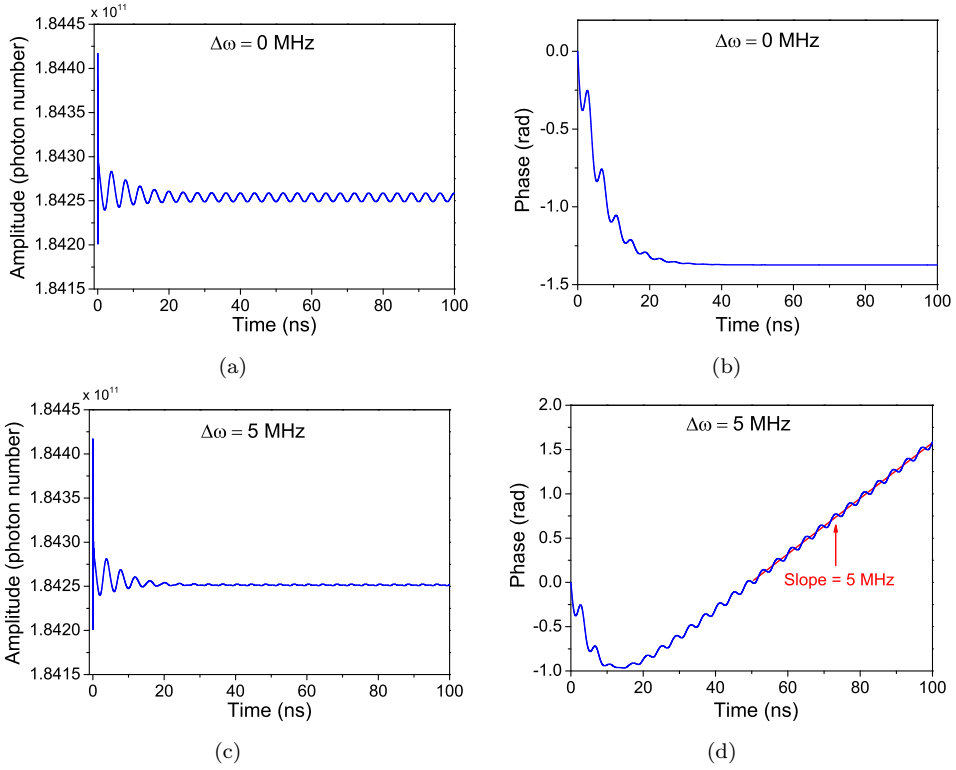

FIGURE 5.6: Examples of the rate equation solutions for amplitude (a, c) and phase (b, d) for three injected comb modes with 250 MHz spacing at two different values of detuning. Injection ratio: –60 dB

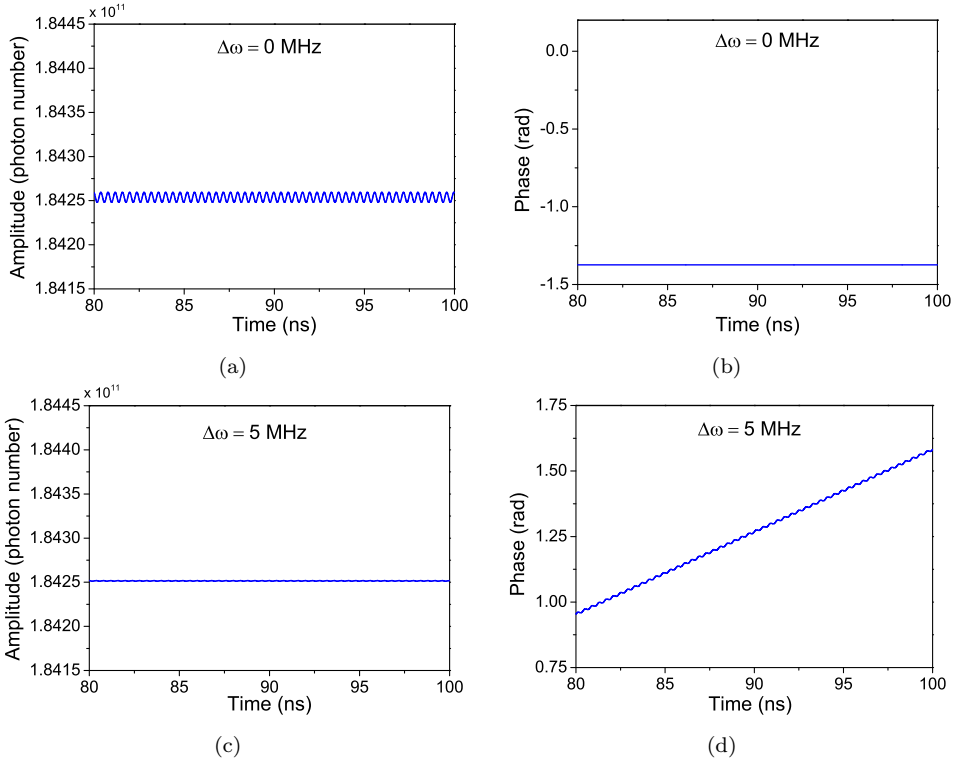

FIGURE 5.7: Rate equation solutions using the same parameters as Figure 5.6, but with a mode spacing of 2.5 GHz. Only the quasi-steady state is shown.

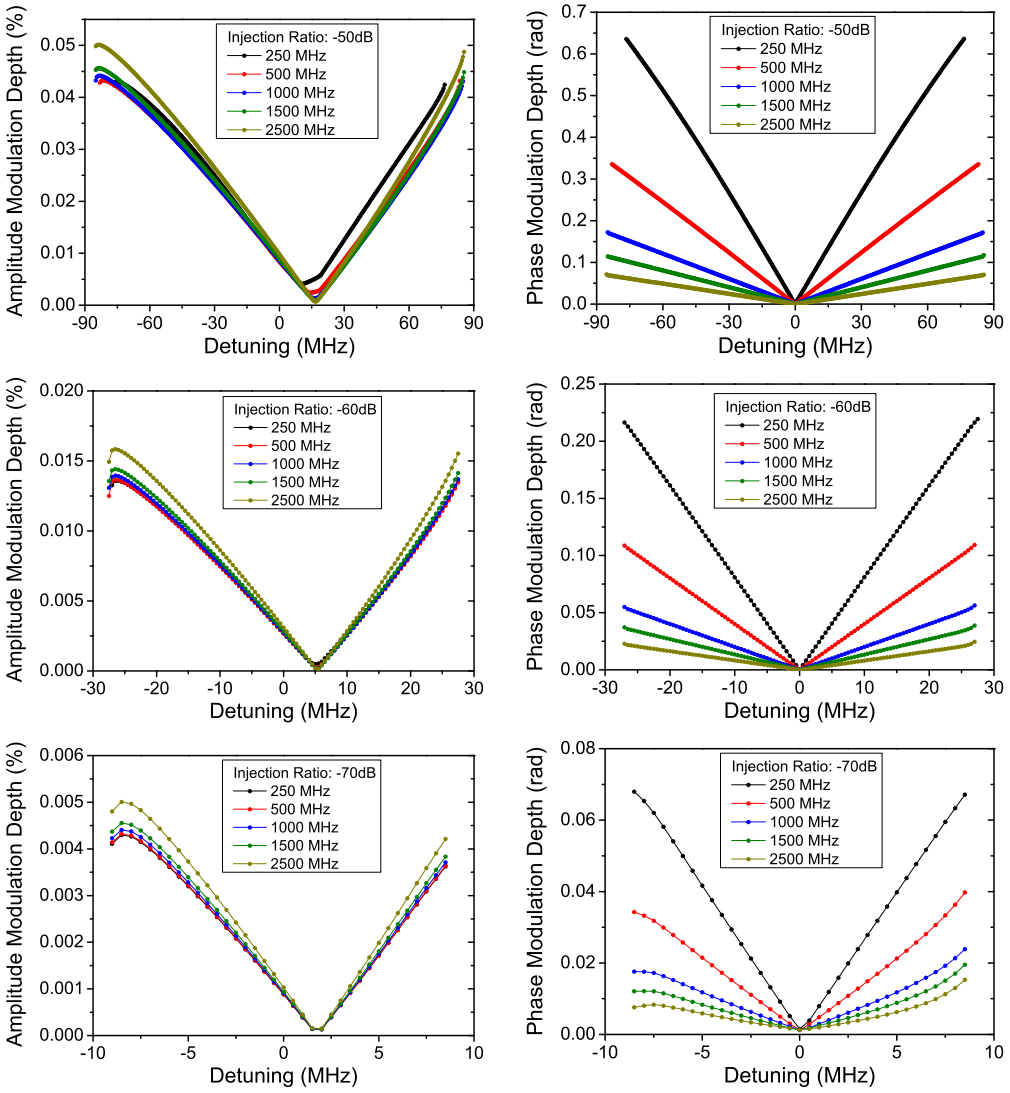

FIGURE 5.8: Amplitude and phase modulation depths for various injection ratios and comb spacings

Section 2.2.2 (Equation (2.7)), and E_{locked} is the constant component of the slave laser amplitude.

The amplitude and phase modulation depths were extracted across the locking ranges for various injection ratios and comb spacings with some examples given in Figure 5.8. Overall, the amplitude modulation depths were always very small and only had small variations with comb spacing. This suggests that the amplitude modulation only had a small effect on the residual comb mode amplification. However, asymmetry with detuning was observed which was similar to the residual comb mode power calculated at low injection ratios (–70 dB) in Figure 5.5. It is likely that only at very low injection ratios does the amplitude modulation have a non-negligible contribution to the residual comb mode amplification.

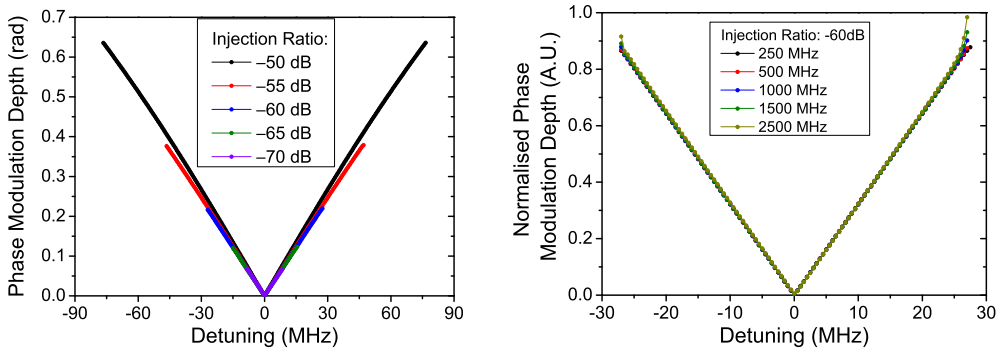

(a) Fixed mode spacing (250 MHz) (b) Modulation depth normalised to mode spacing

FIGURE 5.9: The relationship between phase modulation depth and comb mode spacing

The phase modulation depths were found to be approximately linear and symmetric with detuning, with the maximum modulation occurring at the edges of the locking ranges and the minimum at zero detuning. The phase modulation depth was reduced as the mode spacing was widened, which is consistent with the results in Figure 5.5. It was also found that for a given mode spacing, the phase modulation depth was mostly dependent on the absolute value of the detuning as shown in Figure 5.9(a), with only a small variation with injection ratio. A higher injection ratio simply increased the size of the locking range, which made larger detunings accessible and hence allowed for a larger maximum modulation depth.

The influence of the mode spacing can be seen in Figure 5.9(b). This shows the phase modulation depth at an injection ratio of –60 dB for various mode spacings but was normalised by multiplying the modulation depth by the mode spacing, after which they became equal. This shows that the phase modulation depth is inversely proportional to the mode spacing. From Figure 5.9, the phase modulation depth from the injection of three comb modes has the following approximate relationship with mode spacing and detuning:

$$b \propto \frac{|\Delta\omega|}{\Omega} \tag{5.15}$$

The numerical simulations performed in this section have confirmed that the residual comb mode amplification can be suppressed by keeping the detuning at approximately zero. Furthermore, by analysing the simulation results it was found that the residual comb mode amplification was mostly due to phase modulation induced in the slave laser by the residual injected comb modes. The strength of the phase modulation had a linear relationship with detuning and was inversely proportional to the comb spacing. Amplitude modulation of the slave laser was also induced, but mostly had a negligible contribution to the comb mode amplification as compared to the phase modulation.

5.4 Conclusions and Further Work

This chapter has further investigated the residual comb mode amplification discovered in Chapter 4. The optical power of one of the adjacent residual comb modes was measured using an RF based technique. It was found from this that the residual comb mode amplification could always be suppressed, regardless of the injection ratio, by carefully tuning the frequency detuning between the slave laser and comb mode it is locked to.

Numerical simulations were performed to further investigate this phenomenon using the semiconductor rate equations which were modified for optical injection of an OFC. Initial simulations with 9 injected comb modes had some qualitative resemblance with the experimental results and found that the residual amplification could be reduced by using wider spaced combs. By simplifying the simulated scenario to three comb modes, it was found that the amplification of residual comb modes was mostly due to phase modulation of the slave laser induced by the residual comb modes. The phase modulation could be strongly suppressed by keeping the detuning between the slave laser and the comb mode it is locked to at zero.

The simulations performed here were sufficient to confirm that the residual comb mode amplification was indeed occurring and that it could be suppressed by controlling the detuning. The significantly weaker residual amplification with wider spaced OFCs may be the reason this phenomenon has been scarcely reported or investigated in the literature since it is more common to injection lock slave lasers to wider spaced OFCs. The work presented in this chapter was published as a conference proceeding [9] and since then, an independent follow-up paper was published by Gavrielides [10]. In addition to numerical solutions, this follow-up paper also investigated analytical solutions to the rate equations modified for OFC injection. Other scenarios were also considered, in particular, Gavrielides looked at the case for very narrow spaced OFCs. It was found that in addition to increasing the residual amplification, it also significantly reduced the size of the locking range and could even prevent injection locking from occurring if the spacing was too small. Gavrielides also found that at very wide comb spacings, the residual amplification would grow as the comb spacing approached the relaxation oscillation frequency of the free running slave laser.

There still remains a large number of scenarios yet to be investigated either in this chapter or in [10] which may be of interest. For example, the studied cases so far have all assumed the phases of the injected comb modes were equal, which is not true for OFCs generated using phase modulation or microresonators.

Finally, it is worth noting that the design of the feedback loop for the OIPLL discussed earlier in this thesis (Section 3.2.2) did not take into account any amplification of the residual comb modes and assumed that they were simply reflected from the front facet. The feedback loop still worked as expected even though the amplified residual comb

modes were likely to have an influence on the error signal. For future work, it may be worth re-analysing the expected error signal by taking into account the residual comb mode amplification.

5.5 References

[1] S. Fukushima, C. F. C. Silva, Y. Muramoto, and A. J. Seeds, "Optoelectronic millimeter-wave synthesis using an optical frequency comb generator, optically injection locked lasers, and a unitraveling-carrier photodiode," *Journal of Lightwave Technology*, vol. 21, no. 12, pp. 3043–3051, 2003.

[2] R. Lang, "Injection locking properties of a semiconductor laser," *IEEE Journal of Quantum Electronics*, vol. 18, no. 6, pp. 976–983, 1982.

[3] F. Mogensen, H. Olesen, and G. Jacobsen, "Locking conditions and stability properties for a semiconductor laser with external light injection," *IEEE Journal of Quantum Electronics*, vol. 21, no. 7, pp. 784–793, 1985.

[4] V. Annovazzi-Lodi, S. Donati, and M. Manna, "Chaos and locking in a semiconductor laser due to external injection," *IEEE Journal of Quantum Electronics*, vol. 30, no. 7, pp. 1537–1541, 1994.

[5] T. Simpson, J. Liu, K. F. Huang, and K. Tai, "Nonlinear dynamics induced by external optical injection in semiconductor lasers," *Quantum and Semiclassical Optics: Journal of the European Optical Society Part B*, vol. 9, no. 5, pp. 765–784, 1997.

[6] O. Lidoyne, P. B. Gallion, and D. Erasme, "Modulation properties of an injection-locked semiconductor laser," *IEEE Journal of Quantum Electronics*, vol. 27, no. 3, pp. 344–351, 1991.

[7] E. K. Lau, L. J. Wong, X. Zhao, Y. K. Chen, C. J. Chang-Hasnain, and M. C. Wu, "Bandwidth enhancement by master modulation of optical injection-locked lasers," *Journal of Lightwave Technology*, vol. 26, no. 15, pp. 2584–2593, 2008.

[8] V. Annovazzi-Lodi, A. Scire, M. Sorel, and S. Donati, "Dynamic behavior and locking of a semiconductor laser subjected to external injection," *IEEE Journal of Quantum Electronics*, vol. 34, no. 12, pp. 2350–2357, 1998.

[9] D. S. Wu, D. J. Richardson, and R. Slavík, "Selective amplification of frequency comb modes via optical injection locking of a semiconductor laser: influence of adjacent unlocked comb modes," in *Proceedings of SPIE 8781, Integrated Optics: Physics and Simulations*, p. 87810J, 2013.

[10] A. Gavrielides, "Comb injection and sidebands suppression," *IEEE Journal of Quantum Electronics*, vol. 50, no. 5, pp. 364–371, 2014.

Chapter 6

Waveform Synthesis

The previous two chapters characterised the overall quality of the locking technique presented in this thesis. Specifically, it was found in Chapter 4 that my technique contributes a low amount of additional phase and amplitude noise, which can be kept at a minimum by controlling the injection ratio. Also, in Chapter 5, it was found experimentally that the residual comb modes can be suppressed to less than –50 dB by controlling the frequency detuning. This shows that the OIPLL behaves well as a way to selectively amplify an individual comb mode from a narrow spaced OFC.

This chapter will explore one of the applications which exploits this ability: arbitrary waveform generation. This will be achieved using a Fourier synthesis process where multiple slave lasers, locked to different comb modes, are combined together to form high repetition rate pulses. The shape of these pulses can be altered by individually varying the phase and amplitude of each slave laser prior to their combination.

6.1 Background

The ongoing pursuit of shorter optical pulses has been an active area of research since the first demonstration of the laser in 1960. This is due to the many applications of pulsed lasers across a wide range of fields; some examples include: industrial machining, high-energy physics, and medical applications. Lasers which are able to generate pulses with femtosecond durations are now common place in optics laboratories.

There are also many applications which take advantage of specific temporal pulse shapes and hence there has also been continued research into developing an optical arbitrary waveform generator. This would be analogous to an RF arbitrary waveform generator, where optical signals could be generated with user-defined shapes. Similar to an RF version, an optical arbitrary waveform generator would also be expected to a be a highly useful laboratory tool for conducting various experiments.

6.1.1 Pulse shaping techniques – Previous art

Perhaps the simplest method to generate optical pulses with various power profiles is to externally modulate the power of a cw laser using an amplitude modulator. Bandwidth limitations ($\lesssim$ 40 GHz) are imposed by existing modulators and the RF arbitrary waveform generators required to drive them. This limits the pulse width, the possible shapes, and the repetition rate of the pulses which can be generated using modulation.

Alternative techniques overcome these limitations by using existing techniques to generate short pulses, e.g. using mode-locked lasers. The pulses are then reshaped by manipulating them in the frequency domain. This is known as *linear filtering* since an initial pulse is passed through a passive device with a certain frequency response. This causes a change in the phase and amplitude of the various frequency components of the pulse [1, 2, 3]. In the temporal domain, this corresponds to a change in the pulse shape.

Spatial spectral filtering

Currently, the most common linear filtering technique is spatial filtering. The optical frequency components of a pulse are dispersed spatially using diffraction gratings, as shown in Figure 6.1(a), allowing the different frequency components to be manipulated separately. Early demonstrations of this used fixed amplitude and/or phase masks [4] to generate specific shapes from specific input pulses. A programmable phase mask was later developed by Weiner et al. [5] using liquid crystal spatial light modulators (LC-SLM) which consist of an array of independently controlled liquid crystal modulators, referred to as 'pixels'. Amplitude control was incorporated by using a second LC-SLM oriented 90° from the first which was then followed by a polariser [6].

Alternatives to LC-SLM have also been demonstrated for programmable pulse shaping using acousto-optic modulators (AOMs) [7] which allow custom acoustic gratings to be generated using RF arbitrary waveform generators. This allows the gratings to vary across the AOM which changes how the different spatially separated optical components are diffracted in terms of phase and amplitude.

Pulse shaping can also be achieved using a reflection style geometry as shown in Figure 6.1(b). This is a folded version of Figure 6.1(a) which reduces the number of components required and simplifies the alignment. An early example of this used a movable mirror instead of a spatial light modulator [8] which could be tilted to impart a linear phase shift across the pulse spectrum to delay or advance pulses. Deformable mirrors [9] may also be used to impart other higher order smooth phase variations, e.g. quadratic or cubic, across the optical spectrum. Both of these examples are limited in terms of the complexity of the phase profiles they can generate.

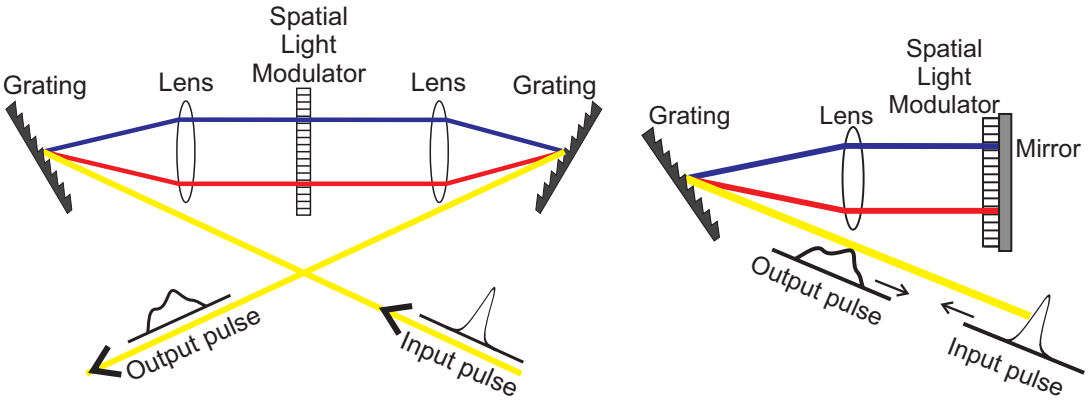

(a) Transmission geometry

(b) Reflection geometry

FIGURE 6.1: Examples of spatial spectral filtering pulse shaping using a modulator array. Images adapted from Weiner, 2011 [3].

More complex pulse shaping can be achieved using a high resolution LC-SLM, which is possible by using devices based on silicon. Liquid crystal on silicon spatial light modulators (LCoS-SLM) are made by depositing a thin layer of liquid crystal on a silicon chip which contains an electrode array to form the individual pixels. An LCoS-SLM operates in reflection by also depositing a mirror in between the liquid crystal and silicon. Using silicon as the platform for the electrodes allows for a high density of electrodes and hence very high resolutions are possible with pixel counts exceeding 10^6 [10]. A two dimensional [11] LCoS-SLM can be used to generate different gratings for different optical frequencies, which gives control of both phase and amplitude (via diffraction). Current commercially available benchtop pulse shapers, such as the Finisar Waveshaper, are based on LCoS technology.

The pulse shapes which can be achieved by spatial filtering is ultimately limited by the resolution of the system. This is given by both the resolution of the spatial light modulators used and also how well the spectral dispersers (gratings) can separate the different frequency components of the pulse. Spectral filtering is inherently a lossy process, since it involves attenuating the spectral components to achieve the desired spectrum. The gratings and modulators also incur additional losses. Additionally, LC-SLMs and LCoS-SLMs have limited power handling capabilities due to the damage threshold of the individual pixels. This restricts the power of the pulses which can be shaped.

As discussed in Chapter 2, the spectrum of a pulse train consists of a number of discrete frequency components with a constant spacing given by the repetition rate (i.e. an OFC). The limited resolution of spectral filtering results in two pulse shaping regimes: line-by-line and group-of-lines pulse shaping. Line-by-line shaping occurs when the resolution of the pulse shaper is higher than the frequency spacing of the comb modes, and each frequency component can be manipulated individually. In contrast, when the resolution of the pulse shaper is lower than the frequency spacing, the modulator processes groups

of adjacent comb modes. The advantage of line-by-line pulse shaping is that it allows for more arbitrarily defined shaped pulses to be generated, e.g. 100% duty cycle waveforms can be generated which is not possible using group-of-lines pulse shaping.

Superstructure fibre Bragg gratings

A fibre Bragg grating is an optical fibre with a periodic variation (comparable to the wavelength of light) of refractive index designed to reflect light across a certain bandwidth. A *superstructured* fibre Bragg grating (SSFBG) is formed when the Bragg grating is non-uniform across its length. The spectral response of the SSFBG is given by the Fourier transform of the refractive index profile. The amplitude and phase across the spectrum of the reflected light can be tailored by the design of the superstructure, allowing for pulse shaping. The generation of rectangular [12], triangle [13], sawtooth [14] and parabolic [15] pulses have been demonstrated using SSFBGs.

An advantage of using SSFBGs is that they are compact devices, unlike spatial filtering which requires bulk optics such as spectral dispersers and modulators. As a fibre optic device, they can be readily integrated in fibre systems, can be fabricated at relatively low cost, and have low loss. The main disadvantage of SSFBGs is their lack of programmability; each grating is written to give a particular output for a particular input pulse. Changes in the input pulse parameters, such as the pulse width or pulse shape, requires different SSFBG to be used. Similarly, different SSFBGs are required for different desired output pulses.

Temporal-domain spectral filtering

Temporal-domain spectral filtering uses the same principle as spatial spectral filtering, however, the spectral components are dispersed in time instead of space as shown in Figure 6.2. An input optical pulse propagates through a dispersive element (e.g. optical fibre) which temporally stretches (i.e. chirps) the pulse. For normal dispersion, the lower frequency components of the pulse will lead, while the higher frequencies will trail. If the pulse is sufficiently stretched, the temporal profile will be proportional to the spectral profile. Spectral filtering can then be achieved by using an electro-optic modulator in conjunction with an RF arbitrary waveform generator. The pulse is then recompressed using a second dispersive element which is the exact conjugate of the first (e.g. using dispersion compensating fibre) to give the shaped pulse at the output.

Pulse shaping using this technique has been demonstrated using amplitude-only [16, 17] and phase-only [18] modulators. Simultaneous control of both amplitude and phase could be implemented using I-Q modulators, but has yet to be demonstrated. The resolution of temporal-domain spectral filtering is limited by the bandwidth of the RF

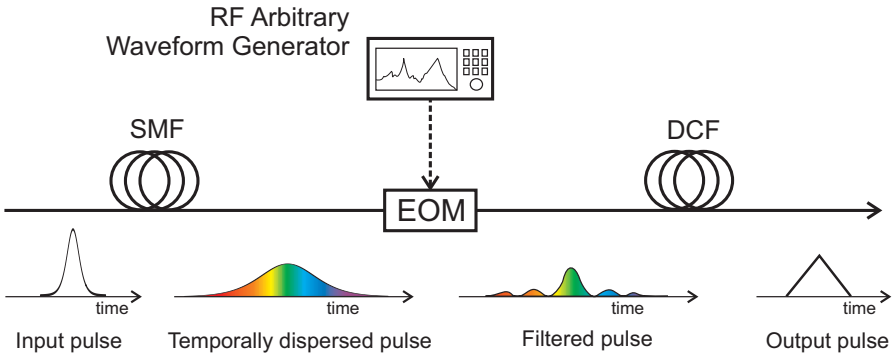

FIGURE 6.2: Conceptual schematic of temporal-domain spectral filtering using single-mode fibre (SMF), dispersion compensating fibre (DCF), and electro-optic modulator (EOM).

arbitrary waveform generator and the amount of pulse stretching possible. Pulses are unable to be stretched too much, since pulse overlapping would occur. This technique is therefore unsuitable for high repetition rate pulses.

Direct Fourier synthesis

The techniques discussed above are all passive techniques in the sense that an input pulse is reshaped to the desired shape by selective amplitude and/or phase manipulation. An alternative to this is to individually synthesise the different frequency components of the pulse using separate cw lasers, each with the desired amplitude and phase. Pulse synthesis using multiple cw lasers is not a common technique since there are many practical challenges. Firstly, for coherent pulses to be generated, the lasers need to be operating at relative frequencies which are precise multiples of the desired repetition rate. This can be achieved using phase locking, but adds a significant degree of complexity. Secondly, since the pulse width (Δt) scales down with increasing number of frequency components, a large number of lasers (N) are required for short pulse generation ($\Delta t \propto 1/N$). Similarly, for shaped pulses, the complexity of the possible shapes also increases with the number of lasers. A large number of lasers adds significant cost but also the complexity of the set-up is compounded since each laser needs to be phase locked.

An early example of Fourier synthesis was demonstrated by Hayes and Laughman [19], who combined up to five CO_2 lasers to generate pulses with repetition rates of 120 MHz. The lasers were phase locked to each other using heterodyne OPLLs. This work was later followed up by Hyodo et al. [20, 21, 22] using three semiconductor lasers. In their experiments, only one of the lasers was phase locked using an OPLL. Four-wave mixing between the other two lasers was utilised to generate two (relatively weak) additional components such that all four frequency components had the same spacing as the original two lasers. The third laser was phase locked to one of these newly generated components using an OPLL. Since the frequency spacing of the three lasers was not limited by any

RF electronics, ultra-high repetition rates of up to 1.8 THz were able to be achieved [22]. Different pulse shapes were also demonstrated, although the complexity of these shapes was limited due to the low number of Fourier components [21].

The advantage of using Fourier synthesis is that the repetition rate is not dependent on cavity resonances or external modulation sources, and can be readily changed by tuning the frequencies of the individual lasers. Also, line-by-line pulse shaping is straight forward since a spectral disperser is not required to separate out the individual frequency components. It should be noted however that a multiplexer with sufficient resolution is still required to combine the lasers with minimal loss. Finally, in contrast to spectral filtering which is inherently a lossy process, Fourier synthesis can directly generate high average power pulses by using high power lasers. This can lead to superior optical signal-to-noise (OSNR) performance since it avoids the need for additional amplifiers which inevitably contribute noise.

Non-linear pulse shaping

The previously discussed methods for pulse shaping were all based on linear techniques to modify the amplitude and phase of different frequency components. An alternative to this is the use of non-linear techniques [23]. Pulse shaping can occur due to the interplay between the non-linear optical interactions, dispersion, and other effects (e.g. optical gain) of a pulse propagating through a non-linear material. Optical soliton generation is perhaps the most well known example of this, where Kerr non-linearities and dispersion are balanced in order to generate a pulse with a constant duration and shape. Other pulse shapes have also been demonstrated using non-linear effects, such as parabolic (similaritons) and triangular waveforms.

A key advantage of non-linear pulse shaping is the occurrence of spectral broadening. This allows the pulse to acquire more frequency components, which potentially allows for more complex pulse shapes to be formed. The main disadvantage is that the pulses generated using non-linear techniques are, in general, highly sensitive to the parameters of the initial pulse, including the power profile and phase profile (i.e. chirp).

6.1.2 Applications of shaped pulses

Some of the specific examples of the applications of optical pulse shaping will be discussed in this section. This is only a small selection of the examples intended to demonstrate the wide range of applications. Further examples can be found in the following review articles on pulse shaping: [1, 2, 3, 23, 24].

Amplification of Ultra-Short Pulses

An early demonstration of optical pulse shaping was used for chirped pulse amplification (CPA) to amplify ultra-short pulses ($\ll$ 1 ps) [25]. Ultra-short pulses are difficult to amplify directly because of their very high peak powers which causes strong non-linear interactions with the amplifier gain medium. For example, self-focussing can occur through the optical Kerr effect which can cause physical damage to the amplifier. CPA overcomes this by first stretching the pulse by a few orders of magnitude using a dispersive element, e.g. optical fibre or gratings, to significantly reduce the peak power. The stretched pulse can then be uniformly amplified since the reduced peak power allows the amplifier to operate without non-linearities. The amplified stretched pulse can be re-compressed using a negative dispersive element to give an amplified ultra-short pulse.

Although the stretching and compressing of the pulse can be thought of as a basic form of pulse shaping, more advanced pulse shaping has been incorporated into CPA systems. Practically, it can be challenging to compress the amplified stretched pulse back to its original pulse width. This is due to difficulties balancing the negative dispersion of the compressor with the dispersion of the stretcher and amplifier, and to also account for non-negligible higher order dispersion. To overcome these challenges, LC-SLM based pulse shapers have been employed to compensate for the unaccounted dispersion in the compressor. This has been used after the CPA system to optimise the amplified pulse and minimise the pulse width, with bandwidth limited pulse widths reported [26]. This configuration limits the pulse energy due to loss from the pulse shaper and the damage threshold of the LC-SLM. Alternatively, the pulse shaper can be placed before the amplifier for pre-compensation [27] of unaccounted dispersion. This configuration was able to significantly shorten the output pulse width, but was unable to achieve bandwidth limited pulses.

Telecommunications

The principle of pulse shaping can also be applied to telecommunications to develop advanced transmission systems [28]. For these systems, OFCs are demultiplexed into individual comb modes and separate modulators can be used to encode phase and amplitude information onto each comb mode. The modulated comb modes are then multiplexed back together to form wavelength-multiplexed data streams. The benefit of this technique is that high bandwidth ($>$ 1 THz), high capacity data streams can be generated using multiple relatively low-speed ($\leq$ 40 GHz) modulators. The system is capable of using any modulation format e.g. on-off keying (OOK), quadrature phase-shift keying (QPSK), and even multi-level formats such as 16 quadrature amplitude modulation (16QAM). The generated waveform may also be pre-compensated for chromatic dispersion in a transmission system.

The disadvantage of using line-by-line pulse shaping in telecommunications is that although complicated waveforms can be generated, they will always be repetitive at the OFC repetition rate. Research is currently directed toward developing *dynamic* optical arbitrary waveform generation, where continuous waveforms (non-repetitive) can be generated [29]. In contrast to line-by-line pulse shaping, the target waveform will span many OFC periods and hence the target spectrum will be continuous. Each comb mode will be modulated to generate a 'spectral slice' of the overall optical spectrum. This is technically challenging since multiplexers (e.g. arrayed waveguide gratings) do not have rectangular pass-band characteristics and hence there will be significant overlap between adjacent spectral slices. Advanced algorithms and digital signal processing techniques are required to account for this. There has been a demonstration of a dynamic arbitrary waveform generation system capable of generating 100 ns duration waveforms over a bandwidth of 20 GHz, using two spectral slices encoded with various modulation formats [30].

Optical signal processing

An early application of shaped ultra-short optical pulses was for use in all-optical switching [31]. A non-linear dual-core optical coupler would couple light from one core to another depending on the instantaneous optical intensity, which would alter the refractive index via the optical Kerr effect [32]. Typical Gaussian or sech shaped pulses have variations in their optical intensities across their pulse profile. This caused the pulse to break up in the coupler with the low intensity wings of the pulse being coupled into the other core while the high intensity central part of the pulse remained in the original core. Square (flat-top) shaped pulses were used to overcome this issue since they have a constant intensity across the pulse duration, allowing the pulse to be entirely switched or unswitched.

Another example of optical signal processing is the use of parabolic pulses to regenerate the timing of short pulse transmission systems [13]. Propagation of a transmission signal through a network can acquire timing jitter between successive pulses. A SSFBG was used to generate an unchirped parabolic pulse train with the same repetition rate as the original transmission signal but with much wider pulse widths, and at a different wavelength. This was combined with the transmission signal and sent through highly non-linear fibre (HNLF). Cross-phase modulation between the two signals caused a shift in wavelength of the transmission pulse which was dependent on the temporal overlap between the pulses. Due to the gradient of the intensity profile of the parabolic pulse, the wavelength shift resulted in a change in group velocity which was linear with respect to the relative delay between the transmission pulse and the centre of the parabolic pulse. The parabolic pulses were then filtered out, and the wavelength-shifted transmission signal was propagated through a length of single mode fibre (SMF) to cancel out this

variation in group velocity such that the period between all successive pulses was equal. The length of SMF required was dependent on the peak power of the parabolic pulses.

The final example presented here used sawtooth shaped pulses for a wavelength conversion system [14, 33]. Similar to the previous example, a SSFBG was used to generate sawtooth pulses at the same repetition rate as the transmission signal, and at a different wavelength. This was combined with the transmission signal and sent through HNLF to induce cross-phase modulation. The constant gradient of the sawtooth pulse profile resulted in a fixed wavelength shift in the transmission signal, provided there was an overlap between the pulses.

Coherent control

Coherent control refers to the control of dynamic processes using laser pulses. Pulse shaping has had a strong impact in this field of research since it allows pulses to be tailored to target specific processes [34]. In this case, the shaped pulses can be thought of as photonic reagents to control the outcomes of various physical and chemical phenomena.

An early demonstration of using shaped pulses for coherent control was to study two-photon absorption in caesium atoms [35]. Since a laser pulse has a broadband spectrum, two-photon absorption occurs between all pairs of photons which sum together to provide the energy for the transition. In this experiment, pulses with a central wavelength corresponding to half the two-photon transition frequency was directed into the caesium vapour. A LC-SLM based pulse shaper was used to apply a symmetric and anti-symmetric spectral phase to the pulse with respect to the half two-photon transition frequency. It was found that due to quantum interference of the system, the level of two-photon absorption was significantly decreased with symmetric phase modulation. In contrast, the anti-symmetric case only had a small reduction in the amount of two-photon absorption, which was believed to be caused by the limited resolution of the pulse shaper. This demonstrated the ability for coherent control of the two-photon excitation.

Shaped ultra-short pulses have also been used to target specific molecular bonds. Laarmann et al. [36] used a LC-SLM based pulse shaper to modify the shape of a 34 fs pulse to break a peptide bond (N1-C3) in a polypeptide molecule (Ac-Phe-NHMe). An evolutionary algorithm was incorporated in a feedback loop to optimise the shaped pulse to maximise the bond breaking. It was found that the optimal shaped pulse for the targeted peptide bond consisted of the original pulse broken up into 4–5 closely spaced pulses.

The final example presented here is the use of shaped pulses to modify the rate of photoisomerisation of a polymer film (Disperse Red 13, DR13) [37]. Photoisomerisation is the process of using light to rearrange the geometric structure of a molecule. The targeted photoisomerisation was caused by two-photon absorption changing one of the

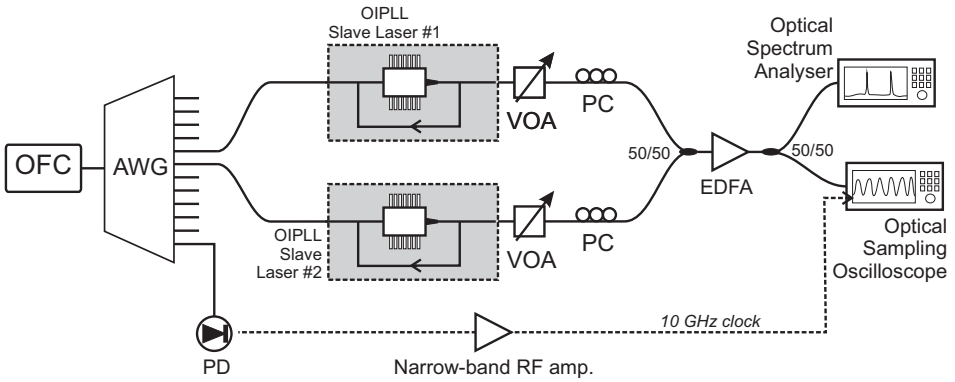

FIGURE 6.3: Experimental set-up for generating and measuring high repetition rate signals using two locked slave lasers.

chemical bonds to a higher energy bond. This also resulted in a change in birefringence. The pulse shape was varied using a deformable mirror based pulse shaper. The rate of photoisomerisation was controlled by controlling the spectral phase of the pulses.

6.2 Fourier synthesis by phase locking to an OFC

My technique for generating arbitrary shaped waveforms is based on the direct Fourier synthesis technique discussed in the previous section. Semiconductor lasers operating at different frequencies are combined together to form pulses with the amplitude and phase of each laser adjusted to achieve the desired waveform. Coherence between the independent lasers is achieved by phase locking the lasers to a common OFC using the OIPLL outlined and characterised in the previous chapters of this thesis.

Proof of principle – two lasers

Previously, in Section 4.3.4, two lasers were locked to two comb modes separated by 1 GHz to measure the phase noise over a 500 MHz bandwidth. In this section, the lasers will be locked to comb modes significantly further apart (100 GHz, 0.8 nm, 400 comb modes) to confirm that the lasers remain coherent and can still be used for Fourier synthesis. The set-up is shown in Figure 6.3, with parameters given in Table 6.1. This set-up is similar to the set-up used to measure phase noise but with the two slave lasers injected with the OFC from adjacent channels of a 100 GHz AWG. The slave lasers were discrete mode semiconductor lasers with no isolators operating at +12 dBm. Newport LB1005 PI controllers were used as feedback controllers (proportional gain: –20 dB, PI corner: 10 Hz).

The temporal waveform was measured using an EXFO PSO-102 optical sampling oscilloscope (OSO). This had a bandwidth of over 500 GHz and an internal timing jitter of 100 fs, as specified by the manufacturer. The combined optical signal was amplified

TABLE 6.1: Component parameters for Figure 6.3

Component	Parameter	Value
AWG	Insertion loss (per channel)	3–5 dB
	Channel bandwidth (3 dB)	50 GHz
	Passband shape	Gaussian
	Connector type	FC/APC
	Fibre type	SMF-28
50/50 Coupler	Excess Loss	0.5 dB
	Connector type	FC/APC
	Fibre type	SMF-28
Variable attenuator	Excess Loss	1.5 dB
	Connector type	FC/APC
	Fibre type	SMF-28
Polarisation controller	Insertion loss	<0.5 dB
	Connector type	FC/APC
	Fibre type	SMF-28
Slave lasers	Type	Discrete mode
	Output Power	+12 dBm
	Connector type	FC/APC
	Fibre type	SMF-28
EDFA	Gain	20 dB
	Connector type	FC/APC
	Fibre type	SMF-28
Photodetector	Bandwidth	20 GHz
	Responsitivity	0.65 A/W
	Optical input type	FC/PC
Narrow-band RF amplifier	Centre frequency	10 GHz
	Bandwidth (approximate)	200 MHz

using an EDFA with a gain of approximately 20 dB to ensure a strong signal could be measured by the OSO. The input signal was attenuated to approximately –5 dBm using the VOAs to ensure that neither the EDFA or the OSO was saturated. The clock signal (trigger) for the OSO was derived directly from the OFC by using another channel of the AWG. The 10 GHz clock signal was generated using a high bandwidth photodetector and selectively amplifying the 40th harmonic of the repetition rate using a narrowband RF amplifier (Wessex Electronics PAN-10006, approximate bandwidth: 10 GHz ± 100 MHz) with an output power of +2.2 dBm. The OSO was uncalibrated and hence the power measured using the device is presented in arbitrary units in this thesis. Waveforms would only be clearly visible on the OSO if the beat frequency between the two lasers was an integer multiple of the 10 GHz clock.

The 100 GHz beat signal and spectrum is shown in Figure 6.4 for injection ratios of –63 dB, corresponding to the optimum injection ratio found in Section 4.3.4. The 64000 sample temporal waveform shows a sine wave, as expected, with a period of 10 ps, corresponding to a frequency of 100 GHz. The rms jitter was calculated to be 263 fs, which corresponded to a phase error variance of 0.027 rad^2.

The optical spectrum shows that the two lasers were separated by the expected 0.8 nm. Additional spectral peaks were observed which were separated by multiples of 0.25 nm

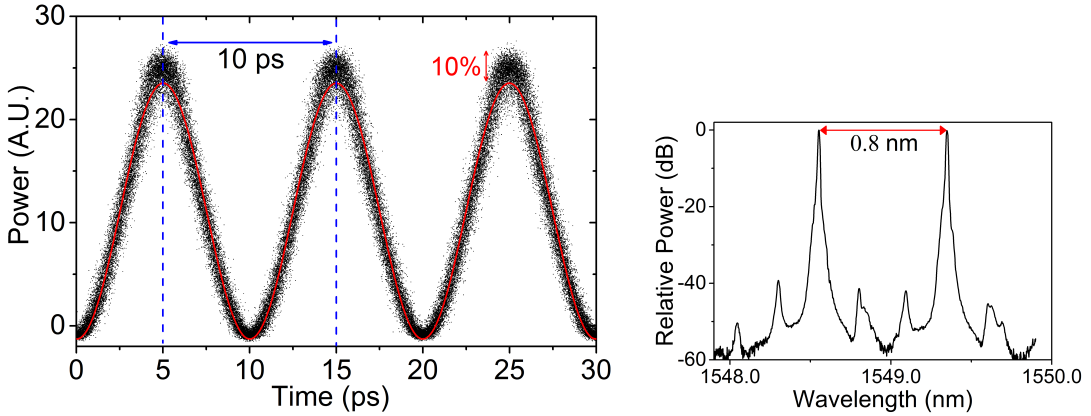

(a) Temporal waveform (black: measured, red: fitted sine wave)

(b) Optical spectrum

FIGURE 6.4: 100 GHz signal generated by two slave lasers.

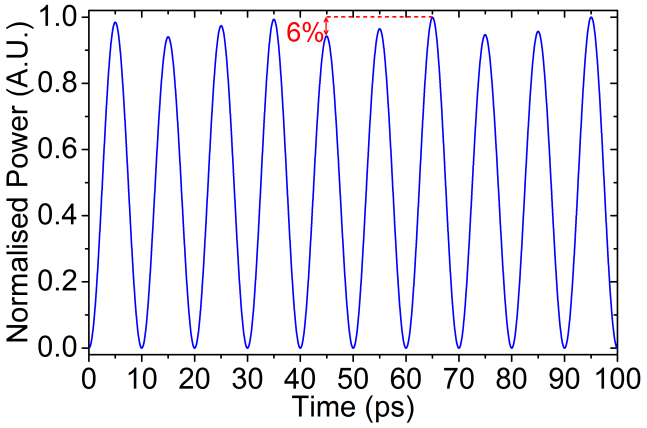

FIGURE 6.5: Experimental set-up for generating and measuring high repetition rate signals using two locked slave lasers.

from the lasing wavelength of the slave lasers. The slave lasers had cavity lengths of approximately 300 μm corresponding to laser sidemodes approximately 1.3 nm away from the lasing mode. Hence the peaks in Figure 6.4(b) did not correspond to the lasers' sidemodes. The origin of these peaks was unclear, but were inherent to the individual slave lasers themselves as they were still present even when they were not subject to any optical injection. Although these sidemodes were at least 40 dB weaker than the lasing modes, they could have still influenced the measured waveform. Figure 6.5 shows the calculated waveform from the spectrum in Figure 6.4(b), with the different modes approximated as delta functions. These sidemodes causes a slow modulation of the peak of each 10 ps period. The OSO is not synchronised to this modulation and hence these variations are distributed across the measured waveform in Figure 6.4(a). This causes strong noise at the peak of the waveform and makes the waveform appear slightly triangular in shape. The approximate variation in peak power in the calculated waveform (6%) was less than the measured values (10%), which was likely due to the approximation of the spectrum with delta function.

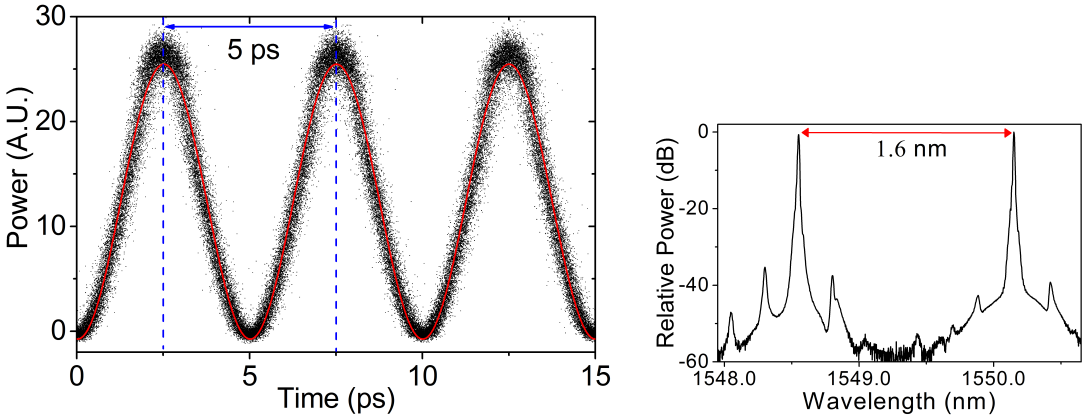

(a) Temporal waveform (black: measured, red: fitted sine wave)

(b) Optical spectrum

FIGURE 6.6: 200 GHz signal generated by two slave lasers.

A 200 GHz signal was also generated by injecting a different AWG channel into one of the slave lasers and locking it to the relevant comb mode. This is shown in Figure 6.6. The rms jitter was calculated to be 142 fs, corresponding to a phase error variance of 0.032 rad^2. The phase error variances calculated from timing jitter for 1, 100, and 200 GHz were 0.029, 0.027, and 0.032 rad^2 respectively[1]. This shows that even at significantly higher repetition rates, the signals generated by the locked slave lasers have similar noise properties as measured in Chapter 4.

The spectrum in Figure 6.6(b) shows an increase in the relative power of the sidemodes. This was due to the higher injection ratios used for the two lasers which can be seen by the larger signal at the base of the main laser modes. The higher injection ratios was mistakenly used in the measurement and were not the same as in the 100 GHz measurement. It was not clear why the sidemode at 1549.8 nm did not increase in power unlike the other sidemodes. Further investigation is required to understand the nature of these sidemodes and how to suppress them.

6.3 Scaling up the number of slave lasers

Pulse synthesis with two slave lasers only allowed sine wave pulses to be generated. More lasers would be required for more complex waveforms. Some of the challenges associated with increasing the number of lasers and their solutions are discussed in this section.

[1]The 1 GHz jitter was measured in Section 4.3.4

6.3.1 Laser diode controller and feedback electronics

Laser diode controller

In the earlier experiments in this thesis, the discrete mode lasers were operated using ILX Lightwave LDC-3724B laser diode controllers for temperature and driving current control. Used in conjunction with a current filter (ILX LNF-320), the lasers operated with low driving current associated noise. These controllers could also be operated with easy to use front panels. However, there were two practical issues associated with these controllers when scaling up the number of lasers. Firstly, these controllers are benchtop sized (comparable to a 19″ rack-mounted unit) and would take up a significant amount of space as the number of lasers increased. Secondly, these controllers were high-end products on the market in terms of price, making them unaffordable for systems using many lasers.

The alternative diode controller chosen was the Wavelength Electronics LDTC0520, which is significantly smaller with dimensions of 6.0 cm×7.4 cm×2.7 cm (palm sized) and with a cost which was approximately one sixth of the ILX controller. Similar noise performance as compared to the ILX controllers could be achieved by using 'home-made' current filters (low-pass filters)[2]. The user interface of the LDTC0520 was limited, with trimmer style potentiometers used to adjust the driving current and temperature. However, these could also be externally controlled using analogue voltages. These controllers also allowed for modulation of the laser by using a time varying external control voltage to control the laser current. This was essential for the OPLL component of the OIPLL.

Feedback controller

The size and cost issues discussed above were also applicable to the Newport LB1005 PI controller previously used for the electronic feedback portion of the OIPLL. The feedback controller was only compensating for very slow variations of master-slave frequency detuning and as such only required a modest feedback bandwidth (10 Hz in the previous experiments). This allowed the use of simple feedback controllers which could be built using standard, low-cost, electronics components (e.g. resistors, capacitors, operational amplifiers etc.). I designed and constructed the PI controllers which were basic inverting, active low-pass filters as shown in Figure 6.7. The capacitor and resistor values were chosen such that the filter cut-off frequency was < 1 Hz and had a variable gain from –30 to –10 dB. These values were not fully optimised because the relaxed requirements on the feedback loop made it unnecessary.

[2] Unpublished work by R. Slavík

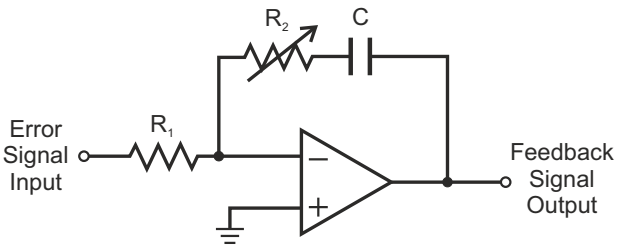

FIGURE 6.7: Schematic of inverting, active low-pass filter used as a basic PI controller.

Combined laser and feedback controller

To improve the user friendliness of the Wavelength Electronics laser drivers, an electronic circuit was designed to control the laser driving current externally. It was particularly important to implement fine control of the current in order to smoothly tune the operating frequency of the slave laser to select which comb mode to injection lock the laser to.

The feedback controller described above was also integrated into this circuit, since it acts on the laser current. Some basic processing of the input error signal was also implemented. Firstly, the error signal could be inverted to allow correct operation of the feedback. Secondly, a voltage offset could be added to the error signal to allow the laser to lock to any detuning within the locking rage.

A photograph of four of the combined laser and feedback controllers is shown in Figure 6.8(a). The Wavelength Electronics drivers are at the top of the photograph, and the current and feedback control circuits are at the bottom. The user interface is shown in Figure 6.8(b)[3]. For each laser, switches were used to turn on/off: the laser, the feedback, the error signal inverter, and the error signal offset. Rotary panel mount potentiometers allowed the fine adjustment of the laser current and error signal offset. A BNC connector was used to supply the input error signal.

6.3.2 Slave Laser Ensemble

Slave laser enclosure

Space considerations also needed to be taken into account for the optical components in the set-up such as the attenuators, polarisation controllers, phase shifters, photodiodes, and couplers. These components are generally small and compact, but as the set-up is scaled up, there becomes a large number of these components. All of the components in the set-up were fiberised for convenient handling and to avoid the need for optical alignment. However, the total amount of optical fibre may also become cumbersome

[3]The unit pictured, containing four laser and feedback controllers, was nicknamed the 'Super Lockbox'.

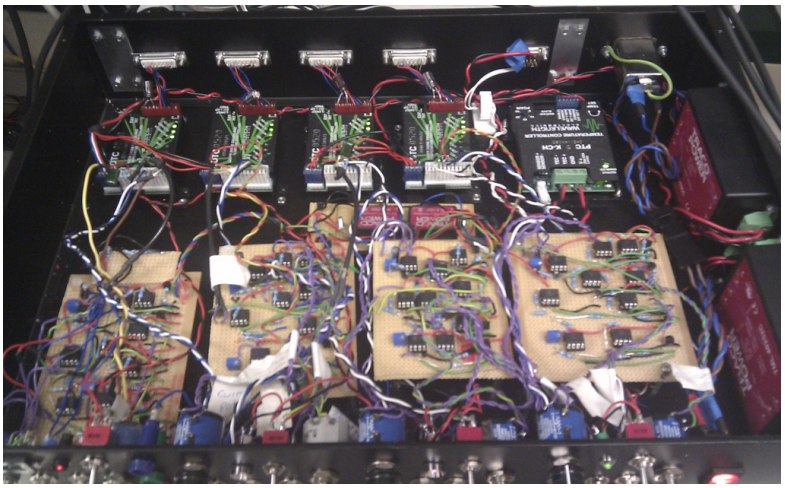

(a) Internal components

(b) Front: user interface

FIGURE 6.8: Photographs of the laser drivers and control electronics (including the feedback controllers)

as the number of lasers increases. To minimise the space requirements of a scaled up system, a single enclosure was designed to house the slave lasers and their individual optical components. The number of slave lasers housed in this enclosure was chosen to be six due to the limited number of slave lasers available at the correct wavelengths.

This enclosure was designed to have only a single optical input (OFC input) and a single optical output (the combined slave lasers) by including the AWGs used as the demultiplexer and multiplexer. A summary of the components used in the enclosure is provided in Table 6.2. For each slave laser, the enclosure also included the optical components from the previously used OIPLL set-up (Figure 3.10). Prior to the lasers being combined, each laser also had: a polarisation controller (PC) for polarisation alignment; a variable attenuators (VOA) for amplitude control; and a fibre phase shifter (PS) for phase control.

Two different types of phase shifters were used in this set-up. Four of the lasers used PZT based ones, which I assembled by winding optical fibre (SMF-28) around a piezoelectric drum and maintaining the tension by gluing the fibre in place. These were able to achieve phase shifts ranging between 0.5–1.0 π/V. High voltage amplifiers were required to ensure a wide continuous phase shift could be achieved. The loss in these 'homemade' PZT

TABLE 6.2: Component parameters for the slave laser ensemble (Figure 6.9)

Component	Parameter	Value
AWG	Insertion loss (per channel)	3–5 dB
	Channel bandwidth (3 dB)	50 GHz
	Passband shape	Gaussian
	Connector type	FC/APC
	Fibre type	SMF-28
90/10 Coupler	Excess Loss	0.5 dB
	Connector type	FC/APC
	Fibre type	SMF-28
Variable attenuators	Excess Loss	1.5 dB
	Connector type	FC/APC
	Fibre type	SMF-28
Polarisation controllers	Insertion loss	<0.5 dB
	Connector type	FC/APC
	Fibre type	SMF-28
Circulators	Insertion loss	1.1 dB
	Connector type	FC/APC
	Fibre type	SMF-28
PZT phase shifters	Insertion loss	1–3 dB
	Connector type	FC/APC
	Fibre type	SMF-28
	Input voltage	0–100 V
Heater based phase shifters	Insertion loss	<0.4 dB
	Connector type	FC/APC
	Fibre type	SMF-28
	Input voltage	0–10 V
Photodetectors	Bandwidth	450 MHz
	Responsivity/Transimpedance gain	24 V/mW (max.)
	Optical input type	FC/APC
Low pass filter (after photodetector)	Cut-off frequency	48 MHz
35 MHz Source	RF output power	1 W

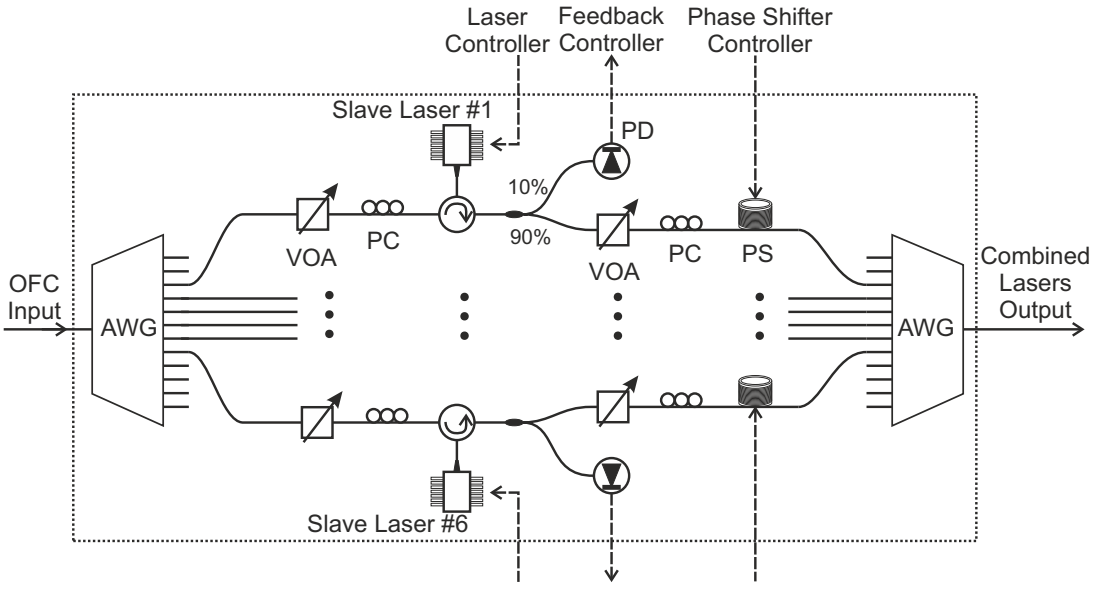

FIGURE 6.9: Schematic of the slave laser enclosure

phase shifters ranged from 1–3 dB. The other type of fibre phase shifter used was based on resistive heating to change the optical path length, and hence the phase. These were manufactured by Phoenix Photonics. These had a small form factor, had a continuous phase shift range of over 50π, and did not require any high voltage amplifiers. However, they had a significantly slower response time than the PZT based phase shifters and required higher current. The loss of the heater based phase shifters was specified to be less than 0.01 dB (not including connector losses), which was significantly less than the 'homemade' PZT based ones.

The components in Figure 6.9 were placed in a rack mountable ($19''$) enclosure as shown in Figure 6.10[4]. This also provided passive phase stabilisation by shielding the optical fibre from thermal and acoustic variations (e.g. from air-conditioning). Multiple levels were required to fit all the components for the six slave lasers. The manually controlled components, attenuators and polarisation controllers, were placed on the upper level for easy accessibility. For each slave laser, three electrical connectors were required. A 15-pin D-SUB connector was used to connect the laser controllers to the lasers; a BNC connector was used for the output of the photodetector for the OPLL; and another BNC connector was used as the input to control the phase shifters. The slave lasers were all discrete mode semiconductor lasers.

Error signal generator

To further reduce the space requirements of the set-up, most of the RF components required to generate the error signal for the OPLL were placed into a single $19''$ enclosure, separate from the optical components. A photograph of this is shown in Figure 6.11. This included amplifiers, filters and mixers such that an error signal output could be generated for each laser requiring a local oscillator input and an input from the photodiodes in the slave laser ensemble. The repetition rate recovery used for the local oscillator was performed external to this enclosure.

For simplicity, the remainder of this thesis will use the term *slave laser ensemble* to refer to the combination of: the set-up of Figure 6.9, the error signal generator, the repetition rate recovery, and the combined laser & feedback controller.

6.3.3 Phase stabilisation

The generation of arbitrary waveforms requires accurate and stable control of the relative phases between the multiple lasers. Each individual slave laser exhibits a high degree of phase stability as a result of the phase locking process. However, there is a significant length (> 5 m) of fibre between when the OFC is initially dispersed and when the slave

[4]Note that in Figure 6.10(d), only four of the lasers were connected at the time.

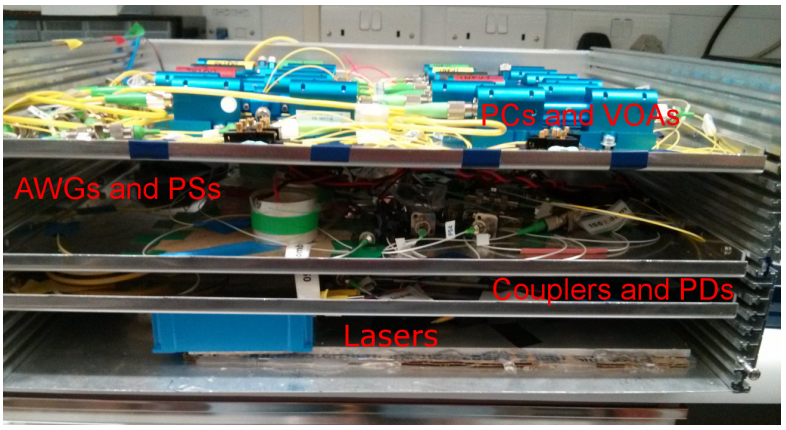

(a) Internal levels

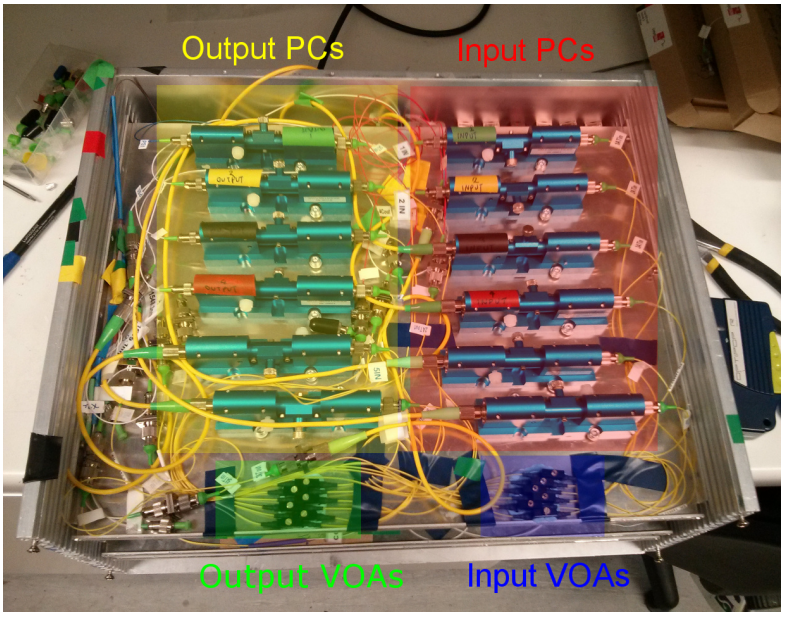

(b) Top level

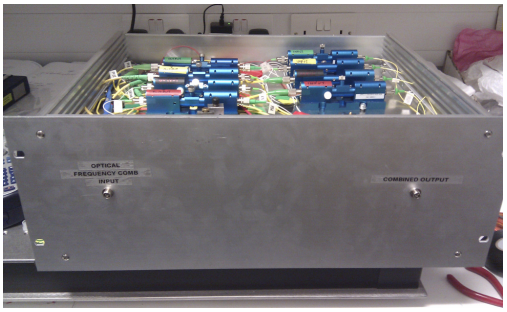

(c) Front optical (FC/APC) connectors

(d) Rear electrical connectors

FIGURE 6.10: Photographs of the enclosure containing the optical components of Figure 6.9.

FIGURE 6.11: Photograph of the error signal generator

lasers are combined by the AWGs in Figure 6.3. Thermal variations in these fibres change the optical path length and hence the relative phases of the lasers when they are combined. This was visible with the beat signals measured in the previous section (Figures 6.4(a) and (b)), where the phase would drift across a range of 2π over a time period of approximately 30 minutes.

Active phase stabilisation was demonstrated earlier in this thesis for the phase noise measurements in Section 4.3.4. This was achieved by locking the phase of the RF beat signal between the lasers with an RF signal derived from the OFC repetition rate. This technique could not be applied to the high repetition rate signals targeted here ($>$ 100 GHz) due to the limited speed of photodetectors and RF components.

An alternative technique was adopted where the relative phases of the lasers were actively stabilised by using the OFC as a reference. This is shown in Figure 6.12. An EDFA was used to amplify the output of the laser ensemble and a portion of the output was used for the phase stabilisation. The EDFA had a gain of approximately 20 dB and the VOAs inside the slave laser ensemble were set so that the launch power in to EDFA input power was –2 to 0 dBm, which prevented its saturation. This was frequency shifted by 35 MHz using an AOM and was combined with the original OFC. Each slave laser generated a 35 MHz beat signal with the original comb mode that it was locked to. The beat signal from each laser could be independently measured by demultiplexing the combined signal using an AWG. The beat signals were detected using various available photodetectors with different responsivities (some also had transimpedance gain). The beat signals were filtered using band-pass filters (passband: 0.1–50 MHz) and amplified using various RF amplifier configurations (total gain: 20–60 dB) such that the RF power was over +5 dBm. An RF mixer was used to measure the phase of this beat signal with respect to the same 35 MHz signal used to drive the AOM. A feedback circuit could then be implemented to keep the phase fixed. A proportional only feedback was implemented which acted on the fibre phase shifters inside the slave laser ensemble. This was done using data acquisition cards installed on a personal computer in conjunction with LabView software. The bandwidth of the feedback was very low ($<$ 10 Hz), but should have been adequate based on the slow phase drift observed.

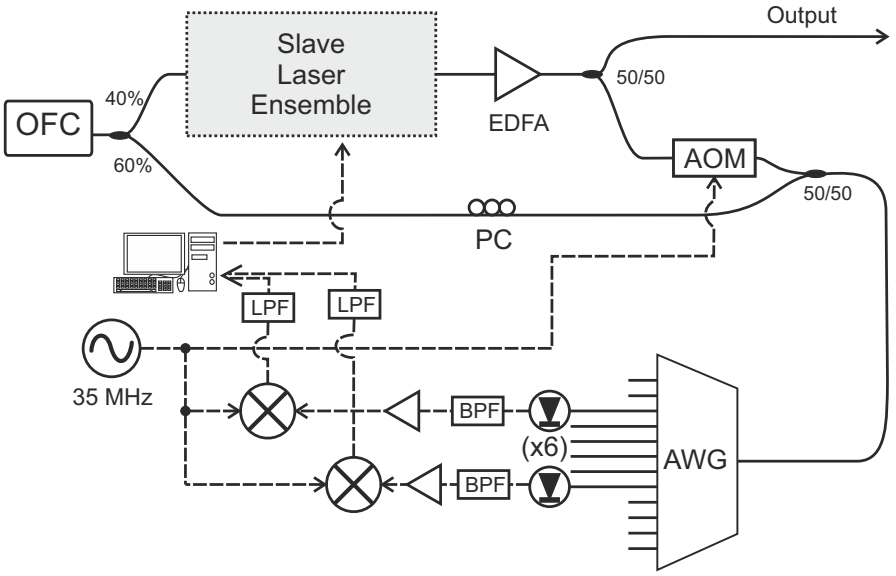

FIGURE 6.12: Phase stabilisation set-up by measuring the phase of each laser with respect to the OFC.

Unfortunately, the performance of this phase stabilisation was poor. Although the phase drift previously observed was very slow (2π in 30 minutes), the phase measured in Figure 6.12 was drifting significantly faster (2π in 1 minute) and contained noise at higher frequencies. This faster phase drift/noise was caused by the measurement set-up. The phase of the slave lasers were measured with respect to the OFC by combining them together. However, the two signals were not common path, and as a result the measurement was highly sensitive to thermal and acoustic variations of optical path length. One method to overcome this would have been to equalise the fibre lengths of the paths between when the OFC is first split, and when it is combined with the laser ensemble. Any thermal or acoustic variations should therefore be present in both paths and be cancelled out. However, this was highly impractical since the fibre lengths of each slave laser were not the same and some components had an unknown fibre length, e.g. the EDFA.

An alternative approach was taken which addressed the issue in the RF domain as shown in Figure 6.13. The same set-up as Figure 6.12 was used to generate a 35 MHz beat signal for each slave laser. However, the phase of each of these beat signals was not measured with respect to the RF signal generator used to drive the AOM. Instead, one of the 35 MHz beat signals was used as a reference signal to measure the phase of the other slave lasers. Since the thermal and acoustic variations of phase are present and equal in all the 35 MHz signals, they are cancelled out by the RF mixer. The noise was significantly reduced using this measurement technique, allowing the relative phase between the lasers to be stabilised using the personal computer with LabView as the feedback controller.

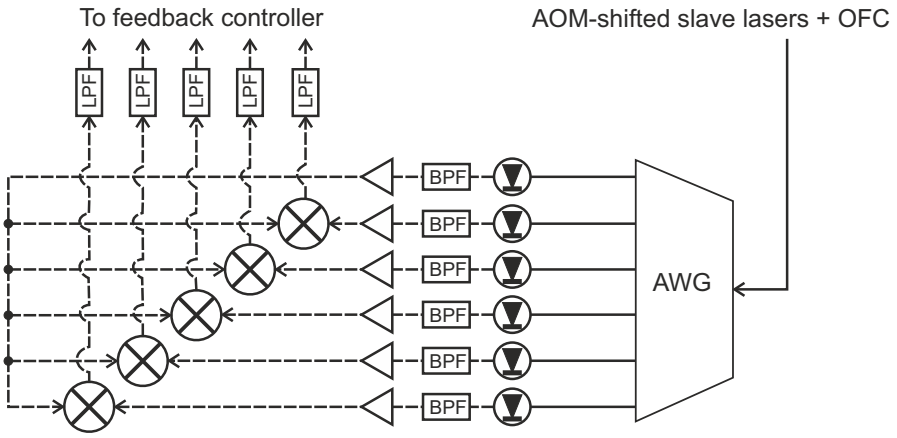

FIGURE 6.13: Phase stabilisation set-up by measuring the relative phase of each laser with respect to each other.

6.4 Partial Fourier synthesis – Set-up

In the previous section, it was shown how the number of slave lasers was scaled up and how the relative phase between the lasers could be stabilised. In this section, I discuss the experimental set-up for partial Fourier synthesis of waveforms. The term *partial* is used here because of the use of additional line-by-line pulse shaping (using a Waveshaper device) to control the phase of the individual slave lasers after they were already combined. The Waveshaper was required in this section primarily because of the limited tunability of the relative phases between the slave lasers with the initial set-up. I emphasise though, that this is not a fundamental limitation of the approach as will be demonstrated in Section 6.6.

6.4.1 Partial Fourier synthesis

The waveforms generated in this section used a Finisar Waveshaper to perform line-by-line pulse shaping. The Waveshaper uses a grating and an LCoS element to perform spatial filtering of both amplitude and phase, as discussed in Section 6.1.1. The Waveshaper was used after the phase stabilised slave lasers were combined to re-disperse the pulse into its separate frequency components to adjust phase and amplitude. The Waveshaper in the partial Fourier synthesis set-up had two functions: to allow measurements of the relative phase between the lasers; and to shape the synthesised pulses.

Measurement of relative phase

Although the relative phase of each laser was stabilised using the technique discussed in Section 6.3.3, the actual relative phases between the lasers after they were combined were unknown. This needed to be known in order to tune them to the required values

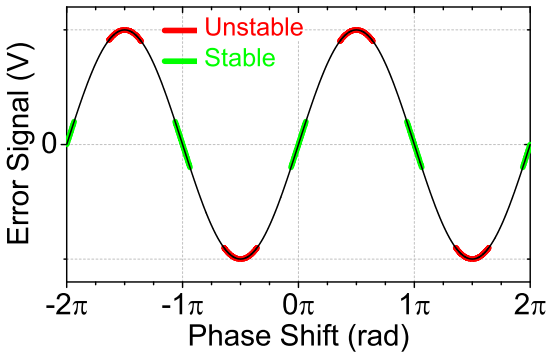

FIGURE 6.14: The error signal for the phase stability feedback loop as a function of phase shift.

for the desired waveform. The relative phases could be determined by measuring the phase of the beat signal between individual pairs of lasers separately on the OSO. The Waveshaper allowed pairs of frequency components to be easily isolated from the others by heavily attenuating the other components temporarily for the measurement.

In principle, this selective attenuation could also be applied before the lasers are combined using the variable attenuators in the slave laser ensemble. However, since I used mechanically controlled attenuators, each time the attenuation was altered, the relative phase (and polarisation) would also be altered due to the high sensitivity of phase before the slave lasers were combined. The LCoS-SLM within the Waveshaper was electrically controlled and did not introduce any undesired changes in phase or polarisation.

Pulse shaping using the Waveshaper

Arbitrary waveform generation requires the control of both amplitude and phase of each slave laser. The relative amplitudes of the lasers could be measured by using an OSA to find their relative power. Their values could be adjusted using the attenuators in the slave laser ensemble, but as discussed above, this needed to be done before the phase measurements were taken.

The phase of each laser could be varied using the phase shifters in the slave laser ensemble. This could be achieved by controlling the locking value of the feedback for phase stabilisation. The error signal has a sinusoidal relationship with phase as shown in Figure 6.14. Locking the phase near the peaks and troughs (red regions in Figure 6.14) of the sinusoid was unstable, and the feedback loop was unable to maintain the desired phase. The relative phases of the lasers therefore could not be tuned continuously across a 2π range, which was required for arbitrary waveform generation. Even when the error signal was locked away from 0 V (outside the green region in Figure 6.14), the phase stability was degraded.

The method I adopted for partial Fourier synthesis was to keep the relative phases locked to 0 V, which was stable. The Waveshaper was used to impart the phase shift required for the desired waveform. The high phase stability from locking to 0 V meant that the Waveshaper was only required to produce a constant phase shift and did not require any additional feedback loops. Since the Waveshaper was already in use for the phase measurements and phase shifting, it was also used for amplitude control. Although this was not necessary, it was more convenient than manually controlling it using the mechanical variable attenuators.

It is worth mentioning that this issue surrounding the phase tunability and stability was later solved and will be discussed later in this chapter (Section 6.6).

6.4.2 Experimental set-up

The experimental set-up for the generation and measurement of partially Fourier synthesised waveforms is shown in Figure 6.15. In these demonstrations, up to six slave lasers were used in the ensemble covering a wavelength range from 1546 nm to 1556 nm. Since the entire OFC was not required, coarse wavelength division multiplexers (CWDM) were used as optical filters to isolate an optical frequency band sufficient for injection locking these lasers. The two CWDMs had passbands of 1500–1564 nm and 1543–1557 nm, resulting in a filtered OFC signal with a bandwidth of 1543–1557 nm entering the slave laser ensemble. The filtered out OFC signals (reflected from the CWDMs) were used for RF generation of the 250 MHz repetition rate signal for the feedback component of the slave laser OIPLL, and also for the 10 GHz clock for the OSO.

The output of the slave laser ensemble was tapped off using an 80/20 coupler, photodetected and displayed on an RF spectrum analyser. The purpose of this was to provide a monitor to easily see if any of the slave lasers had lost their phase locking. The remaining 80% of the signal was amplified and divided into two. One portion was used for the phase stabilisation by frequency shifting the signal using an AOM and combining it with the filtered OFC injection signal. This was then processed using the set-up in Figure 6.13. The other portion of the amplified output of the slave laser ensemble was sent to the Waveshaper.

The VOAs at the output of each of the lasers within the slave laser ensemble were set such that the power of each laser was approximately equal. Figure 6.15 shows the approximate power levels in the set-up when 5 or 6 slave lasers were operational. Lower power needed to be used for fewer lasers to prevent damage to the Waveshaper, which could handle a maximum power of +13 dBm per laser. To generate strong signals for the phase stabilisation error signal generator, the EDFA was operated close to saturation with an output power of approximately +20 dBm. Depending on the desired waveform, the total optical power of the signal may have been heavily attenuated by the Waveshaper.

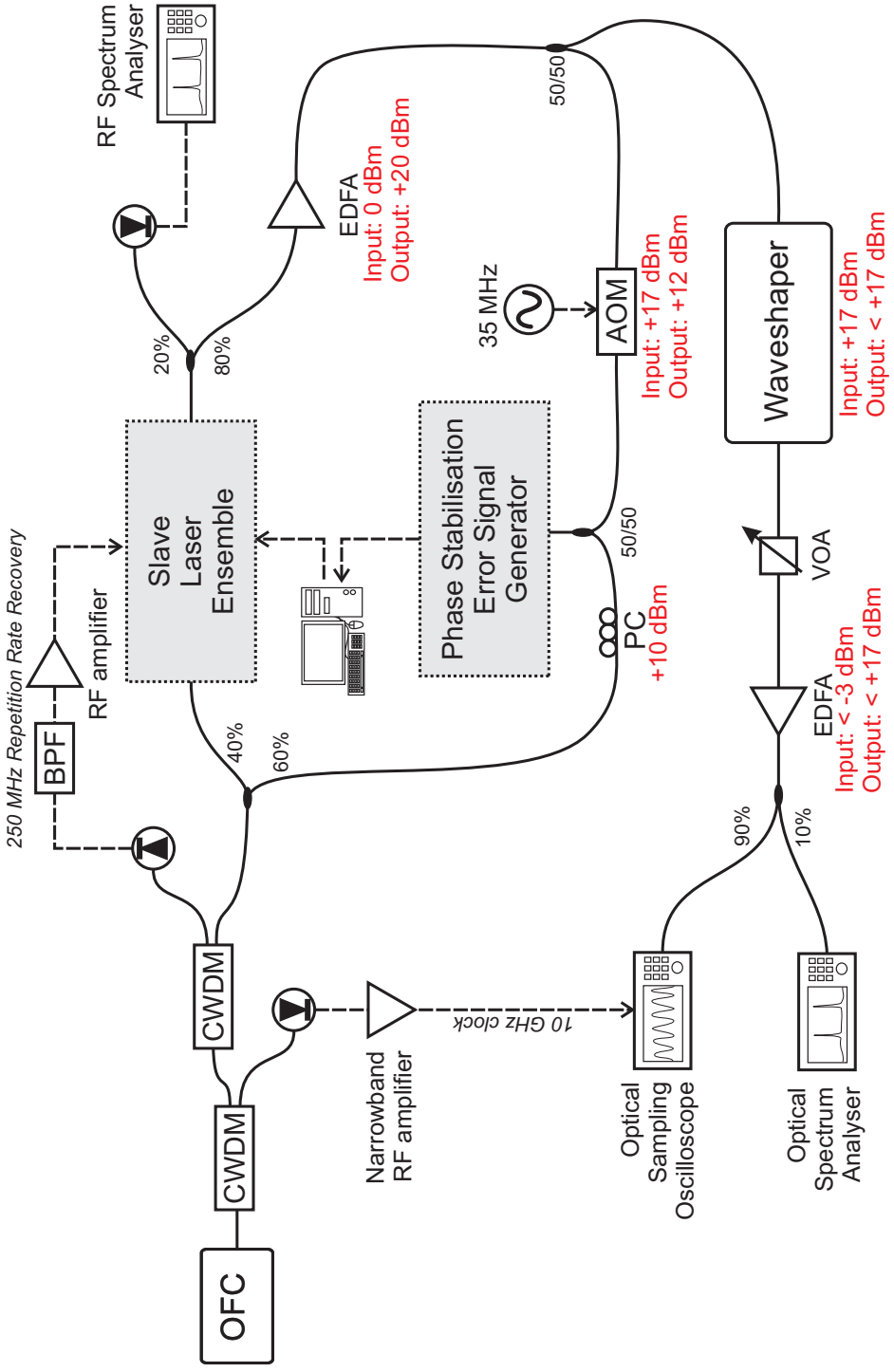

FIGURE 6.15: The set-up used for the generation and measurement of partially Fourier Synthesised waveforms. The phase stabilisation error signal generator contains the components shown in Figure 6.13. The maximum optical powers are given in red for various components when 5 or 6 slave lasers are used and have equal powers at the output of the slave laser ensemble.

Therefore, to generate the clearest measurable signal, the output of the Waveshaper was amplified using an additional EDFA. A variable attenuator before the EDFA was used to prevent saturation. The photodetector inside the OSO also experienced saturation for temporal peak power of approximately 50 mW (+17 dBm) and hence the input into the final EDFA was always less than –3 dBm. Part of the EDFA output was tapped off to an OSA to measure the relative power of the different frequency components.

6.5 Partial Fourier synthesis – Results

The waveforms generated using the set-up discussed in the previous section are presented here. This section is divided into different subsections for the different number of lasers used in the Fourier synthesis.

6.5.1 Three Lasers

The results for three lasers were achieved without the Waveshaper and hence they represent a simple example of actual (non-partial) Fourier synthesis.

Pulses

Pulse trains with a single pulse per period were targeted first. This could be achieved by setting the +100 and –100 GHz Fourier components (lasers) to be –3 dB relative to the centre component. In this case, with three slave lasers, the relative phases between the lasers were not measured but were instead estimated. This was done by tuning the relative phases to minimise the power in between successive pulses, which corresponded to equal relative phases between the combined lasers. The phases were tuned by changing the locking position of the phase stabilisation feedback as discussed in Section 6.4.1. Since the tuning range of the phase was limited, patience was required to wait for the relative phases to drift into a state where the target phases were accessible.

The parameters of the lasers are given in Table 6.3. Figure 6.16 shows the 16000 sample waveform measured on the OSO and the optical spectrum. The relative power of each laser was off target by less than 1 dB. Despite this, the pulses were clearly visible with only a small amount of power in-between them. The peak of the satellite pulse was suppressed by a linear factor of approximately 16 (–12 dB) compared to the peak of the main pulse. The injection ratios used for the injection locking of each laser ranged between –45 and –55 dB, which was higher than the optimum injection ratio. This can be seen by the high level of spectral noise near the laser peaks in Figure 6.16(b).

TABLE 6.3: Three lasers — single pulse parameters

Laser Index	Wavelength (nm)	Relative Frequency (GHz)	Relative Intensity (dB)
1	1548.55	+100	–3.8
2	1549.35	0	0
3	1550.15	–100	–3.4

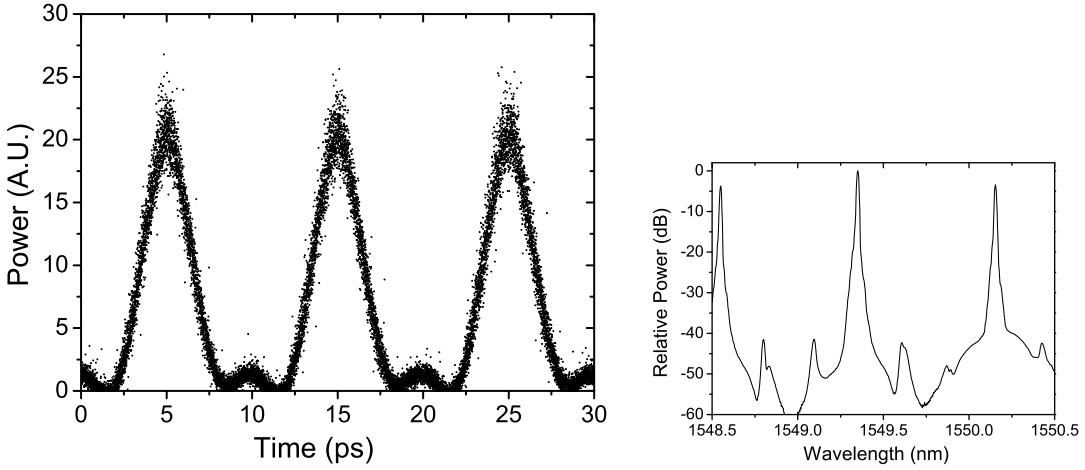

(a) Temporal waveform (b) Optical spectrum

FIGURE 6.16: 100 GHz pulses generated by three slave lasers.

TABLE 6.4: Three lasers — double pulse parameters

Laser Index	Wavelength (nm)	Relative Frequency (GHz)	Relative Intensity (dB)
1	1548.55	+100	–3.8
2	1549.35	0	0
3	1550.15	–100	–0.1

Double Pulses

The types of waveforms possible was limited with only three slave lasers. As a quick demonstration, a double pulse train was demonstrated with one pulse having a peak power of approximately half of the other. This is shown in Figure 6.17 using the parameters in Table 6.4. The injection ratios were reduced from the previous measurements to range between –55 to –65 dB and were expected to be in a region where the phase noise associated with the injection locking was at a minimum. Despite this, the waveform in Figure 6.17(a) appeared more noisy than the single pulse. This was because the double pulse waveform was more sensitive to fluctuations in relative phase than the single pulse.

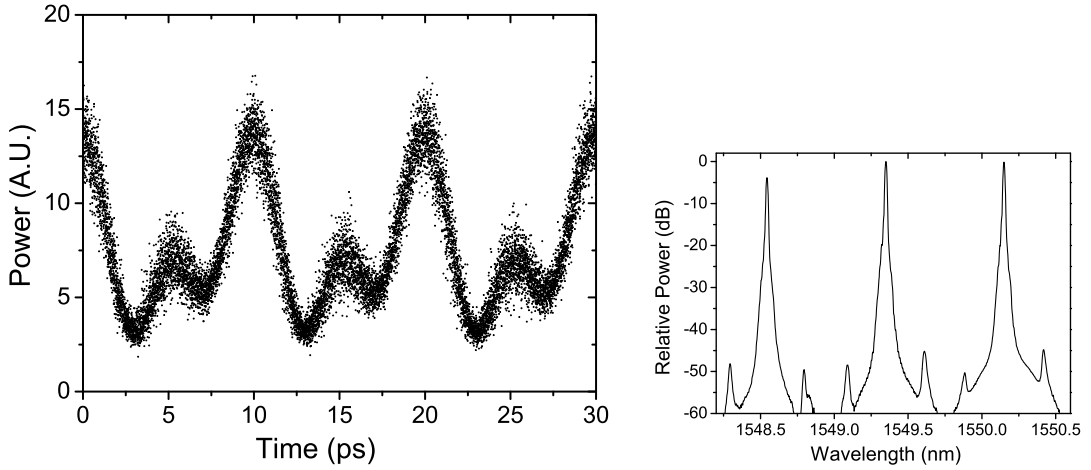

(a) Temporal waveform (b) Optical spectrum

FIGURE 6.17: 100 GHz pulse doublets generated by three slave lasers.

6.5.2 Four Lasers

In this section, four slave lasers were used with a frequency spacing of 100 GHz. As the number of slave lasers used for the Fourier synthesis increased, more complicated shapes could be generated. This also made it more difficult to tune the relative phases of the lasers visually, as was done with three lasers. As a result, the full set-up in Figure 6.15 was utilised to measure the relative phases of the lasers. The relative phase of each laser was measured with respect to laser #2 (1549.37 nm) by using the Waveshaper to isolate pairs of lasers. Once the stabilised relative phase of each laser was known, they could be tuned to the desired value using the Waveshaper. The relative power of each laser was still set using the attenuators inside the slave laser ensemble.

The relative power and phases of the slave lasers required to generate a particular waveform was calculated using non-linear fitting in Matlab. Only a particular power profile was targeted as no constraints were placed on the phase profile of the waveform. The non-linear fitting would find values for E_k^2 and ϕ_k in the equation

$$I_{total} = E_{total} \times E_{total}^{*} \ , \tag{6.1}$$

where

$$E_{total} = \sum_{k=1}^{4} E_k \, e^{i[(\omega_0 + \delta\omega_k)t + \phi_k]} \ , \tag{6.2}$$

where k is the laser index. E_k^2 is the power, ϕ_k the phase, and $\delta\omega_k$ is the relative angular frequency of each laser. ω_0 is the nominal optical angular frequency of the waveform. An example of an ideal rectangular waveform and the targeted waveform, as calculated from the fitting, is shown in Figure 6.18. In the following sections, the values given for the targeted relative phases were rounded to the nearest $^{\pi}/_{2}$ if their difference was within ± 0.1 rad.

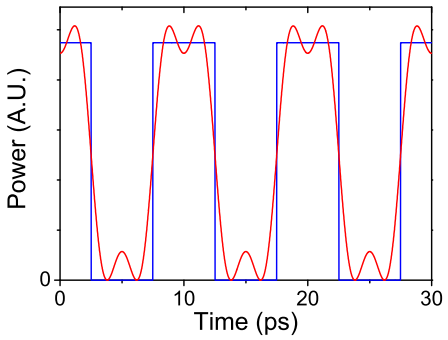

FIGURE 6.18: An example of a non-linear fit using four slave lasers (red) for an ideal rectangular pulse train (blue)

Square pulses

The first waveform attempted was a rectangular (flat-top) pulse train with a 50% duty cycle, as shown in Figure 6.18. The laser parameters are given in Table 6.5 and the measured waveform and spectrum is shown in Figure 6.19. The waveform measurements in this section were recorded with 64000 samples. The red line in Figure 6.19(a) shows the calculated power profile of the waveform using the measured parameters (not targeted) in Table 6.5, but has been translated in time and scaled with a multiplicative factor to fit the data. There is a reasonable resemblance between the measured and calculated waveform, however, there was a larger than expect amount of power in-between the pulses. It should also be noted that the targeted rectangular-like pulse still contained a noticeable ripple across the waveform due to the limitations of using only four frequency components, as seen in Figure 6.18.

Parabolic pulses

Figure 6.20 shows the parabolic pulses generated using four lasers with the parameters in Table 6.6. The targeted pulses had a 50% duty cycle, however, similar to the rectangular-like pulses, there was considerably more power in-between the pulses than expected.

Triangular pulses

Triangle shaped pulses were generated as shown in Figure 6.21 using the parameters in Table 6.7. The targeted pulses had a 100% duty cycle. Out of the various pulses generated with four slave lasers, the triangular pulses had the best agreement with calculations.

TABLE 6.5: Four lasers — rectangular pulse parameters

Laser Index	Wavelength (nm)	Relative Frequency (GHz)	Relative Intensity (dB)	Targeted Relative Phase (rad)
1	1548.57	+100	–0.5	$^{3\pi}/_{2}$
2	1549.37	0	0	N.A.
3	1550.18	–100	–8.1	$^{\pi}/_{2}$
4	1550.98	–200	–8.7	0

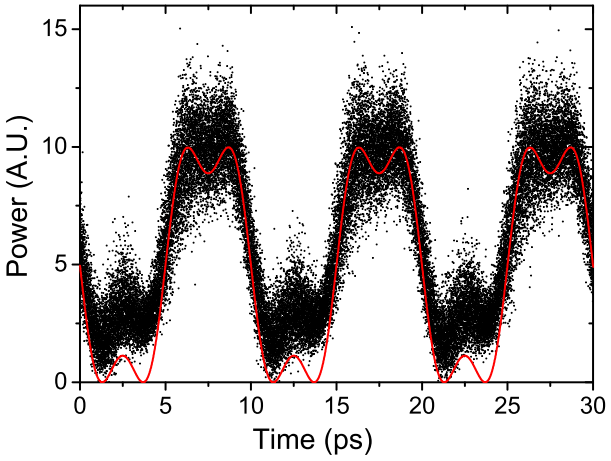

(a) Temporal waveform (black: measured, red: calculated)

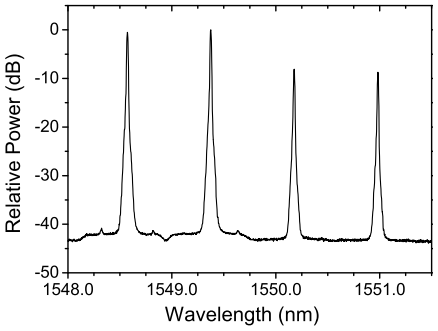

(b) Optical spectrum

FIGURE 6.19: 100 GHz rectangular pulses generated by four slave lasers.

TABLE 6.6: Four lasers — parabola pulse parameters

Laser Index	Wavelength (nm)	Relative Frequency (GHz)	Relative Intensity (dB)	Targeted Relative Phase (rad)
1	1548.57	+100	–2.0	π
2	1549.37	0	0	N.A.
3	1550.18	–100	–5.3	π
4	1550.98	–200	–15.8	0

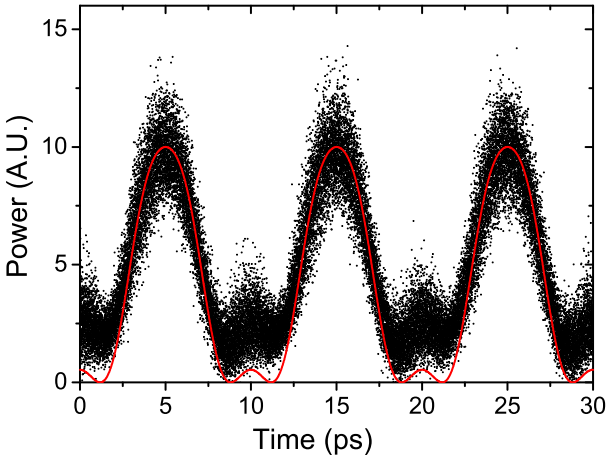

(a) Temporal waveform (black: measured, red: calculated)

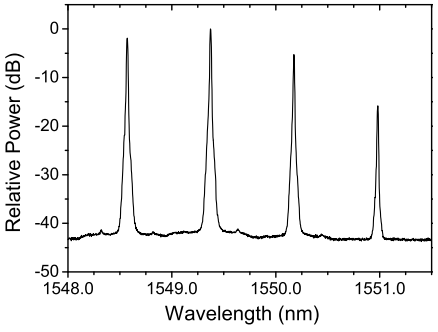

(b) Optical spectrum

FIGURE 6.20: 100 GHz parabolic pulses generated by four slave lasers.

Sawtooth

Finally, a sawtooth pulse was attempted using the four slave lasers (Table 6.8 & Figure 6.22). There was a poor match between the measured and calculated waveforms. This was the only asymmetric pulse shape targeted, which may have been more sensitive to phase mismatch. This was also likely to be the reason why the targeted relative phases did not round off to $^{\pi}/_{2}$ values.

Discussion

This section has shown that more types of waveforms could be generated by using more slave lasers, with varying levels of success. With all of the measured waveforms, it appeared that there was an overall increase in noise with four lasers as compared to three. One possible reason for this was because the oscilloscope was set to record 64000 samples per measurements (compared to 16000 in the previous measurements for three lasers). Any jitter in the signal would therefore seem more apparent with the larger number of samples, even for the same amount of jitter. The additional EDFA which was used in conjunction with the Waveshaper would have also contributed additional noise to the system.

Although a larger variety of waveforms could be generated with four lasers, it can be seen that most of the targeted waveforms were still quite poor fits to their ideal cases. Additionally, there was an appreciable difference between the measured and targeted waveforms. In particular, the 50% duty cycle pulse trains (parabolic and rectangular) had a significantly larger amount of power in-between the pulses than expected. This may have been due to misalignment of polarisation of the slave lasers as they were combined in these measurements, resulting in a constant power offset in the waveform. The other possibility is that the relative phases of the lasers did not match the targeted values. This was likely since in these experiments, the relative phases of the lasers were only measured once for calibration. The desired phases were programmed into the Waveshaper with the assumption that the Waveshaper would accurately generate the required phase shifts. In hindsight, the relative phases should have been remeasured after this to ensure they were at their expected values.

TABLE 6.7: Four lasers — triangular pulse parameters

Laser Index	Wavelength (nm)	Relative Frequency (GHz)	Relative Intensity (dB)	Targeted Relative Phase (rad)
1	1548.57	+100	–1.7	0
2	1549.37	0	0	N.A.
3	1550.18	–100	–16.0	0
4	1550.98	–200	–18.4	π

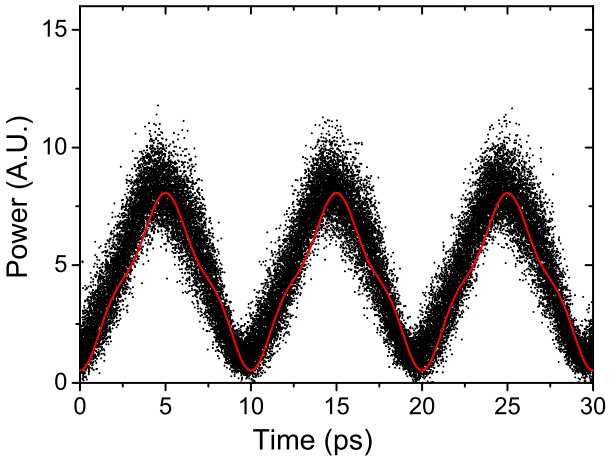

(a) Temporal waveform (black: measured, red: calculated)

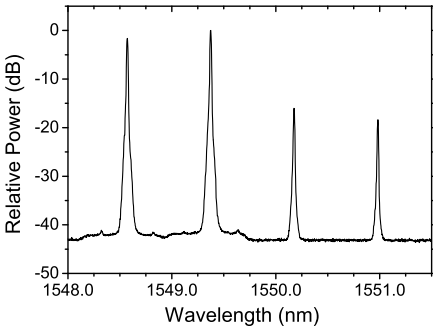

(b) Optical spectrum

FIGURE 6.21: 100 GHz triangular pulses generated by four slave lasers.

TABLE 6.8: Four lasers — sawtooth pulse parameters

Laser Index	Wavelength (nm)	Relative Frequency (GHz)	Relative Intensity (dB)	Targeted Relative Phase (rad)
1	1548.57	+100	–6.1	–0.77
2	1549.37	0	0	N.A.
3	1550.18	–100	–6.3	2.37
4	1550.98	–200	–9.0	0.81

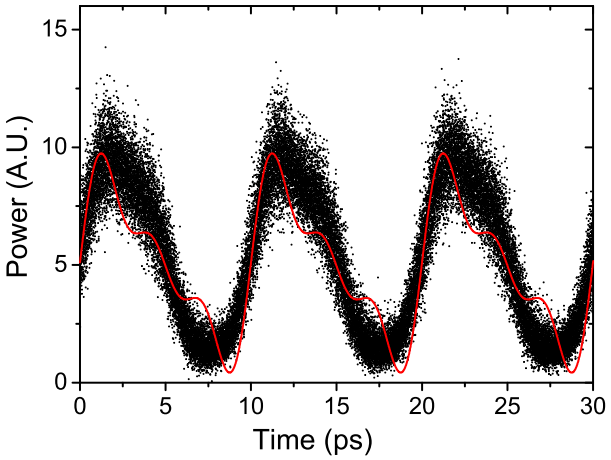

(a) Temporal waveform (black:measured, red: calculated)

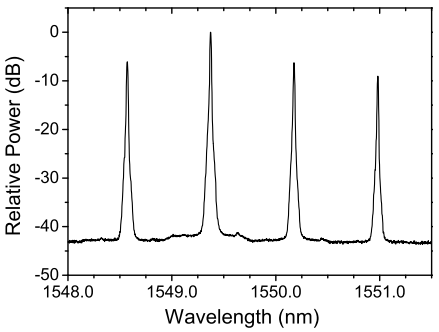

(b) Optical spectrum

FIGURE 6.22: 100 GHz sawtooth-like pulses generated by four slave lasers.

6.5.3 Five Lasers

In this section, waveforms generated with five slave lasers are demonstrated. The previous sections using three and four lasers were effectively 'learning stages' to become better acquainted with Fourier synthesis. Some of the key results of this chapter are presented in the following sections using five and six lasers.

The five lasers used in this section did not have an equal frequency spacing between them, as shown in Table 6.9. This was chosen to allow a couple of well known waveforms (rectangular and triangular) to be generated using their Fourier transforms (sinc and sinc^2 spectra). By using a spectrum based on their Fourier transforms, the waveforms can be generated with constant phase (i.e. chirp-free). This flexibility in the choice of frequency components is one of the key advantages of using OFC phase locked lasers for Fourier synthesis.

TABLE 6.9: Five lasers indexing

Laser Index	Wavelength (nm)	Relative Frequency (GHz)
1	1548.81	+300
2	1549.40	+100
3	1550.20	0
4	1551.00	–100
5	1552.61	–300

One of the issues from Section 6.5.2 was the uncertainty of the relative phase of each laser. This was addressed with five lasers by repeating the phase measurements each time after the Waveshaper was reprogrammed to ensure that each frequency component approximately had the correct phase. The phase stability feedback (Figure 6.13) was improved by ensuring that the photodetector inputs had the maximum optical power possible without saturating them. This resulted in better error signals being generated and hence more stable locking. The Waveshaper was also used for amplitude control to minimise disturbances to the aligned polarisation of the lasers. The EDFAs were replaced with models that had a gain flattening filter and automatic gain control which enabled it to maintain a constant gain of 20 dB across the entire amplification bandwidth and regardless of the input power.

Calibration

As with four lasers, the relative phases of the slave lasers needed to first be measured for calibration which was again done with laser #2 as the reference. This was done more carefully and systematically with five lasers, which will be discussed here. The uncalibrated 100 GHz waveform is shown in Figure 6.23(a). The Waveshaper was used to isolate laser #2 and one other laser by heavily attenuating the other lasers. The beat signal between the two lasers was recorded by the OSO and post-processing was used

to fit a cosine wave to measure the phase. The phase noise of the lasers and the OSO contributed to the timing jitter of the measured beat signal. This jitter was calculated and interpreted as the uncertainty in the phase measurement.

The polarisations of the lasers were all aligned with respect to laser #2, which was kept constant. This was done at the same time as the phase measurements when each laser was isolated with laser #2. The alignment was made by maximising the amplitude of the beat signal. The polarisations could remain aligned for long periods of time due to the lasers and fibre being enclosed in the slave laser ensemble, which provided thermal and acoustic insulation. Perturbations were also reduced because the Waveshaper was used to control the relative power of the lasers instead of the manual attenuators, as was the case with four lasers.

For the calibration, the lasers were set to have approximately equal power. A waveform was also calculated using the measured parameters in Table 6.10 and is plotted in red in Figure 6.23(a) with a multiplication factor to fit the data. There is a very good agreement between the two, showing that the relative phases of the lasers had been accurately measured.

The measured phases are shown in Figure 6.23(c) and are summarised in Table 6.10. It should be noted that laser #5 was significantly noisier than the other lasers. This can be seen by the larger jitter (with a corresponding phase error of 0.4 rad) associated with the phase measurement, which was double that for the other lasers (phase error of 0.2 rad). Similar to the other lasers, this was a 200 kHz linewidth discrete mode laser and was butterfly packaged. However, it was packaged[5] into a separate module which also included the driving electronics (laser and TEC controller) and the fusion spliced circulator. The length of fibre between the laser and circulator was estimated to be approximately 30% longer and was confined in a much smaller space, requiring a smaller bend radius of the fibre. These factors reduce the OIL stability, as discussed in Section 3.2.1, which was likely to increase the level of phase noise.

TABLE 6.10: Five lasers — calibration

Laser Index	Relative Intensity (dB)	Measured Relative Phase (rad)
1	–0.4	–1.4 ± 0.2
2	–0.3	N.A.
3	0	2.2 ± 0.2
4	–0.4	1.4 ± 0.2
5	–0.6	–0.8 ± 0.4

Using the calibration data, the relative phases of the lasers were aligned using the Waveshaper as shown in Figure 6.24. The post-calibration phase measurements are summarised in Table 6.11 and shows that all the relative phases were close to zero, with the exception of laser #1 which was slightly off-target beyond its error bounds. The

[5]This was done by TeraXion Inc.

measured waveform is plotted with the calculated waveform using the targeted values in Figure 6.23(a) and are in good agreement with one another.

TABLE 6.11: Five lasers — post-calibration

Laser Index	Measured Intensity (dB)	Measured Relative Phase (rad)	Targeted Relative Phase (rad)
1	–0.4	–0.4 ± 0.2	0
2	–0.3	N.A.	N.A.
3	0	0.0 ± 0.2	0
4	–0.4	–0.2 ± 0.2	0
5	–0.6	0.4 ± 0.4	0

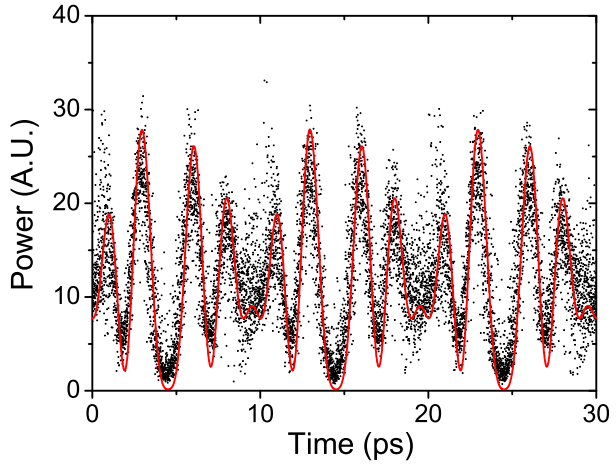

(a) Temporal waveform (black: measured, red: calculated from measured power and phases)

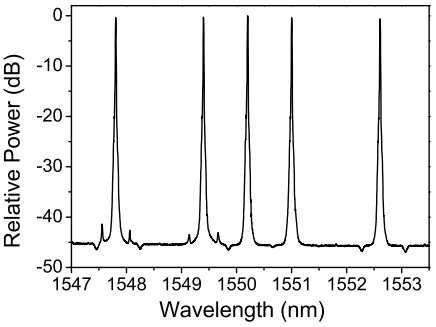

(b) Optical spectrum

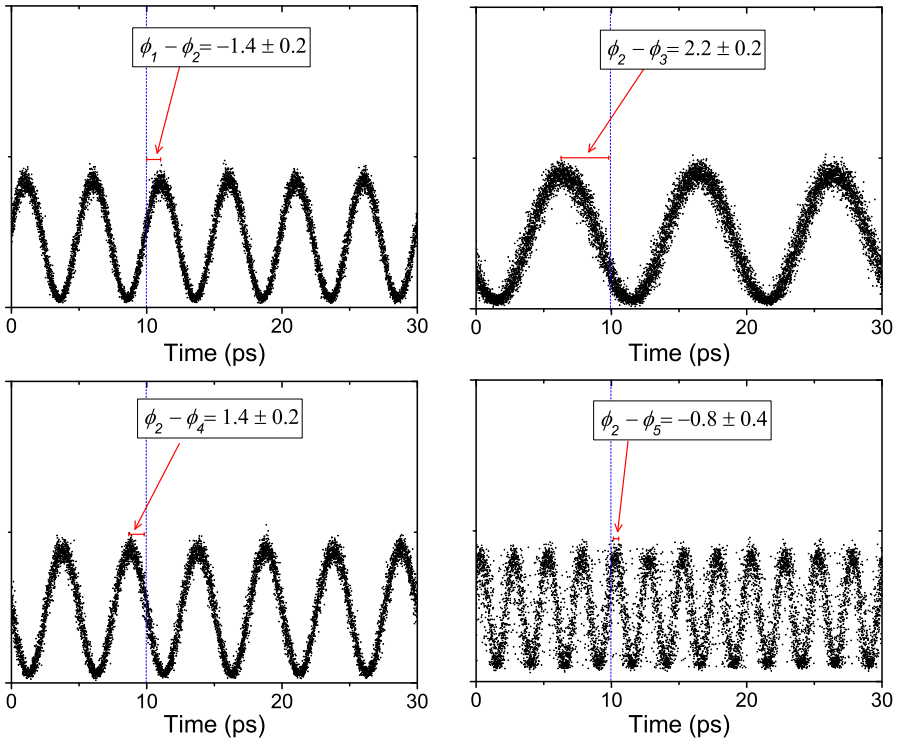

(c) Measured phases

FIGURE 6.23: The uncalibrated waveform (a) and spectrum (b) generated by five lasers. (c) The measurements of the relative phase of each slave laser with respect to laser #2.

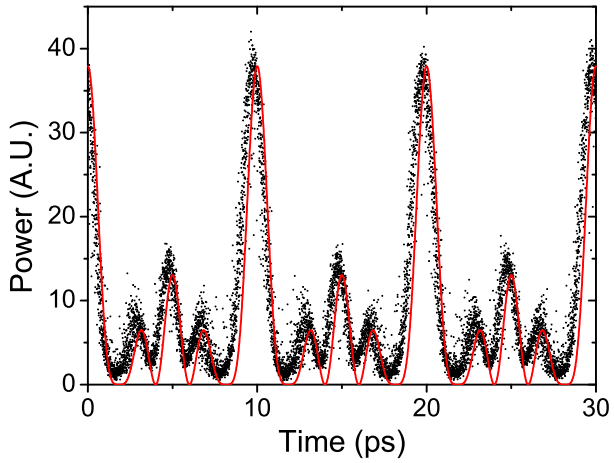

(a) Temporal waveform (black: measured, red: targeted)

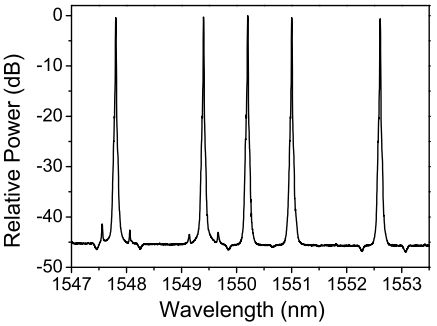

(b) Optical spectrum

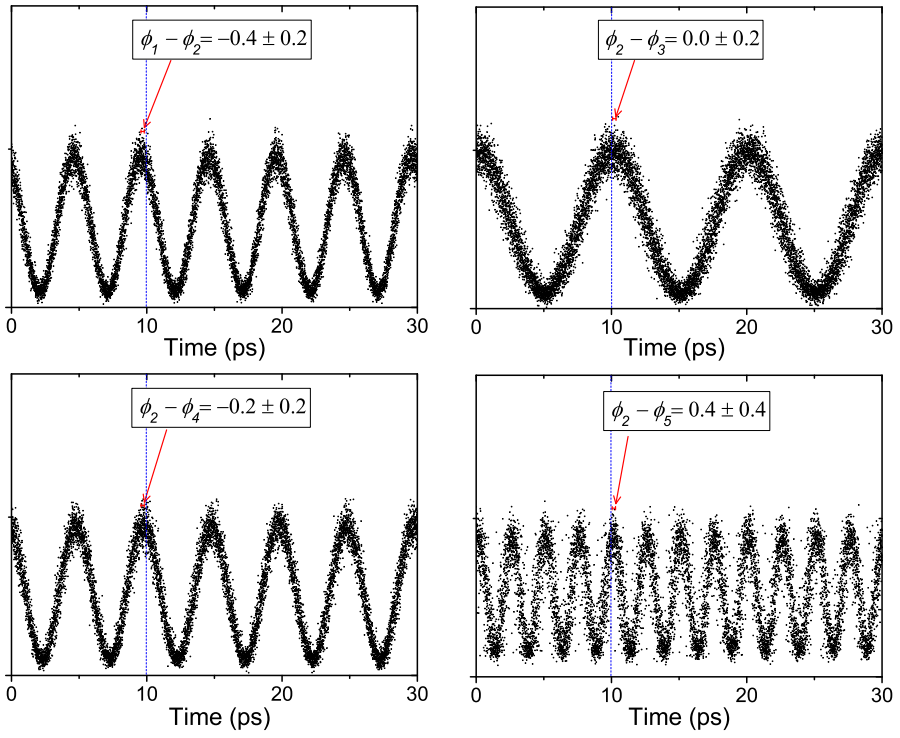

(c) Measured phases

FIGURE 6.24: 100 GHz pulse train generated by five slave lasers after phase calibration.

sinc-spectrum rectangular pulses

Similar to with four lasers, a rectangular-like waveform was again targeted using five lasers. However, this time the targeted spectrum was based on the Fourier transform of a pulse train with a flat electric field amplitude profile and a 50% duty cycle. This corresponds to a spectrum with a sinc profile, as shown in Figure 6.25. This is also the reason behind the choice of frequency spacing of the five slave lasers, since the ±200 GHz components have zero amplitude and therefore lasers at these frequencies were not required. With only five frequency components, the generated waveform was still not expected to reproduce the flat-top profile well. It should be noted that the OSO measures power, not the electric field amplitude, of the optical pulse train. However, in this case, the power of an ideal flat-top amplitude pulse should still be flat-top.

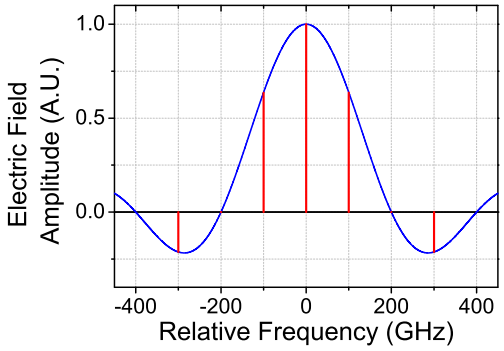

FIGURE 6.25: Fourier transform of a 50% duty cycle rectangular pulse train (blue) and the discrete number of slave lasers (red).

The targeted relative power of the lasers were the square of the electric field amplitudes. The components with negative amplitudes corresponded to a phase of π relative to the positive amplitude components, which had relative phases of zero amongst themselves. The measured waveform and spectrum are shown in Figure 6.26, and the parameters are summarised in Table 6.12. There was a reduction of noise in the vicinity of the lasers in the spectrum (Figure 6.26(b)) due to the Waveshaper attenuating over a 100 GHz channel to control the relative power of the lasers.

Figure 6.26(a) shows that there was good agreement between the targeted waveform (red) and the measured waveform despite the mismatch between the measured and targeted phases. This was quantified by calculating a normalised standard deviation over a single period between the measured and calculated waveforms. The data was normalised to the peak power of the calculated waveform, and was done to allow for comparisons between different waveforms. The normalised standard deviation of the sinc-spectrum waveform in Figure 6.26(a) was 0.09.

The phase across the waveform was also plotted (blue) based on the measured relative phase for each of the lasers. In the ideal case (the targeted phase values), the phase

should be constant across the entire waveform. However, there was a mismatch between the measured and targeted phases which resulted in some small fluctuations in the phase.

TABLE 6.12: Five lasers — sinc-rectangular pulses

Laser Index	Measured Intensity (dB)	Targeted Intensity (dB)	Measured Relative Phase (rad)	Targeted Relative Phase (rad)
1	–13.5	–13.5	3.7 ± 0.2	π
2	–4.3	–3.9	–	–
3	0	0	0.1 ± 0.2	0
4	–4.4	–3.9	0.3 ± 0.2	0
5	–13.6	–13.5	3.6 ± 0.4	π

The stability of the pulse train is shown in Figure 6.26(c). For this, a continuous measurement of the waveform was made over a period of two minutes using the OSO. The data is displayed as a heat map showing the frequency of the measured samples over the two minute measurement period. The heat map is colour graded with black representing zero frequency and white representing the maximum frequency of samples. The waveform is well defined in this heat map, showing that there was very little drift over the two minutes. Even though timing jitter was present in the individual waveform measurements, the heat map shows that this was averaged out over longer periods of time. The stability of the waveform in the heat map was quantified by calculating the FWHM of the frequency of samples (z-axis) at the rising and falling edges. This was done for a fixed power level which was approximately half of the maximum peak power of the waveform. This will be referred to as the *edge sample frequency FWHM* and was calculated to 0.31 ± 0.04 ps for the sinc-spectrum waveform.

Apodised sinc-spectrum rectangular pulses

The limited number of frequency components available resulted in the sinc-spectrum rectangular wave having a large ripple across the top of the pulse. The ripple of the temporal waveform could be reduced by apodising the spectrum. Apodisation is a general term which refers to the process of smoothing sidelobes. In this case, apodisation refers to attenuating the non-zero relative frequency components. The reduction in the ripple at the top of the pulse comes at the cost of reduced sharpness at the edges of the pulse.

TABLE 6.13: Five lasers — apodised sinc-rectangular pulses

Laser Index	Measured Intensity (dB)	Targeted Intensity (dB)	Measured Relative Phase (rad)	Targeted Relative Phase (rad)
1	–20.6	–20	2.8 ± 0.2	π
2	–5.2	–5	–	–
3	0	0	–0.2 ± 0.2	0
4	–5.5	–5	–0.5 ± 0.2	0
5	–21.0	–20	2.2 ± 0.4	π

Apodisation was applied by further attenuating the ±100 GHz and ±300 GHz components in the sinc-spectrum by approximately 1 dB and 7 dB respectively. This is

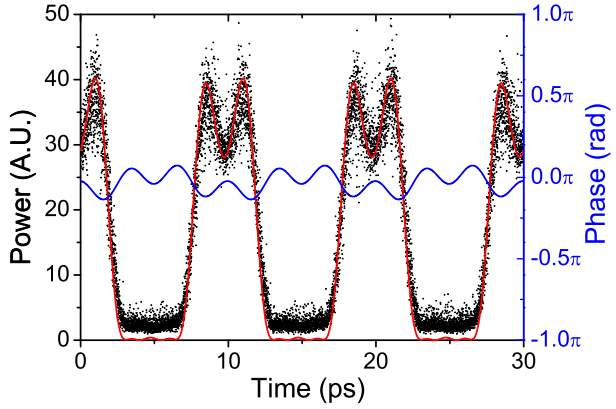

(a) Temporal waveform (black: measured power, red: targeted power, blue: calculated phase)

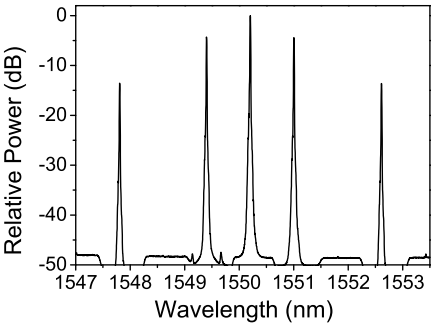

(b) Optical spectrum

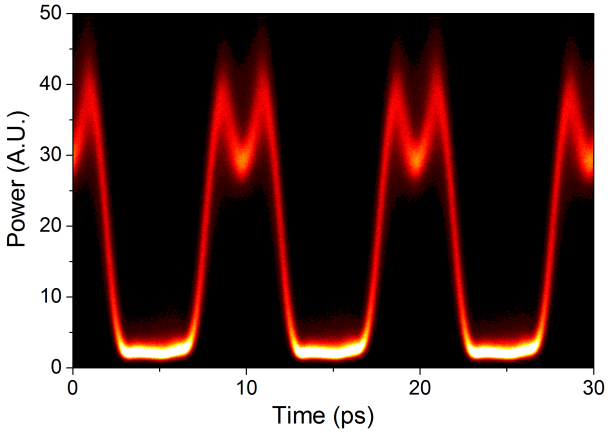

(c) Two minute heat map

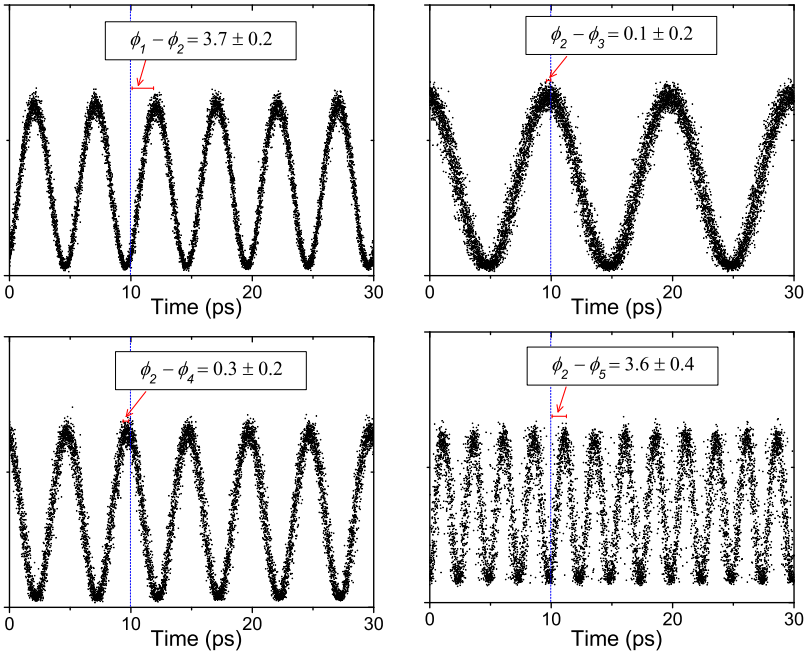

(d) Measured phases

FIGURE 6.26: 100 GHz rectangular pulses generated by five slave lasers with a sinc-spectrum.

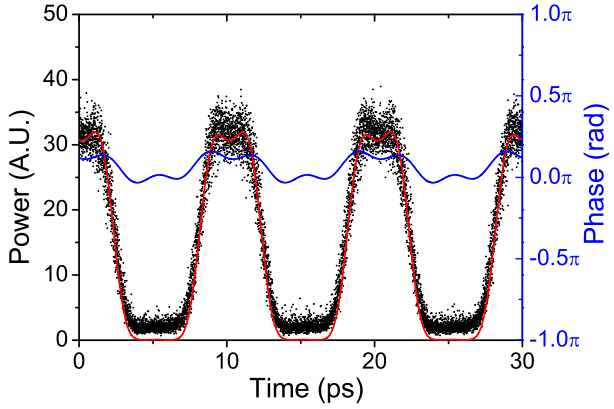

(a) Temporal waveform (black: measured power, red: targeted power, blue: calculated phase)

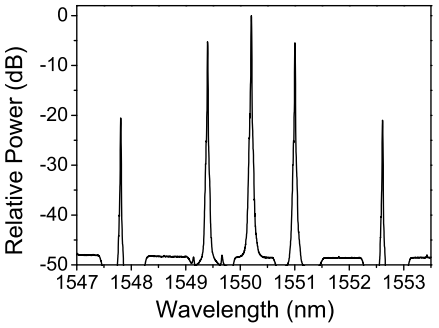

(b) Optical spectrum

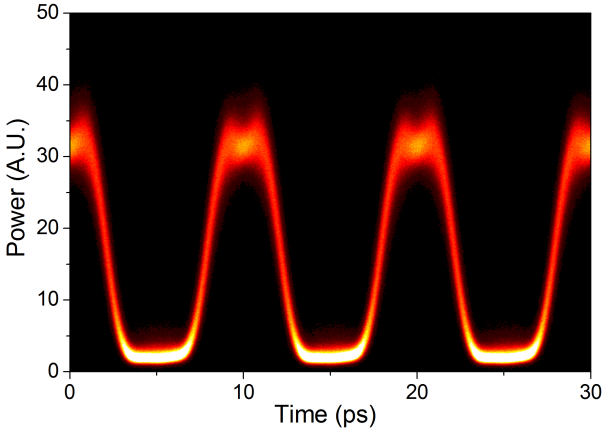

(c) Two minute heat map of the measured samples

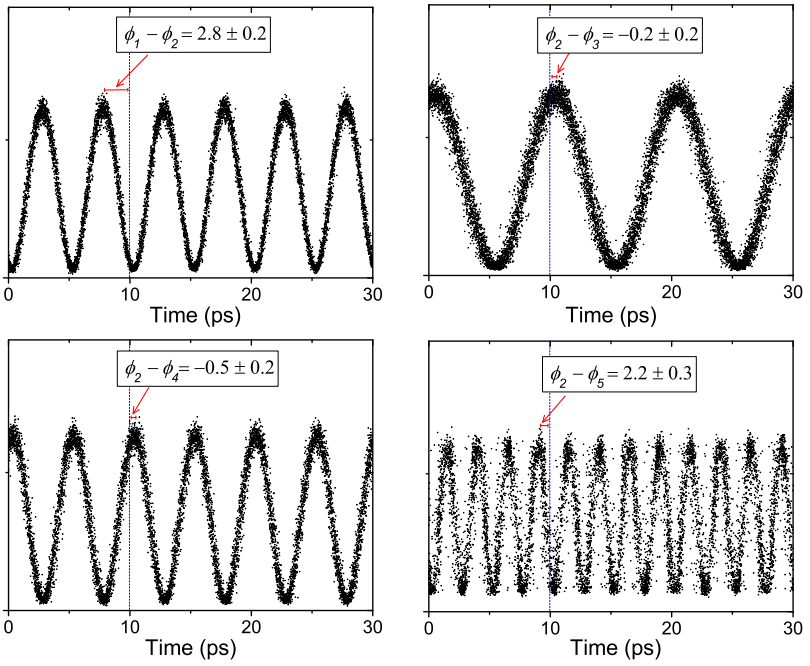

(d) Measured phases

FIGURE 6.27: 100 GHz rectangular pulses generated by five slave lasers with an apodised sinc-spectrum.

approximately a Gaussian apodisation function with a FWHM of 191 GHz. The measured and targeted values are summarised in Table 6.13 and the measurements are shown in Figure 6.27. The relative phases were found to have a significant mismatch between the measured and targeted values. Despite this, there was still a very good agreement between the measured and targeted waveforms in Figure 6.27(a) with a normalised standard deviation of 0.08. Similar to the sinc-spectrum rectangular wave, the phase of the optical carrier was not constant as it should be in the ideal case but instead oscillated due to the mismatch between the measured and targeted relative phases. The two minute heat map is shown in Figure 6.27(c). This had an edge sample frequency FWHM of 0.34 ± 0.04 ps, which is comparable to the unapodised waveform.

sinc^2-spectrum dark parabolic pulses

The final waveform demonstrated using five slave lasers was based on a sinc^2-spectrum, which results in a temporal waveform with a triangular electric field amplitude which linearly increases and decreases with time. The power profile of a triangular electric field amplitude waveform becomes parabolic. This is known as a dark parabolic pulse since the region between pulse peaks has the shape of a positive-parabola[6].

Table 6.14: Five lasers — sinc^2-spectrum dark parabolic pulses

Laser Index	Measured Intensity (dB)	Targeted Intensity (dB)	Measured Relative Phase (rad)	Targeted Relative Phase (rad)
1	–27.4	–27.0	0.0 ± 0.1	0
2	–8.3	–7.8	–	–
3	0	0	-0.1 ± 0.2	0
4	–8.3	–7.8	-0.2 ± 0.2	0
5	–28.0	–27.0	-0.3 ± 0.4	0

The measurement of the dark parabolic pulse train is shown in Figure 6.28 and the parameters are summarised in Table 6.14. There was a very good agreement between the targeted and measured waveforms in Figure 6.28(a). The normalised standard deviation was 0.007, which was significantly better than the values calculated for the sinc-spectrum based waveforms. This was due to the good alignment of the relative phases of the slave lasers which also resulted in a near-constant phase profile across the waveform. The two minute heat map in Figure 6.28(c) has an edge sample frequency FWHM of 0.46 ± 0.06 ps, showing that the dark parabolic waveform is less stable than the sinc- and apodised sinc-spectrum based waveforms.

Discussion: phase mismatch

The mismatch between the measured and targeted relative phases of the slave lasers was a persistent issue in this section. This resulted in non-constant phase profiles across the

[6]This is a contrast to a regular (bright) parabolic pulse, which the pulse itself resembles a negative-parabola

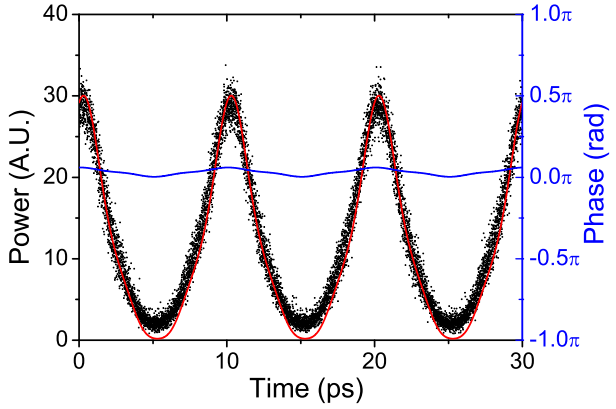

(a) Temporal waveform (black: measured power, red: targeted power, blue: calculated phase)

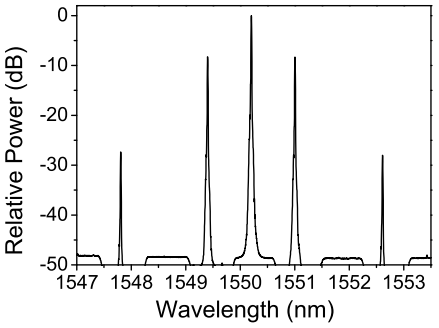

(b) Optical spectrum

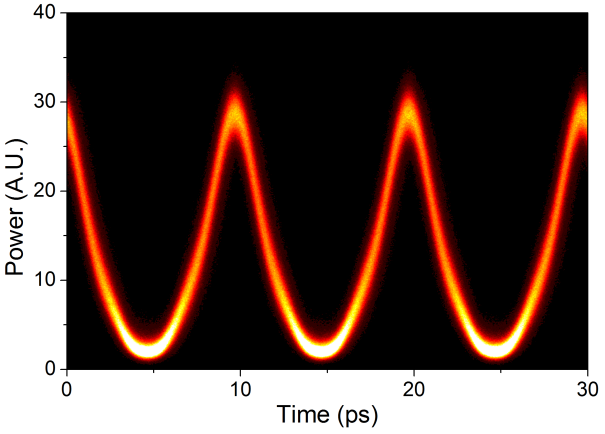

(c) Two minute heat map of the measured samples

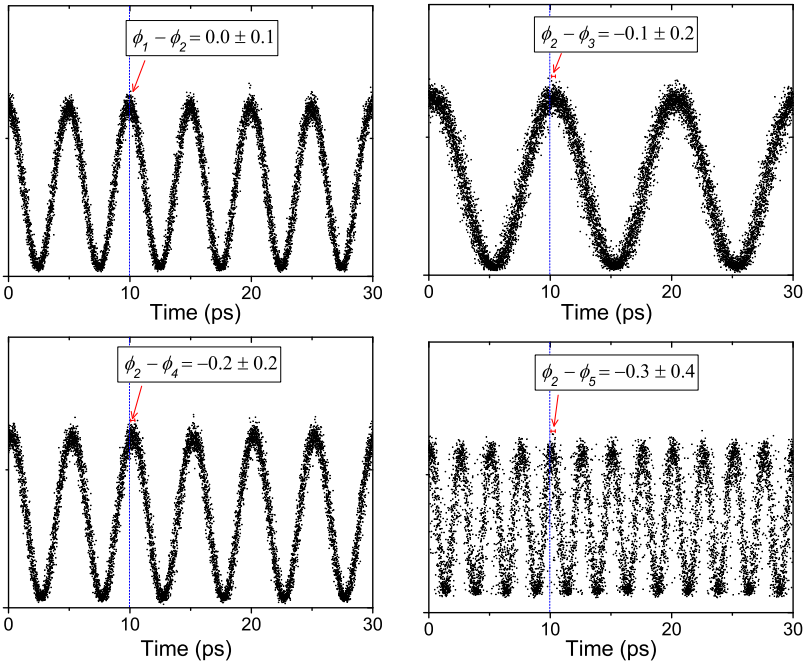

(d) Measured phases

FIGURE 6.28: 100 GHz dark parabolic pulses generated by five slave lasers with a sinc^2-spectrum.

waveforms, which was most evident with the sinc-spectrum rectangular waveforms. Despite the relative phases being off target, the power profiles were still in good agreement with the targeted waveform.

One of the possible reasons for the phase mismatch could be attributed to drift in the phase of the clock signal for the OSO. This signal was derived from the repetition rate of the OFC which needed to travel trough optical fibre and therefore was susceptible to slow phase drifts from thermal effects. This drift in clock phase resulted in a translation in time of the measured waveforms, which corresponded to a linear phase relationship for each laser with relative frequency. However, this linear phase shift does not alter the phase profile of the waveform and hence was not the only cause for the phase mismatch. The likely causes for the remaining mismatch was due to: the error of the phase measurements due to jitter of the OSO and the signal itself; and the accuracy of the phase shift imparted by the Waveshaper.

The phase mismatch could be minimised by actively adjusting the phase shift imparted by the Waveshaper. Unfortunately, this was highly inconvenient because the relative phases were calculated using post-processing. However, it would be possible to program the OSO to give real-time phase measurements. The Waveshaper output could then be updated to give the correct phase values. This could be done either manually or automatically using software.

6.5.4 Six Lasers

The final demonstration of partial Fourier synthesis was achieved with six slave lasers. The operating wavelengths are given in Table 6.15, with the first five being the same as those used in the previous section. The addition of the sixth laser breaks the frequency symmetry of the system and hence the waveforms generated using all six lasers are less likely to have a constant phase profile. Similar to when four lasers were used (Section 6.5.2), the targeted waveforms were based on their power profiles only and the required power and phase of the slave lasers were calculated using non-linear fitting.

TABLE 6.15: Six lasers indexing

Laser Index	Wavelength (nm)	Relative Frequency (GHz)
1	1548.81	+400
2	1549.40	+200
3	1550.20	+100
4	1551.00	0
5	1552.61	–200
6	1554.23	–400

The relative phases of the lasers were calibrated using the same method which was discussed for five lasers. Laser #2 was again used as the reference laser to generate the beat signals.

Triangular pulses

Triangular pulses were generated using the phase and amplitude parameters given in Table 6.16 with the generated waveform shown in Figure 6.29. The expected phase of the waveform was calculated from the targeted relative phase values. This was found to oscillate smoothly across the period of the waveform with a frequency matching the repetition rate of the waveform (100 GHz). This waveform more closely resembles an ideal triangular waveform than the case with four lasers (Section 6.5.2), highlighting the advantage of having more frequency components available. The normalised standard deviation between the measured and calculated waveforms was calculated to be 0.1.

TABLE 6.16: Six lasers — triangular pulses

Laser Index	Measured Intensity (dB)	Targeted Intensity (dB)	Targeted Relative Phase (rad)
1	–36.9	–37.0	0
2	–22.0	–21.6	–
3	0	0	0
4	–3.4	–3.3	π
5	–22.9	–22.0	π
6	–34.5	–33.0	π

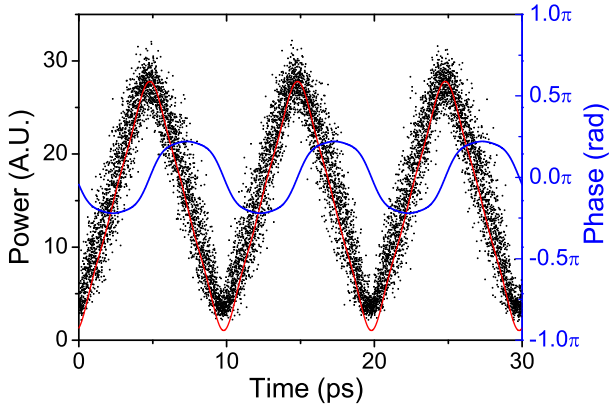

(a) Temporal waveform (black: measured power, red: targeted power, blue: expected phase)

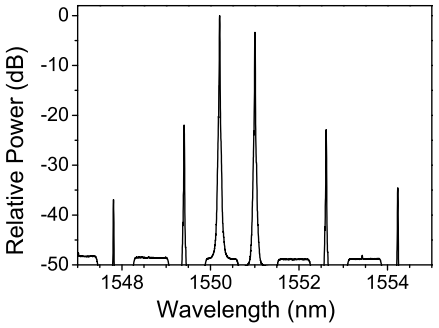

(b) Optical spectrum

FIGURE 6.29: 100 GHz triangular pulse train generated using six slave lasers.

Parabolic pulses

The generation of (bright) parabolic pulses with 50% duty cycle is shown in Figure 6.30 using the parameters in Table 6.17. The calculated normalised standard deviation between the measured and calculated parabolic waveforms was 0.1.

TABLE 6.17: Six lasers — parabolic pulses

Laser Index	Measured Intensity (dB)	Targeted Intensity (dB)	Targeted Relative Phase (rad)
1	–18.9	–19.0	0
2	–4.9	–4.9	–
3	0	0	π
4	–2.6	–2.6	0
5	–12.0	–11.4	π
6	–25.1	–24.6	0

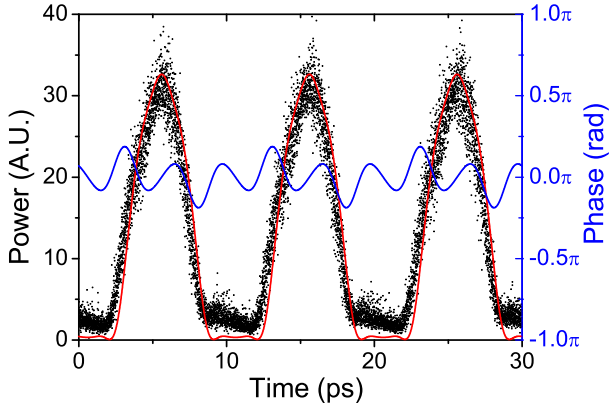

(a) Temporal waveform (black: measured power, red: targeted power, blue: expected phase)

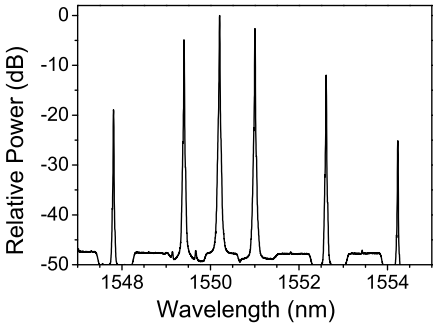

(b) Optical spectrum

FIGURE 6.30: 100 GHz parabolic pulse train generated using six slave lasers.

Sawtooth

The final waveform targeted with six lasers was a sawtooth pulse train. This is shown in Figure 6.31 using the parameters in Table 6.18. Similar to the case for four lasers, this had the poorest match between targeted and measured waveforms with a normalised standard deviation of 0.2. However, with six lasers, the waveform more closely resembled a sawtooth power profile. Unlike the triangular or parabolic pulses, the targeted relative phases of the lasers were not simply 0 or π. The waveform was therefore more likely to be sensitive to phase mismatches. This was also the likely reason for the presence of the step-like feature in the centre of the sawtooth wave.

TABLE 6.18: Five lasers — sawtooth pulses

Laser Index	Measured Intensity (dB)	Targeted Intensity (dB)	Targeted Relative Phase (rad)
1	–18.6	–18.9	6.11
2	–4.2	–4.3	–
3	–1.2	–1.3	6.23
4	0	0	4.01
5	–10.8	–10.5	4.29
6	–16.5	–16.0	4.64

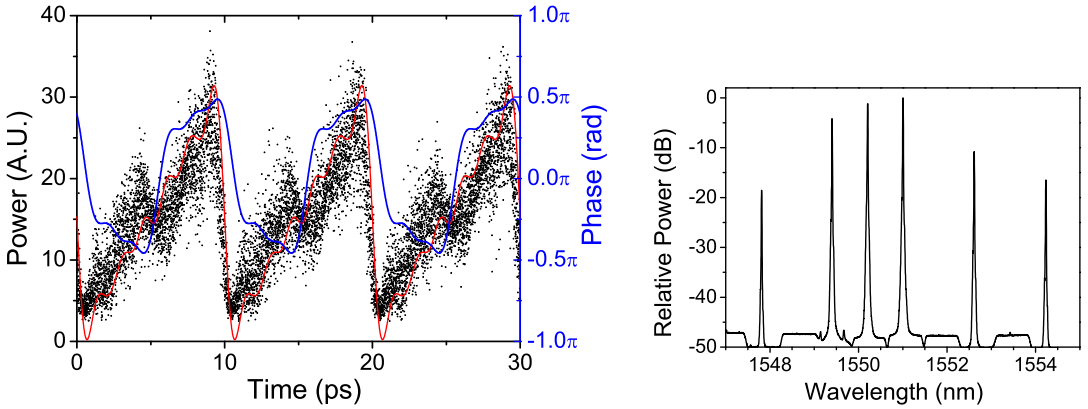

(a) Temporal waveform (black: measured power, red: targeted power, blue: expected phase)

(b) Optical spectrum

FIGURE 6.31: 100 GHz sawtooth-like pulses generated using six slave lasers.

Discussion

This section has shown that waveforms generated with six lasers more closely resemble their ideal waveforms than with four lasers. This is consistent with Fourier theory since there are more frequency components present. In particular, the targeted triangular and parabolic pulses are close matches to their ideal cases as shown in Figure 6.32. The asymmetry and sharp discontinuity of the sawtooth waveform results in more frequency components being required for a better fit. Each of the generated waveforms still have some power offset, which was previously discussed in Section 6.5.2.

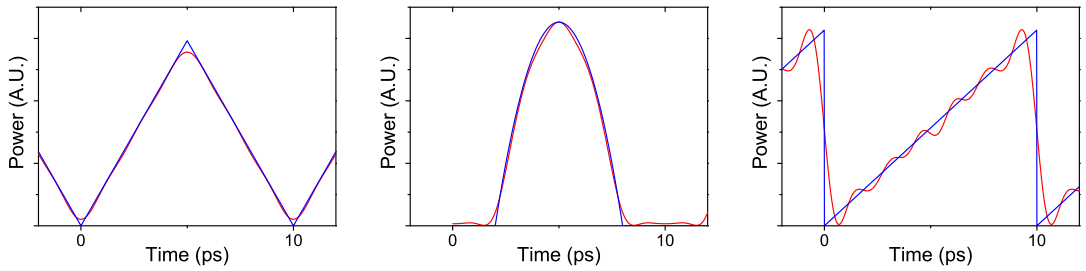

(a) Triangular (b) Parabolic (c) Sawtooth

FIGURE 6.32: Comparison between targeted (red) and ideal (blue) waveforms.

Although not presented here, two minute heat maps were also measured for the waveforms generated with six slave lasers. These additional measurements are provided in Appendix C. Similar to the waveforms generated with five lasers, these waveforms were found to be stable over two minutes. However, as expected from the larger normalised standard deviation of these waveforms compared to those generated with 5 lasers, the edge sample frequency FWHM was also larger. These were calculated to be 1.11 ± 0.08 ps, 0.73 ± 0.06 ps, and 1.2 ± 0.2 ps for the triangular, parabolic, and sawtooth waveforms respectively.

It was found when calibrating the relative phases of the six lasers that the beat signal between laser #2 and #6 (600 GHz) had a significantly smaller amplitude than the others. This was despite the two lasers having approximately equal power and with the beat signal maximised by aligning their polarisations. The reason for this was believed to be due to the bandwidth limitation of the OSO, which was specified by the manufacturer to be approximately 500 GHz. The bandwidth of the OSO was measured using the six available slave lasers by generating beat signals between various pairs of lasers and measuring the peak-to-peak amplitudes. The lasers were set to have the same power and polarisations. Examples are shown in Figure 6.33(a)–(c), and the measured bandwidth in Figure 6.33(d). The error bars are estimated based on the noise of the beat signals. This shows that 800 GHz is the approximate 3 dB bandwidth of the OSO. This limited bandwidth would have also contributed to the power offset present in the measured waveforms.

Adding more lasers to the slave laser ensemble would, in principle, be expected to improve the convergence of the waveforms to their ideal cases. To achieve this, the active control of phase discussed in Section 6.5.3 would be required to ensure each laser had the correct relative phase. Also, the bandwidth limitation of the OSO would require a smaller frequency spacing between lasers if additional ones were to be added whilst using the same OSO. The narrower frequency spacing would ensure that the generated waveforms could be measured accurately.

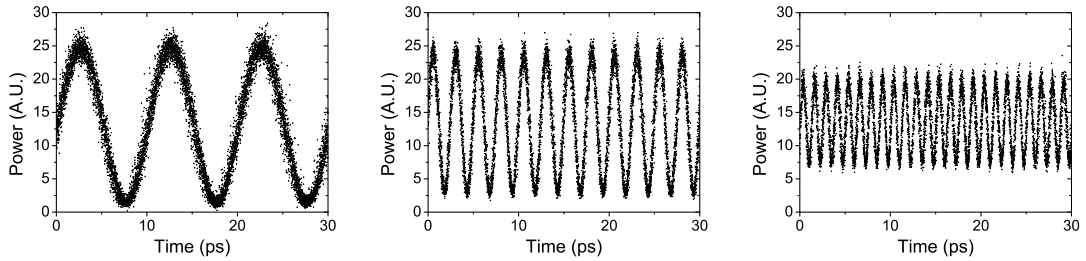

(a) 100 GHz beat signal (b) 400 GHz beat signal (c) 800 GHz beat signal

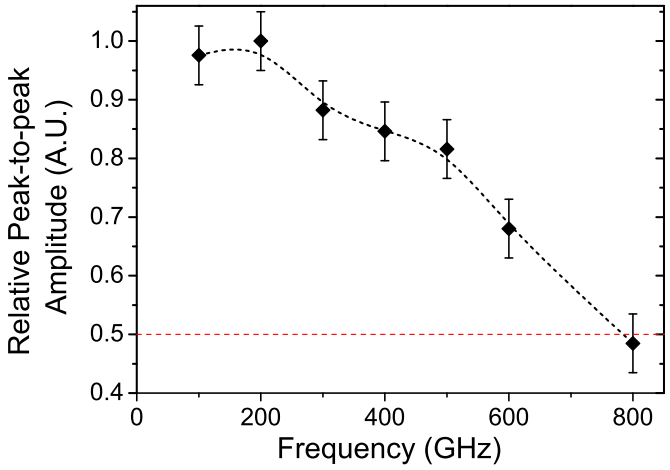

(d) OSO bandwidth characterisation

FIGURE 6.33: The OSO bandwidth measured from the beat signals between various pairs of lasers.

6.6 Full Fourier Synthesis

Partial Fourier synthesis was demonstrated in Section 6.4 with the generation of various waveforms using a Waveshaper device. This was an inefficient process since access to the individual frequency components was already possible inside the slave laser ensemble before they were combined together. In this section, I demonstrate that full Fourier synthesis was indeed possible.

6.6.1 Phase control

In Section 6.4.1, the limited ability to accurately vary the relative phases of each laser due to the unstable locking positions of the feedback loop was discussed. The ability to tune the stabilised phase could be achieved despite this limitation by using additional phase shifters in the phase stabilisation error signal generator as shown in Figure 6.34(a). The only alteration from Figure 6.13 is the inclusion of the RF phase shifters to vary the phase of the 35 MHz beat signals. Shifting the phase of the RF signal entering the mixer causes the error signal function to be translated as a function of optical phase, as shown in Figure 6.34(b). By keeping the feedback locked to a certain error signal value (e.g. 0 V, where the locking was stable) and imparting an RF phase shift, the relative phase of the slave laser could be varied while remaining actively stabilised. The amount of optical phase shift, relative to the reference OFC, was directly equal to the RF phase shift applied.

The RF phase shifters used were Minicircuits JSPHS-51+, with the phase shift controlled by an external voltage. The five phase shifters were controlled using an Arduino microcontroller with a computer (software) interface. Ideally, this would be integrated with the LabView feedback program used for the phase stabilisation, but was not possible in this case due to an insufficient number of available data acquisition cards. Although these phase shifters only had a π phase shift range, the entire 2π range was accessible by switching the feedback locking position to either the rising or falling slope, i.e. by inverting the feedback gain.

6.6.2 Demonstration

The relative amplitude and phase of each slave laser could be controlled without the Waveshaper by using the manual attenuators and RF phase shifters. This represents full Fourier synthesis. However, the Waveshaper was still required to perform the phase calibration, i.e. to isolate pairs of slave lasers to measure their relative phases. The experimental set-up was therefore the same as in Figure 6.15, but with the RF phase shifters implemented in the phase stabilisation error signal generator. To minimise the

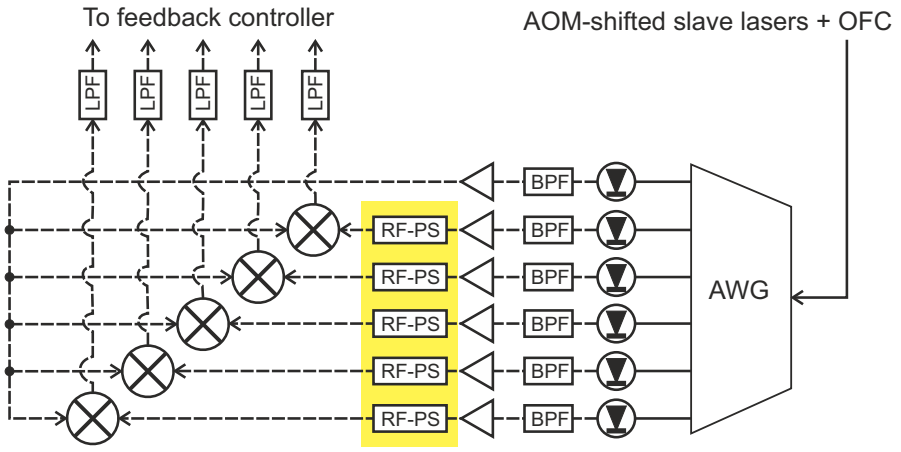

(a) Phase stabilisation with phase tunability using RF phase shifters (RF-PS).

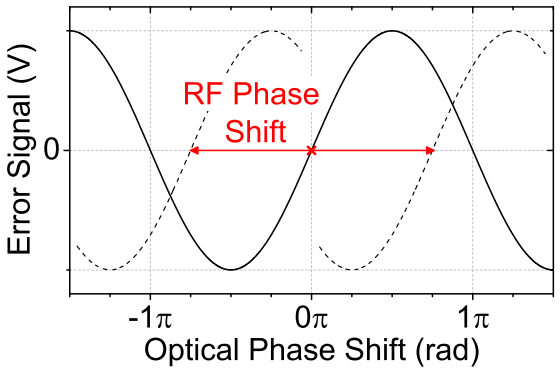

(b) Error signal as a function of optical phase shift.

FIGURE 6.34: Phase control using RF Phase shifters

effect of the sensitivity of phase and polarisation due to the manual attenuators, the relative power of each laser was set first.

For this demonstration, sinc-spectrum and apodised sinc-spectrum rectangular waveforms using five slave lasers were generated. This allowed the results to be directly compared with those in Section 6.5.3 using partial Fourier synthesis.

Sinc-spectrum rectangular pulses

The sinc-spectrum waveform generated without the Waveshaper is shown in Figure 6.35 and the measured parameters are given in Table 6.19. The relative phases of the lasers were able to be set to similar values as those in Section 6.5.3. This shows that the RF phase shifters were able to control the relative phases of the lasers with a similar level of accuracy as the Waveshaper. As expected from the relative phase measurements, the power profile of the waveform is in good agreement with the targeted waveform as shown in Figure 6.35(a). The normalised standard deviation was 0.09, which was the same as the waveform generated with the Waveshaper. The two minute heat map in Figure 6.35(c) shows a similar level of stability (edge sample frequency FWHM:

0.28 ± 0.04 ps) as in Section 6.5.3, which demonstrates that the RF phase shifters do not introduce any instability.

TABLE 6.19: Five lasers — sinc-spectrum rectangular pulses (no Waveshaper)

Laser Index	Measured Intensity (dB)	Targeted Intensity (dB)	Measured Relative Phase (rad)	Targeted Relative Phase (rad)
1	–12.8	–13.5	3.6 ± 0.2	π
2	–3.9	–3.9	–	–
3	0	0	0.1 ± 0.2	0
4	–4.2	–3.9	0.3 ± 0.2	0
5	–13.1	–13.5	3.6 ± 0.4	π

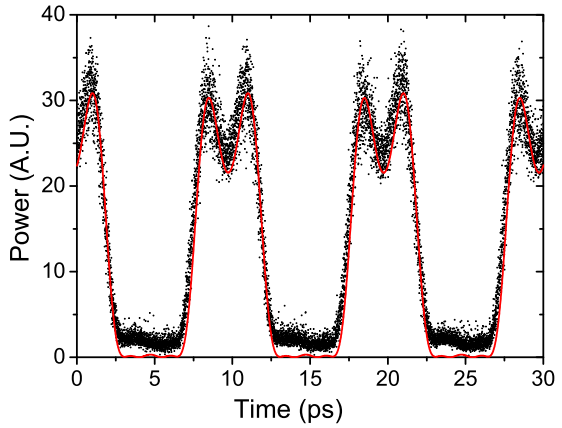

(a) Temporal waveform (black: measured, red: targeted)

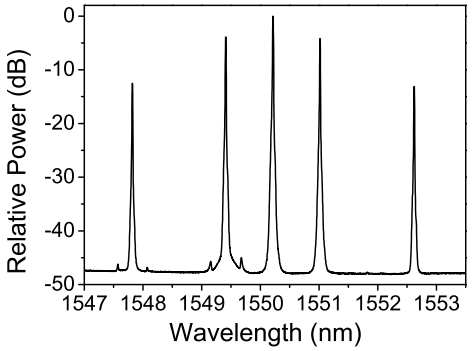

(b) Optical spectrum

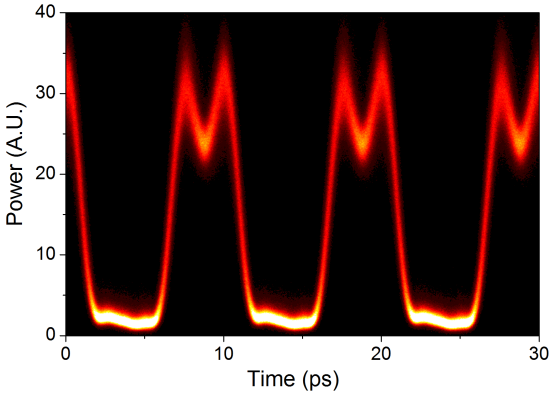

(c) Two minute heat map

FIGURE 6.35: Full Fourier synthesis of a 100 GHz sinc-spectrum rectangular pulse train generated by five slave lasers.

Apodised sinc-spectrum rectangular pulses

The apodised sinc-spectrum was generated directly after the un-apodised version above. The RF phase shifters were not altered from the previous measurement and only the attenuators were adjusted to perform the apodisation. The polarisation needed to be aligned again afterwards. The generated waveform is shown in Figure 6.36, and again

the power profile had the expected shape. The normalised standard deviation was 0.08, which was also the same as the waveform generated using the Waveshaper. A similar level of stability is also shown in the heat map in Figure 6.36(c), with a edge sample frequency FWHM of 0.42 ± 0.04 ps, which is only slightly larger than for the case using the Waveshaper. However, Table 6.20 shows that the measured relative phases were significantly off target. The reason for this is clear from Figure 6.36(a), where the waveform has been translated in time compared to the un-apodised waveform in Figure 6.35(a). The relative phases were recalculated with respect to laser #3, and their deviations from the targeted phase are shown in Figure 6.36(d). The slope of the linear phase shift in Figure 6.36(d) was approximately π rad/100 GHz, which corresponds to a time translation of 5 ps. This expected time translation matches the waveform measured in Figure 6.36(a).

TABLE 6.20: Five lasers — apodised sinc-spectrum rectangular pulses (no Waveshaper)

Laser Index	Measured Intensity (dB)	Targeted Intensity (dB)	Measured Relative Phase (rad)	Targeted Relative Phase (rad)
1	–19.9	–20	2.8 ± 0.2	π
2	–4.9	–5	–	–
3	0	0	2.9 ± 0.2	0
4	–4.9	–5	5.9 ± 0.2	0
5	–20.1	–20	2.2 ± 0.4	π

The reason for the temporal translation was due to the a change in phase of laser #2, which occurred when the manual attenuators were adjusted. Recall that laser #2 itself was not actively phase stabilised since it was used as the reference for all the other lasers. Laser #2 was therefore allowed to drift, with the phase stabilisation feedback compensating for this drift in the other lasers to maintain the fixed relative phases. However, the phase of each laser with respect to the OSO clock does change due to the drift in laser #2, which resulted in a change of phase of the waveform i.e. a time translation.

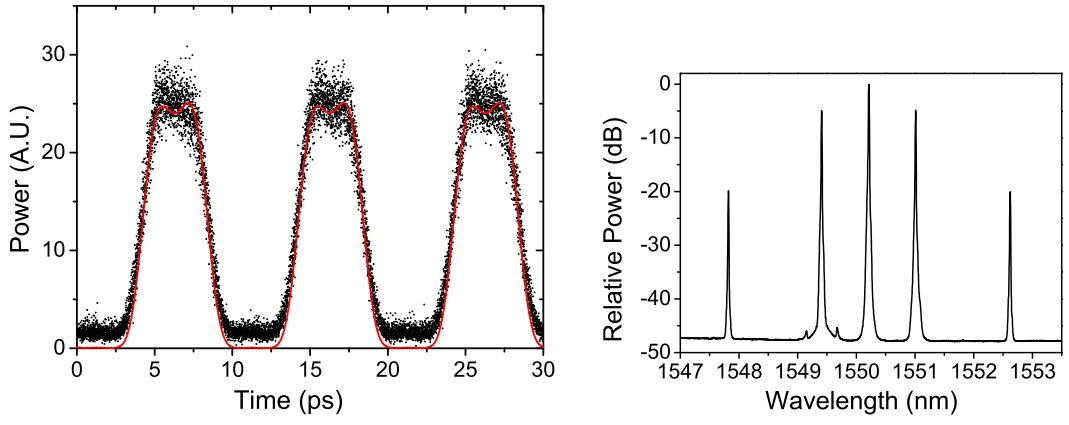

(a) Temporal waveform (black: measured, red: targeted)

(b) Optical spectrum

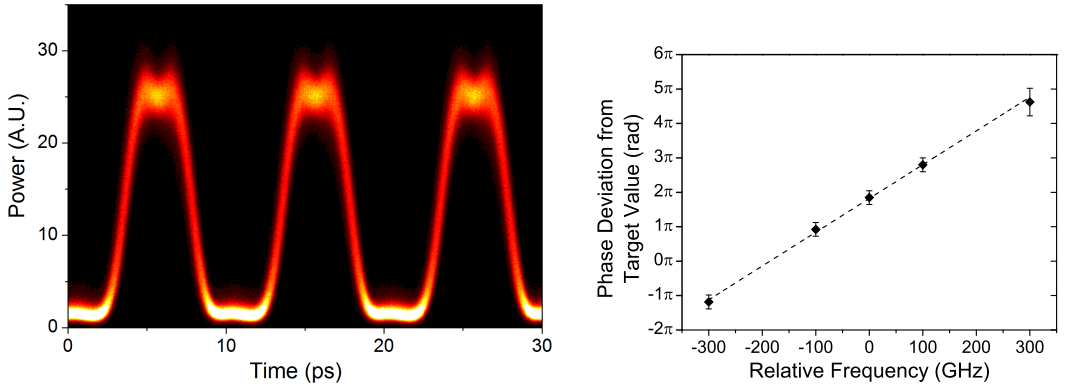

(c) Two minute heat map

(d) Linear phase shift of waveform

FIGURE 6.36: Full Fourier synthesis of a 100 GHz apodised sinc-spectrum rectangular pulse train generated by five slave lasers. The targeted waveform in (a) was translated in time to fit the data.

6.7 Further improvements (future work)

The previous section has shown that Fourier synthesis of stable, high repetition rate waveforms can be achieved without the need for a Waveshaper to control the relative amplitudes and phases. This section will discuss potential methods to further improve the system.

6.7.1 Improving the current system

Although the Waveshaper was not used for amplitude or phase control in Section 6.6, it was still required to isolate pairs of slave lasers to measure their relative phases. In principle, this could have been done within the slave laser ensemble by using the attenuators prior to the lasers being combined. However, this was not possible in the set-up used because the mechanically controlled attenuators would introduce phase and polarisation variations each time they were adjusted. This could be overcome by using a combination of electrically controlled optical attenuators and shutters. This would allow the relative power of each laser to be controlled without changing its phase or polarisation, as well as allowing pairs of lasers to be easily isolated. Since this would allow both relative phase and amplitude to be controlled electronically, this could then be combined into a single control system. This system would therefore have the same functionality as the Waveshaper as used in these experiments.

This system utilised a large amount of electrical components such as RF amplifiers, phase shifters, mixers and filters. Over 50 individual components were used in this set-up, each requiring coaxial cables for interconnects and occupying a large volume of space. All of the components used are also available as surface mount components which are significantly smaller than their bulk form counterparts. It would therefore be possible to design and fabricate printed circuit boards (PCBs) to replace the bulk components and the coaxial interconnect cables used to form the error signal generators for the OIPLLs and the phase stabilisation. This would greatly reduce the size of the overall set-up as well as potentially reducing the cost.

The use of polarisation maintaining (PM) fibre within the slave laser ensemble could reduce the size of the set-up by removing two polarisation controllers per slave laser. This would also eliminate the need to manually align the polarisation of both the input and output of the slave lasers. PM fibre may also improve the phase stability of the system by minimising polarisation dependent fluctuations of optical path lengths. An alternative to PM fibre would be to implement active polarisation locking using polarisation trackers.

Finally, the performance of the set-up may also be improved by using a wider spaced OFC. As previously discussed in Chapter 5, the residual comb modes from the injection locking process experience amplification, and hence they can behave as noise in the

system. This effect is reduced with wider comb spacings and it would also allow for higher injection ratios to be used to improve the stability of the injection locking. However, a wider comb spacing would require higher bandwidth RF components for the feedback loop in the OIPLL which could significantly increase the cost and performance of the system. Also, wider spaced OFCs which span the required bandwidth for high repetition rate Fourier synthesis are more difficult to generate.

6.7.2 Photonic Integration

In the long-term, it can be envisioned that the optical portion of the set-up could also be miniaturised into a photonic integrated circuit (PIC). Many of the components required have already been demonstrated in an integrated form, as outlined in the review paper by Heck et al. [38]. This includes the lasers, low-loss AWGs, circulators [39], phase modulators, and attenuators (in the form of Mach-Zehnder modulators). Furthermore, the master laser could also be integrated into the PIC by using other types of OFCGs such as EOM- or microresonator- based OFCs.

A PIC would not only significantly reduce the size of the system, but also have the advantage of having very short optical path lengths. This would suppress the effects of thermal phase variations and reduce the already low requirements for phase stabilisation. The optical paths lengths of the slave lasers can also be made equal by design, further improving the phase stability of the system. A PIC would also provide good polarisation stability.

The combination of a PIC for the optical components and PCBs for the electrical components could result in a highly compact and portable device. This could potentially have numerous applications across a wide range of fields.

6.8 Conclusions

This chapter has demonstrated optical waveform generation as one of the applications of the OIPLL phase locking technique which was introduced and characterised earlier in this thesis. Waveform generation was achieved based on the principle of Fourier synthesis, where multiple lasers operating at different frequencies were combined together to generate the waveforms. The OIPLL was utilised to ensure that the lasers were coherent with one another by locking them to a common OFC.

A combination of Fourier synthesis and line-by-line pulse shaping using a Waveshaper (after the lasers were combined) was used to generate various waveforms. Up to six slave lasers were used to generate: Gaussian, rectangular, triangular, dark- & bright-parabolic, and sawtooth pulses. As expected from Fourier theory, the convergence of

these waveforms to their ideal cases improved as the number of lasers increased. The generated pulse trains were measured to have good stability over a two minute period.

Full Fourier synthesis was also demonstrated with the waveforms being generated without the Waveshaper being used for amplitude or phase control. The power profiles and stability of these waveforms were the same as those generated using partial Fourier synthesis. As future work, the Waveshaper could be removed completely from the set-up by implementing electrically controlled attenuators inside the slave laser ensemble.

The experiments performed in this chapter were ultimately limited by two factors. Firstly, the limited number of slave lasers available at the required wavelengths restricted the complexity of the generated waveforms. Secondly, the bandwidth of the OSO limited the measurements possible. This would have prevented high speed features of the waveforms to be properly resolved if they were generated at higher repetition rates.

The physical size of the set-up was able to be condensed by using multi-tiered enclosures to house the various optical and RF components in the slave laser ensemble. However, it can be envisioned that the set-up can be shrunk further by using a combination of electrical and photonic integration using PCBs and PICs. This could potentially lead to the development of a compact sized optical waveform synthesiser which could prove to be as useful as the RF arbitrary waveform generator has been for lower speed applications.

6.9 References

[1] A. M. Weiner, "Femtosecond optical pulse shaping and processing," *Progress in Quantum Electronics*, vol. 19, no. 3, pp. 161–237, 1995.

[2] A. M. Weiner, "Femtosecond pulse shaping using spatial light modulators," *Review of Scientific Instruments*, vol. 71, no. 5, pp. 1929–1960, 2000.

[3] A. M. Weiner, "Ultrafast optical pulse shaping: A tutorial review," *Optics Communications*, vol. 284, no. 15, pp. 3669–3692, 2011.

[4] J. Agostinelli, G. Harvey, T. Stone, and C. Gabel, "Optical pulse shaping with a grating pair," *Applied Optics*, vol. 18, no. 14, pp. 2500–2504, 1979.

[5] A. M. Weiner, D. E. Leaird, J. S. Patel, and J. R. Wullert, "Programmable femtosecond pulse shaping by use of a multielement liquid-crystal phase modulator," *Optics Letters*, vol. 15, no. 6, pp. 326–328, 1990.

[6] M. M. Wefers and K. A. Nelson, "Generation of high-fidelity programmable ultrafast optical waveforms," *Optics Letters*, vol. 20, no. 9, pp. 1047–1049, 1995.

[7] M. A. Dugan, J. X. Tull, and W. S. Warren, "High-resolution acousto-optic shaping of unamplified and amplified femtosecond laser pulses," *Journal of the Optical Society of America B*, vol. 14, no. 9, pp. 2348–2358, 1997.

[8] K. F. Kwong, D. Yankelevich, K. C. Chu, J. P. Heritage, and A. Dienes, "400-Hz mechanical scanning optical delay line," *Optics Letters*, vol. 18, no. 7, pp. 558–560, 1993.

[9] E. Zeek, K. Maginnis, S. Backus, U. Russek, M. Murnane, G. Mourou, H. Kapteyn, and G. Vdovin, "Pulse compression by use of deformable mirrors," *Optics Letters*, vol. 24, no. 7, pp. 493–495, 1999.

[10] E. Frumker and Y. Silberberg, "Femtosecond pulse shaping using a two-dimensional liquid-crystal spatial light modulator," *Optics Letters*, vol. 32, no. 11, pp. 1384–1386, 2007.

[11] J. W. Wilson, P. Schlup, and R. A. Bartels, "Ultrafast phase and amplitude pulse shaping with a single, one-dimensional, high-resolution phase mask," *Optics Express*, vol. 15, no. 14, pp. 8979–8987, 2007.

[12] P. Petropoulos, M. Ibsen, A. D. Ellis, and D. J. Richardson, "Rectangular pulse generation based on pulse reshaping using a superstructured fiber bragg grating," *Journal of Lightwave Technology*, vol. 19, no. 5, pp. 746–752, 2001.

[13] F. Parmigiani, P. Petropoulos, M. Ibsen, and D. Richardson, "Pulse retiming based on XPM using parabolic pulses formed in a fiber Bragg grating," *IEEE Photonics Technology Letters*, vol. 18, no. 7, pp. 829–831, 2006.

[14] F. Parmigiani, M. Ibsen, T. T. Ng, L. Provost, P. Petropoulos, and D. J. Richardson, "An efficient wavelength converter exploiting a grating-based saw-tooth pulse shaper," *IEEE Photonics Technology Letters*, vol. 20, no. 17, pp. 1461–1463, 2008.

[15] T. T. Ng, F. Parmigiani, M. Ibsen, Z. Zhang, P. Petropoulos, and D. J. Richardson, "Compensation of linear distortions by using XPM with parabolic pulses as a time lens," *IEEE Photonics Technology Letters*, vol. 20, no. 13, pp. 1097–1099, 2008.

[16] P. C. Chou, H. A. Haus, and J. F. Brennan III, "Reconfigurable time-domain spectral shaping of an optical pulse stretched by a fiber Bragg grating," *Optics Letters*, vol. 25, no. 8, pp. 524–526, 2000.

[17] M. Li, Y. Han, S. Pan, and J. Yao, "Experimental demonstration of symmetrical waveform generation based on amplitude-only modulation in a fiber-based temporal pulse shaping system," *IEEE Photonics Technology Letters*, vol. 23, no. 11, pp. 715–717, 2011.

[18] J. Azaña, N. K. Berger, B. Levit, and B. Fischer, "Reconfigurable generation of high-repetition-rate optical pulse sequences based on time-domain phase-only filtering," *Optics Letters*, vol. 30, no. 23, pp. 3228–3230, 2005.

[19] C. Hayes and L. Laughman, "Generation of coherent optical pulses," *Applied Optics*, vol. 16, no. 2, pp. 263–264, 1977.

[20] M. Hyodo, N. Onodera, and K. S. Abedin, "Fourier synthesis of 9.6-GHz optical-pulse trains by phase locking of three continuous-wave semiconductor lasers," *Optics Letters*, vol. 24, no. 5, pp. 303–305, 1999.

[21] M. Hyodo, K. Abedin, and N. Onodera, "Generation of arbitrary optical waveforms by Fourier synthesis using three continuous-wave semiconductor lasers," *Electronics Letters*, vol. 36, no. 3, pp. 224–225, 2000.

[22] M. Hyodo, K. S. Abedin, and N. Onodera, "Fourier synthesis of 1.8-THz optical-pulse trains by phase locking of three independent semiconductor lasers," *Optics Letters*, vol. 26, no. 6, pp. 340–342, 2001.

[23] S. Boscolo and C. Finot, "Nonlinear pulse shaping in fibres for pulse generation and optical processing," *International Journal of Optics*, vol. 2012, pp. 1–14, 2012.

[24] S. T. Cundiff and A. M. Weiner, "Optical arbitrary waveform generation," *Nature Photonics*, vol. 4, no. 11, pp. 760–766, 2010.

[25] D. Strickland and G. Mourou, "Compression of amplified chirped optical pulses," *Optics Communications*, vol. 56, no. 3, pp. 219–221, 1985.

[26] T. Brixner, M. Strehle, and G. Gerber, "Feedback-controlled optimization of amplified femtosecond laser pulses," *Applied Physics B: Lasers and Optics*, vol. 68, no. 2, pp. 281–284, 1999.

[27] A. Efimov and D. H. Reitze, "Programmable dispersion compensation and pulse shaping in a 26-fs chirped-pulse amplifier," *Optics Letters*, vol. 23, no. 20, pp. 1612–1614, 1998.

[28] D. Geisler, N. Fontaine, T. He, R. P. Scott, L. Paraschis, J. P. Heritage, and S. J. B. Yoo, "Modulation-format agile, reconfigurable Tb/s transmitter based on optical arbitrary waveform generation," *Optics Express*, vol. 17, no. 18, pp. 15911–15925, 2009.

[29] R. P. Scott, N. K. Fontaine, J. P. Heritage, and S. J. B. Yoo, "Dynamic optical arbitrary waveform generation and measurement," *Optics Express*, vol. 18, no. 18, pp. 18655–18670, 2010.

[30] D. J. Geisler, N. K. Fontaine, R. P. Scott, T. He, L. Paraschis, O. Gerstel, J. P. Heritage, and S. J. B. Yoo, "Bandwidth scalable, coherent transmitter based on the parallel synthesis of multiple spectral slices using optical arbitrary waveform generation," *Optics Express*, vol. 19, no. 9, pp. 8242–8253, 2011.

[31] A. Weiner, Y. Silberberg, H. Fouckhardt, D. Leaird, M. Saifi, M. Andrejco, and P. Smith, "Use of femtosecond square pulses to avoid pulse breakup in all-optical switching," *IEEE Journal of Quantum Electronics*, vol. 25, no. 12, pp. 2648–2655, 1989.

[32] S. R. Friberg, A. M. Weiner, Y. Silberberg, B. G. Sfez, and P. S. Smith, "Femtosecond switching in a dual-core-fiber nonlinear coupler," *Optics Letters*, vol. 13, no. 10, pp. 904–906, 1988.

[33] F. Parmigiani, M. Ibsen, P. Petropoulos, and D. Richardson, "Efficient all-optical wavelength-conversion scheme based on a saw-tooth pulse shaper," *IEEE Photonics Technology Letters*, vol. 21, no. 24, pp. 1837–1839, 2009.

[34] P. Nuernberger, G. Vogt, T. Brixner, and G. Gerber, "Femtosecond quantum control of molecular dynamics in the condensed phase," *Physical Chemistry Chemical Physics*, vol. 9, no. 20, pp. 2470–2497, 2007.

[35] D. Meshulach and Y. Silberberg, "Coherent quantum control of two-photon transitions by a femtosecond laser pulse," *Nature*, vol. 396, no. 6708, pp. 239–242, 1998.

[36] T. Laarmann, I. Shchatsinin, P. Singh, N. Zhavoronkov, C. P. Schulz, and I. V. Hertel, "Femtosecond pulse shaping as analytic tool in mass spectrometry of complex polyatomic systems," *Journal of Physics B: Atomic, Molecular and Optical Physics*, vol. 41, no. 7, p. 074005, 2008.

[37] C. Mendonça, U. Neves, I. Guedes, S. Zilio, and L. Misoguti, "Coherent control of optically induced birefringence in azoaromatic molecules," *Physical Review A*, vol. 74, no. 2, p. 025401, 2006.

[38] M. Heck, J. Bauters, M. Davenport, J. Doylend, S. Jain, G. Kurczveil, S. Srinivasan, Y. Tang, and J. Bowers, "Hybrid silicon photonic integrated circuit technology," *IEEE Journal of Selected Topics in Quantum Electronics*, vol. 19, no. 4, p. 6100117, 2013.

[39] N. Sugimoto, T. Shintaku, A. Tate, H. Terui, M. Shimokozono, E. Kubota, M. Ishii, and Y. Inoue, "Waveguide polarization-independent optical circulator," *IEEE Photonics Technology Letters*, vol. 11, no. 3, pp. 355–357, 1999.

Chapter 7

Conclusions

The research in this thesis has investigated the concept of phase locking semiconductor lasers to individual modes of an OFC using an OIPLL. The phase locking process causes the semiconductor slave laser to adopt the frequency characteristics of the comb mode it is locked to. The output power of the locked slave laser is essentially the same as in its free running state, and hence the phase locking process can be thought of as a narrowband optical amplifier, which was used to extract individual comb modes from an OFC. For this thesis, lasers were phase locked to a relatively narrow spaced (250 MHz) fibre based OFC. These types of OFCs are predominantly used in the fields of frequency and time metrology, and spectroscopy due to their excellent frequency stability. The ability to extract individual comb modes with high gain can potentially enable more applications for these types of OFCs.

The foundation of this thesis was the technique used to perform the phase locking, the OIPLL. This was primarily based on optical injection locking, where light from the OFC was directly injected into the optical cavity of the slave laser, which under certain conditions, could phase lock to an individual comb mode due to optical coupling. One of these conditions was that the locking range had to be significantly narrower than the comb spacing to prevent injection locking to multiple comb modes simultaneously. Narrow locking ranges were achieved by using a very low injection power as compared to the output power of the slave laser, i.e. a low injection ratio. Locking was demonstrated using injection ratios as low as –70 dB, which effectively corresponded to optical gains of up to 70 dB.

The narrow locking ranges made the locking process susceptible to frequency drift of the slave laser or the OFC, which would cause unlocking to occur. This was overcome by using a low bandwidth electronic feedback system (an OPLL) to keep the frequency detuning between the slave laser and the comb mode it was locked to at a fixed value. This allowed the slave laser to remain injection locked for long periods of time by actively compensating for any frequency drift in the lasers. Although this combined system of

injection locking and electronic feedback has been demonstrated before, I have implemented it with very narrow locking ranges which allowed me to injection lock my lasers to a single comb mode of a narrow spaced OFC. Also, unlike in previous demonstrations, my implementation did not require any ultra-narrowband pre-filtering of the injection signal, or dithering of the error signal for the electronic feedback.

The quality of the locking process was investigated by measuring the residual noise of the phase locked slave laser relative to the comb mode it was locked to. The long-term frequency stability was characterised by measuring the Allan deviation over a period of 8 hours. Overall, the long-term operating frequency of the slave laser was highly stable as the Allan deviation was found to be 9.1×10^{-17} at an averaging time of 1 s, and reached a minimum of 4.4×10^{-19} at 1000 s. The short-term stability was characterised by measuring the residual phase noise across a measurement bandwidth from 100 Hz to 500 MHz. From this, it was found that an optimum injection ratio exists which minimised the integrated phase noise across the measurement bandwidth. At the optimum injection ratio, the size of the locking range balanced the noise contributions from having either too small or too large of a locking range. It was concluded from these results that this phase locking technique could be used for various applications, so long as the injection ratio is kept at the optimum value for the best noise performance.

Although the slave laser could be phase locked to an individual comb mode, the residual injected comb modes were still present in the slave laser output. Indeed, the residual comb modes were actually amplified from their injected powers, but were never as large as the phase locked lasing mode of the slave laser. It was found experimentally that the amount of amplification was dependent on the master-slave frequency detuning and the injection ratio. Larger amplification was possible for higher injection ratios. However, regardless of the injection ratio, the amplification could always be suppressed by controlling the value of the detuning. I performed numerical modelling of the injection locking process to further investigate this unexpected phenomenon. The semiconductor laser rate equations were modified to accommodate the OFC injection. The underlying cause of the amplification was found to be mostly due to phase modulation induced in the slave laser by the residual injected comb modes. Amplitude modulation also contributed to the amplification, but was negligible as compared to the phase modulation, except at very low injection ratios. From these results, it was concluded that in addition to using the optimum injection ratio for the best noise performance, the slave laser should also be set to zero detuning to minimise the effects of the residual comb modes.

The final chapter of this thesis explored one of the applications which could utilise this phase locking technique – Fourier synthesis of high repetition rate waveforms. This utilised multiple independent slave lasers which were locked to different modes of a common OFC to make them coherent with one another. By combining the outputs of the lasers together, each laser could then behave as a different frequency component of a Fourier series. The waveforms generated were manipulated by controlling the phase

and amplitude of each laser individually. To ensure stable waveforms were generated, a phase stabilisation system was required to control the relative phases of the slave lasers as they were combined. This also allowed the relative phases to be tuned to the desired value for a given waveform, whereas the relative amplitudes were simply controlled using variable optical attenuators.

I used up to six slave lasers to generate waveforms with repetition rates of 100 GHz. A variety of waveforms with different intensity profiles were demonstrated including rectangular, triangular, parabolic and sawtooth pulses. The resemblance of these waveforms to their ideal waveforms had mixed results and was ultimately limited by the number of available Fourier components (slave lasers). However, as a proof of principle experiment, the results were able to successfully demonstrate Fourier synthesis using multiple OFC locked lasers. Improved agreement between the generated and ideal waveforms are expected by scaling up the number of slave lasers used.

Concurrent work and suggestions for future work

Even though the phase locking process was found to be of high quality in Chapter 4, the noise properties could be improved further. The use of polarisation maintaining fibre and components between the OFC and slave laser would minimise fluctuations of the injection ratio due to polarisation variations. Although the noise performance was acceptable for the application targeted in this thesis, the low frequency phase noise could have been significantly reduced by using high bandwidth phase lock loops, which might be important for high accuracy metrology applications. Furthermore, the long-term frequency stability characterisation was incomplete as it was only measured at a single injection ratio. In fact, both the long- and short-term noise properties of the phase locking process could be further characterised by measuring the noise dependence on the master-slave detuning.

It is also important to keep in mind that the Fourier synthesiser set-up presented in Chapter 6 was only a proof of principle prototype. The device itself could be significantly improved by discarding the programmable filter (Waveshaper) which, in the end, was used only for calibration purposes, not for line-by-line pulse shaping. This could be enabled by implementing electrically controlled optical attenuators in the set-up to selectively filter individual slave lasers (Fourier components) with minimal phase or polarisation perturbations. The use of slave lasers with higher output power could also remove the need for optical amplifiers.

Considering more long-term future directions, the most directly related one I envision is towards the development of a Fourier synthesiser using a combination of photonic and electronic integration. This would potentially allow for a device which would be compact in size and also contain more slave lasers to increase the number of available Fourier

components. The small size would also be expected to improve phase and polarisation stability issues associated with thermal fluctuations.

Further development of the Fourier synthesiser could also allow it to be used for further applications, with one example being for tailored THz generation. One of the current methods used to generate THz pulses uses photoconductive antennae [1]. Optical pulses are used to excite free carriers (electrons and holes) in a semiconductor material, which are then separated and accelerated by an external voltage through an antenna structure. This causes the antenna to radiate at THz frequencies across a bandwidth which is determined by the response time of the semiconductor material and the antenna structure. I speculate that the generated THz waveform can be customised by controlling the intensity profile of the optical pulses used to excite photoconductive antennae to generate THz pulses. A Fourier synthesiser would allow customisable, high power, and low noise optical pulses to generated for this purpose.

The phase locking technique presented in this thesis could also be utilised as the basis for numerous applications other than Fourier synthesis. Some of these other applications are already being pursued by others in my research group here in Southampton. One such application is in the field of frequency metrology. Feasibility studies have been undertaken to test the use of the phase locking technique for ultra-stable optical frequency dissemination, specifically for signal regeneration and wavelength conversion [2, 3]. For this application, the ultra-stable single frequency signal will be used to generate an OFC using an electro-optic modulator, and a slave laser will be phase locked to one of the generated comb modes. The slave laser effectively regenerates the original signal at a different wavelength, but with some additional noise from the locking process. Research is currently being undertaken to further reduce this additional noise.

Another application which uses the phase locking technique from this thesis is in the field of telecommunications. Research has been undertaken to use the phase locking technique for homodyne detection of orthogonal frequency division multiplexing (OFDM) signal by using it for carrier recovery [4]. Homodyne detection requires an optical local oscillator at the receiver to recover the transmitted data. This local oscillator is required to be at the same frequency as the carrier of the data signal. It is common for the local oscillator frequency to be estimated, but this results in a relatively large number of errors in the received data. The carrier frequency may also be transmitted with the data, but requires a large portion of bandwidth around the carrier to be data-free (the guardband) in order for it to be cleanly recovered. In [4], it was shown that the phase locking technique from this thesis can be used to lock the frequency of the local oscillator to the transmitted carrier signal. The ability to achieve stable, long-term locking at low injection ratios means the slave laser can behave as a narrowband amplifier and hence the size of the guardband can be reduced, which increases spectral efficiency.

Final remarks

In conclusion, the phase locking technique presented in this thesis, which was used here to extract comb modes from narrow spaced OFCs, has great potential to be a useful tool in a wide range of fields. Research is currently being undertaken where this technique has successfully been used for frequency metrology and telecommunications applications. In this thesis, its application for Fourier synthesis of optical waveforms was successfully pursued as a proof of principle experiment. Further development of the prototype presented here could result in a compact device which could have many applications in a wide of range of fields.

7.1 References

[1] P. Smith, D. Auston, and M. Nuss, "Subpicosecond photoconducting dipole antennas," *IEEE Journal of Quantum Electronics*, vol. 24, no. 2, pp. 255–260, 1988.

[2] J. Kim, D. Wu, G. Marra, D. J. Richardson, and R. Slavík, "Stability Characterization of an Optical Injection Phase Locked Loop for Optical Frequency Transfer Applications," in *2014 CLEO: Science and Innovations*, p. SW30, 2014.

[3] J. Kim, D. S. Wu, G. Marra, D. J. Richardson, and R. Slavík, "Wavelength Conversion by Injection Locking to an Optical Comb for Optical Frequency Transfer Applications," in *EPS-QEOD Europhoton Conference*, pp. ThB–T1–O–02, 2014.

[4] Z. Liu, J. Kim, D. S. Wu, D. J. Richardson, and R. Slavík, "Homodyne OFDM with Optical Injection Locking for Carrier Recovery," *Journal of Lightwave Technology (accepted)*, 2014.

Appendix A

Acousto-Optic Modulator Induced Amplitude Noise

For the measurements in Section 4.2.1, it was discovered that a non-insignificant residual RF signal at 35 MHz was present even when the slave laser was not locked. This is shown in Figure A.1. The residual signal (when the laser was unlocked, and the beat signal tuned away from 35 MHz) varied from –15 to –20 dB as compared to the locked signal. Although this corresponds to being at least 30 times weaker (in a linear scale), it is possible that it could have affected the previous measurements.

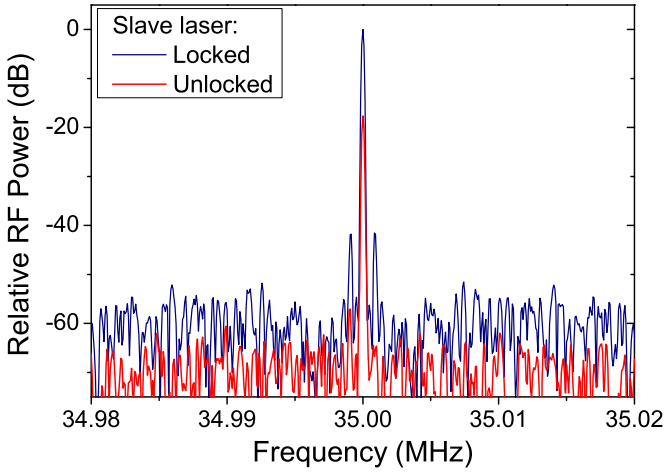

FIGURE A.1: The RF beat signal at 35 MHz when the slave laser is locked and unlocked. Injection ratio: –65 dB.

The reference arm was disconnected from the set-up, such that the photodetector was only measuring the AOM frequency shifted slave laser output. The residual signal was still present which shows that the residual beat signal was not due to the residual comb modes present in the slave laser output, but was caused by amplitude modulation induced by the AOM. It is unknown how this AOM induced noise would affect the measurements. The AOM noise was suppressed in the subsequent phase noise measurements by

reducing it's relative power by increasing the power of the signal of interest Section 4.3.1 by using two locked slave lasers.

Appendix B

Phase Noise of a Single Slave Laser from Two Identical Lasers

In Section 4.3.1, it was claimed that the phase noise of a single OIPLL locked slave laser could be calculated from a measurement involving two slave lasers locked. The claim that the phase noise of a single laser was simply half of the measured value using two lasers is justified in this appendix.

A schematic of the experimental set-up is reproduced in Figure B.1. It is first assumed that the two lasers had similar noise and operating properties. This was justified because the two lasers used were manufactured in the same batch and had the same specifications. For this analysis, it is assumed that the lasers were locked to the same comb mode. The two locked lasers would operate at the same frequency, but one of them was frequency shifted by $\Delta\omega$ through the acousto-optic modulator. The intensity measured by the photodetector is:

$$I_{tot} = E_1^2 + E_2^2 + 2E_1E_2\cos(\Delta\omega t + \phi_1(t) - \phi_2(t)) \ ,$$

where E_1 and E_2 are the amplitudes of the electric fields of laser #1 and #2 respectively; and $\phi_1(t)$ and $\phi_2(t)$ are the time dependent phase noise terms of the two lasers. The residual comb modes were not taken into consideration in this analysis. An RF band-pass filter can be used to isolate the oscillating cosine term with an angular frequency of $\Delta\omega$. The filtered output voltage of the photodetector (with gain of k_{photo}) is given by:

$$V_{photo} = 2k_{photo}E_1E_2\cos(\Delta\omega t + \phi_1(t) - \phi_2(t)) \ .$$

An RF mixer, with a conversion factor of k_{mixer}, can be used to down-convert this oscillating signal to baseband using a local oscillator at the same frequency. If a noise-free reference signal is used as the local oscillator, $R\cos(\Delta\omega t + \phi_r)$, then the mixer

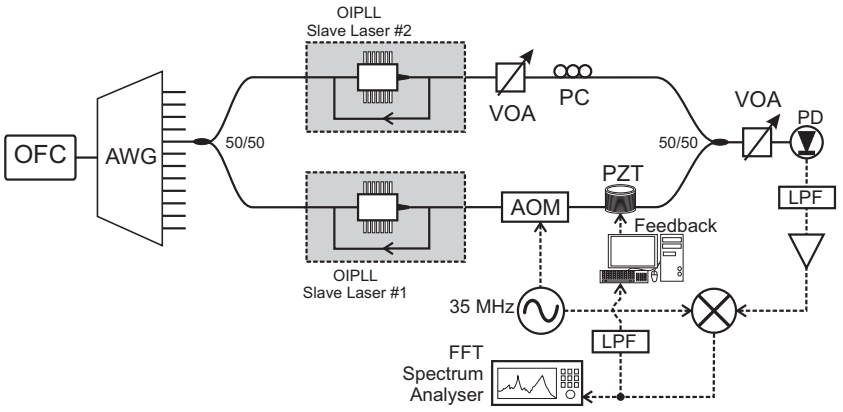

FIGURE B.1: Schematic of the set-up used to measure phase noise. AWG: arrayed waveguide grating, AOM: acousto-optic modulator, PZT: Lead Zirconate Titantate (piezoelectric phase shifter), LPF: low-pass filter, VOA: variable optical attenuator, PC: polarisation controller. This is a reproduction of Figure 4.8

output is equal to:

$$\begin{aligned} S &= [2k_{photo}k_{mixer}E_1E_2R]\cos(\Delta\omega t + \phi_1(t) - \phi_2(t))\cos(\Delta\omega t + \phi_r) \ , \\ &= K_d[\cos(\phi_1 - \phi_2 - \phi_r) + \cos(2\Delta\omega t + \phi_1(t) - \phi_2(t) + \phi_r)] \ , \end{aligned} \tag{B.1}$$

where $K_d = k_{photo}k_{mixer}E_1E_2R$ is the phase detector sensitivity. The second term in (B.1), which has a frequency of $2\Delta\omega$, can be filtered out using an RF low-pass filter. ϕ_r can be tuned to be $^{-\pi}/_2$ such that:

$$\begin{aligned} S &= K_d\cos(\phi_1(t) - \phi_2(t) + \pi/2) \ , \\ &= K_d[\phi_1(t) - \phi_2(t)] \ , \end{aligned} \tag{B.2}$$

where the cosine small angle approximation was invoked.

The phase noise is measured using an RF spectrum analyser which measures the power spectral density which is proportional to the square of the signal S:

$$\begin{aligned} S^2 &= K_d^2\left(\phi_1(t) - \phi_2(t)\right)^2 \ , \\ &= K_d^2\left(\phi_1(t)^2 + \phi_2(t)^2 - 2\phi_1(t)\phi_2(t)\right) \ . \end{aligned} \tag{B.3}$$

If it is assumed that both lasers are identical but independent, then the phase noise (a random process) can be considered to have equal expected values such that $\mathbb{E}[\phi_1(t)^2] = \mathbb{E}[\phi_2(t)^2]$. However, since the lasers are independent, then the expected value of the cross-term in (B.3) is equal to zero, i.e. $\mathbb{E}[\phi_1(t)\phi_2(t)] = 0$. Therefore, for time averaged measurements

$$S^2 = 2 \times \left(K_d\phi_1(t)\right)^2 \ , \tag{B.4}$$

and the phase noise power spectral density of a single laser is half the measured power spectral density.

Appendix C

Additional Measurements of Fourier Synthesised Waveforms

In this appendix, further stability measurements of the waveforms generated in Section 6.5.3 and 6.5.4 are presented.

Heat maps for waveforms generated with six lasers

The two minute heat maps for waveforms synthesised using six slave lasers are presented here. As stated in Section 6.5.4, these show similar stability to those generated with five slave lasers.

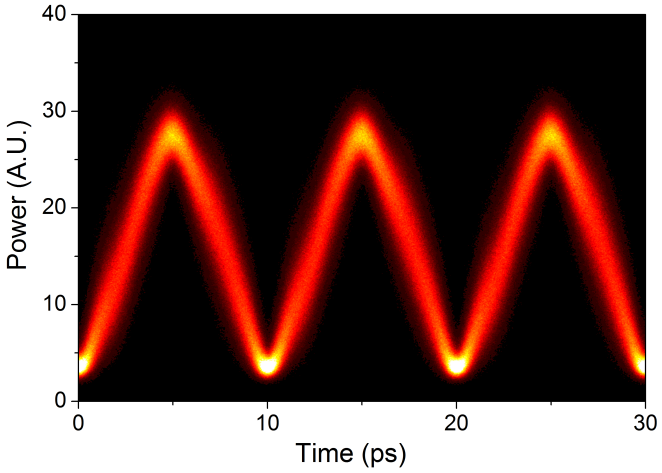

FIGURE C.1: Two minute heat map for a triangular waveform generated using six slave lasers. Edge sample frequency FWHM: 1.11 ± 0.08 ps.

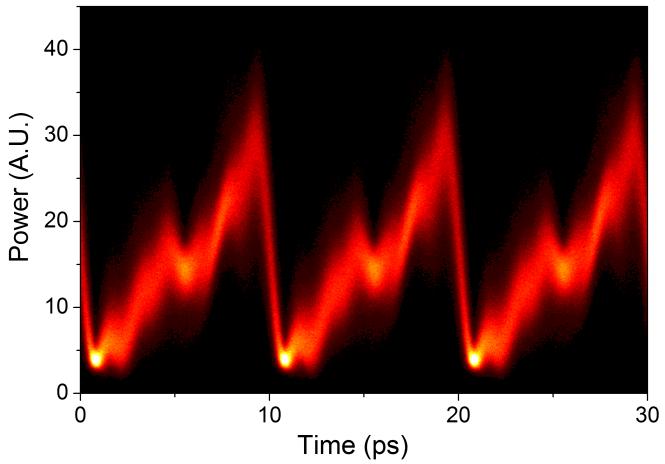

FIGURE C.2: Two minute heat map for a sawtooth waveform generated using six slave lasers. Edge sample frequency FWHM: 1.2 ± 0.2 ps.

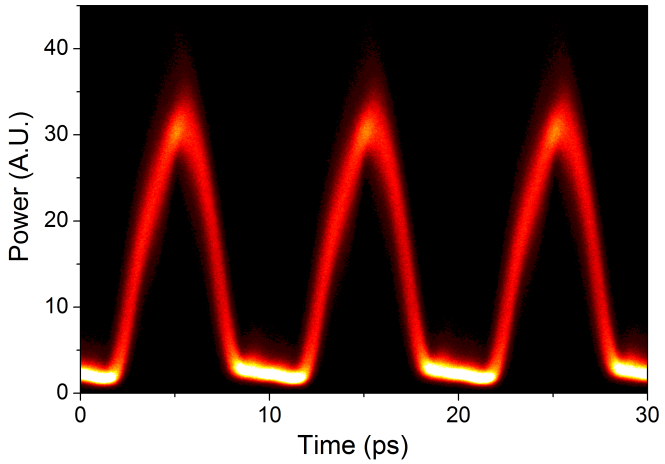

FIGURE C.3: Two minute heat map for a parabolic waveform generated using six slave lasers. Edge sample frequency FWHM: 0.73 ± 0.06 ps.

Infinite persistence measurements of waveforms

Measurements were also taken of the synthesised waveforms with the optical sampling oscilloscope set to infinite persistence. For this, measurements were taken over a period of two minutes, but unlike the heat maps, the measured sampled are overlaid on top of previous measurements. The following plots do not show the number or frequency of overlapping samples as was the case for the heat maps, but instead shows the absolute spread of samples over the measurement period. The results shown here confirm that there was indeed good stability in the measured waveforms.

Five slave lasers (Section 6.5.3)

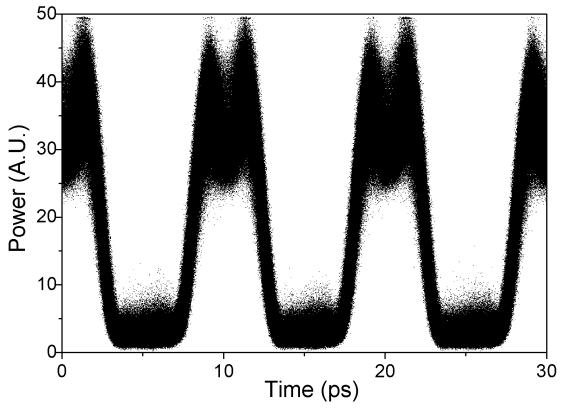

FIGURE C.4: Two minute infinite persistence measurement for a sinc-spectrum square pulse train generated by five slave lasers.

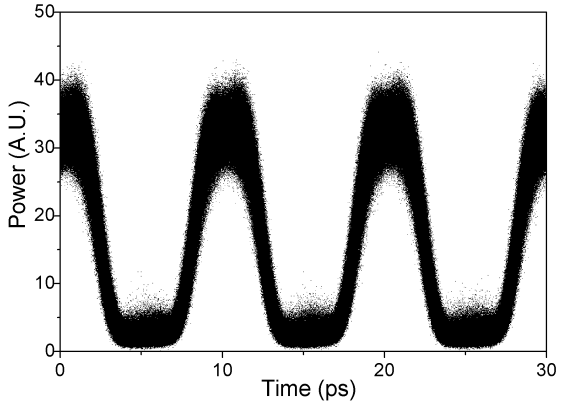

FIGURE C.5: Two minute infinite persistence measurement for an apodised sinc-spectrum square pulse train generated by five slave lasers.

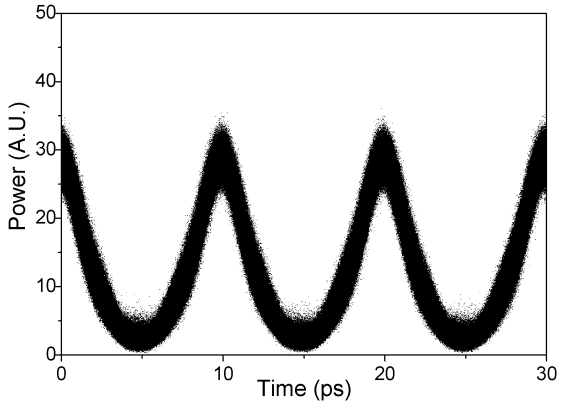

FIGURE C.6: Two minute infinite persistence measurement for a dark parabolic pulse train generated by five slave lasers.

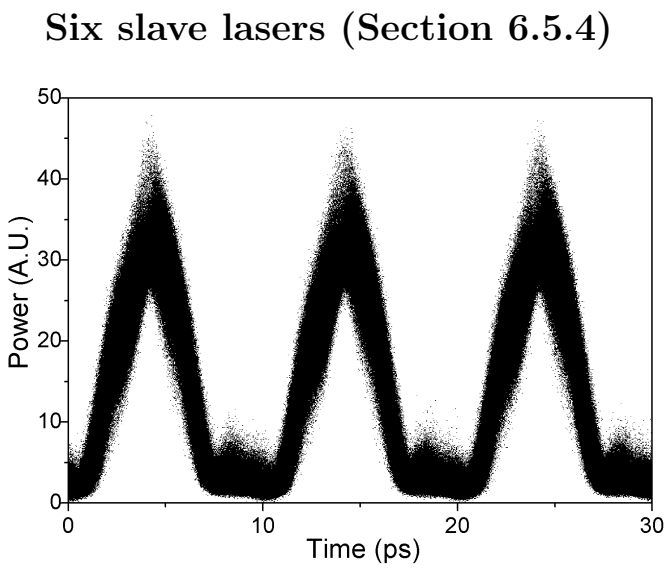

FIGURE C.7: Two minute infinite persistence measurement for a bright parabolic pulse train generated by six slave lasers.

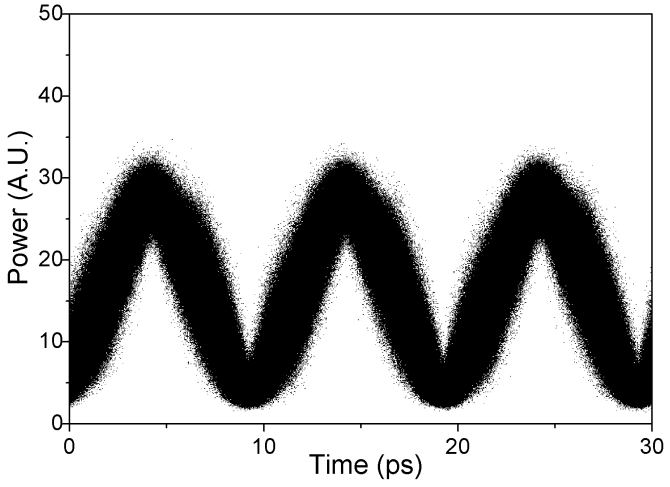

FIGURE C.8: Two minute infinite persistence measurement for a triangular pulse train generated by six slave lasers.